NEW STRUCTURES FOR AlGaAs LASERS AND AVALANCHE PHOTODETECTORS

Thesis by

Henry A. Blauvelt

In Partial Fulfillment of the Requirements

for the Degree of

Doctor of Philosophy

California Institute of Technology

Pasadena, California

1983

(Submitted October 26, 1982)

To my Parents

-Acknowledgements-

I would like to take this opportunity to express my appreciation to my adviser, Professor Amnon Yariv, for his encouragement and support throughout my graduate studies at Caltech. I have profited greatly from the experience gained under his supervision in the quantum electronics group.

I am especially indebted to Dr. Shlomo Margalit for many fruitful discussions and for his guidance. His constant willingness to discuss new ideas was of tremendous value. Special thanks are due also to Dr. Nadav Bar-Chaim for his collaboration on some of the work described in this thesis and for teaching me how to grow crystals by liquid phase epitaxy.

I would also like to express my thanks to the other members, past and present, of the quantum electronics group with whom I have worked these past years: Dr. Israel Ury, Dr. Kam Lau, Dr. Daniel Wilt, Dr. Pei-Chuang Chen, Dr. Joseph Katz, Dr. Uziel Koren, Mr. Chris Harder, Mr. Liew-Chuang Chiu, Mr. Paul Yu, and Mr. Stephen Smith. I am also indebted to Mr. Desmond Armstrong for his assistance with the experimental apparatus. I also thank Mr. Lawrence Begay for his help in constructing some of the experimental apparatus used in this study.

I am thankful for the financial support received from the California Institute of Technology, the National Science Foundation, and the Office of Naval Research.

Finally, my deepest appreciation goes to my parents for thier constant support and encouragement of my undertaking this work.

Abstract

This thesis describes the fabrication and the properties of five new semiconductor laser diode structures. All of these devices were grown from the GaAs-AlGaAs ternary system using the liquid phase epitaxial technique. In addition, a new low noise avalanche photodetector is proposed.

The first example is a new technique for fabricating cleaved mirrors without cleaving through the substrate. This technique, called micro-cleavage, has potential applications for both opto-electronic integrated circuits and for the fabrication of short cavity length lasers. In this technique, cantilevers are formed by a sequence of etching steps. These cantilevers are subsequently cleaved using ultrasonic vibrations.

Three devices related to high power single mode lasers are described. The first of these is the large optical cavity buried heterostructure window laser. The output power of semiconductor lasers, particularly during pulsed operation is limited by catastrophic mirror damage which occurs at power densities above a pulse width dependent damage threshold. The damage occurs due to local heating up to the melting point of the active region in the vicinity of the cleaved mirror facets. However, catastrophic mirror damage can be avoided by isolating the active layer from the cleaved mirrors, as is done in these window lasers. The second device related to high power that is described is the Inverted Strip Buried Heterostructure laser. These lasers combine many of the best features of both the buried optical guide lasers and the strip buried heterostructure that have been previously developed elsewhere. The inverted strip buried heterostructure lasers have significantly better beam quality than buried optical guide lasers and can be operated in the fundamental spatial mode for larger emitting

areas (and therefore greater output power). The third device related to high power lasers is a variation of a buried heterostructure laser in which the injected current is confined to a narrow section in the center of the active layer. The optical gain is therefore also confined to a narrow section in the center of the active layer. By doing so the fundamental mode is much better matched to the optical gain than the higher order spatial modes. The result is that fundamental mode operation is possible for buried heterostructure lasers with active layer widths up to 8 μm. When the current is injected uniformly into the active layer, fundamental mode operation is possible only for active layer widths less than 2 μm. In addition to the descriptions of these devices a theoretical chapter on high power single mode lasers is included.

The final laser structure that is described is a single liquid phase epitaxial growth laser structure in which the current is restricted to flow between two narrow stripes located above and below the active layer. This structure, which is fabricated using a meltback-growth technique allows the current injection to be restricted to a very narrow section of the active layer, which results in several interesting properties which are described and explained using a simple model.

The final subject of this thesis is a multilayer avalanche photodetector (APD) which has been proposed for low noise applications. The noise generated by an APD is dependent on the statistics of the carrier multiplication process, since positive feedback effects, which exist when both electrons and holes produce secondary pairs, can greatly amplify any current fluctuations. Significantly more noise is generated if the electron and hole ionization rates (α,β) are equal than if only one carrier produces secondary pairs. The multilayer structure described and analyzed in this chapter is expected to have impact ionization which is dominated by electrons and therefore would be of importance for low noise applications.

CONTENTS

Chapter I

INTRODUCTION

1.1 Semiconductor Laser Diodes

Since the first observations of lasing action in GaAs in 1962[1-4], semiconductor laser diodes have been the focus of great attention because of their tremendous commercial potential. In the past twenty years great improvements have been made in the performance and reliability of semiconductor lasers. By reducing the threshold currents of the laser diodes, to as low as 4 mA in buried heterostructure lasers[5], continuous operation at room temperature has been made possible. Lasers which operate continuously and stably in a single spatial mode and frequency at output powers up to 40 mW have been demonstrated[6,7]. Laser reliability has been improved to the point where some laser structures have expected lifetimes exceeding 10^6 hours.

Throughout this thesis, a familiarity with semiconductor lasers is assumed. Comprehensive treatments of semiconductor laser diodes can be found in the books by Casey and Panish[8], Kressel and Butler[9] , and Thompson[10].

Laser diodes have numerous unique properties which make them attractive for a number of important applications. Laser diodes are very small in size, they are highly efficient, and they can be modulated at frequencies up to several GHz by directly modulating the laser current. Semiconductor laser diodes also have the potential for duplicating the low cost and high reliability characteristics of semiconductor electronic devices. Most of the major applications of semiconductor laser diodes involve the use of laser diodes in the storage and transmission of information. Laser diodes are being used as the transmitters for high speed communication through optical fibers. Laser diodes will soon appear in the rapidly expanding consumer electronics market to be used to

optically read high density audio and video information stored on discs. Storage and retrieval of information from high density disc recording has potential applications in the computer industry. The characteristics of laser diodes also make them potentially attractive for document generation applications such as laser printers and copiers.

Fiber optic communication has been the subject of intense research recently. Of particular interest are fiber optic communication systems which use glass fibers as the transmission medium and semiconductor devices as the light sources and detectors[11]. Fiber optic communication systems have a number of advantages as compared to conventional microwave transmitting systems. Optical fibers are light weight, have very low attenuations, are free from interference, and have large transmission bandwidths. The semiconductor light sources and detectors in optical communication systems are small, highly efficient, capable of operating at GHz frequencies, and have the potential for low cost and high reliability.

Semiconductor laser research for optical communications has concentrated primarily on III-V materials. In particular, the ternary $Al_xGa_{1-x}As$ grown on GaAs substrates and the quaternary $In_xGa_{1-x}As_yP_{1-y}$ lasers grown on InP substrates have received the most attention. By adjusting the mole fractions of the atomic constituents, the emitting wavelength of these semiconductor lasers can be varied. AlGaAs lasers have been fabricated with wavelengths ranging from 0.68 μm to 0.88 μm. InGaAsP lasers have been fabricated with wavelengths ranging from 1.0 μm to 1.7 μm. Of particular interest for optical communications is the wavelength range of 1.3-1.6 μm. This is the wavelength region where silica optical fibers have the lowest loss and least optical dispersion. Attenuations as low as 0.2 dB/Km have been reported at 1.55 μm[12]. By comparison the best optical fibers have losses of 2 dB/Km at the wavelength of GaAs lasers of 0.88 μm.

Because of this, InGaAsP lasers are the preferred transmitting sources for long distance optical communication systems. However, AlGaAs lasers have many advantages which make them more attractive for short distance, high speed communications applications where low fiber losses and dispersion are not critical. AlGaAs laser technology has received the most attention and is more advanced than that of InGaAsP lasers. AlGaAs lasers are significantly less sensitive to temperature variations, which is a major problem with long wavelength quaternary lasers. The technology for fabricating GaAs electronic circuits is also more advanced than that of InP making monolithic integration of AlGaAs lasers with GaAs electronic devices more attractive than the integration of InGaAsP lasers with InP electronic circuits.

The advantages of integrated optoelectronic circuits (IOEC) combining AlGaAs lasers and GaAs electronic circuits have been recognized for some time[13]. These advantages include size, cost, and reliability. In addition, the reduction of parasitic reactances, which would otherwise result from device interconnections, can lead to significant improvements in the speed and noise performances of the optoelectronic circuits.

The problem of designing and fabricating IOECs is mostly one of devising means to make the technologies of GaAs electronic circuits and AlGaAs lasers compatible with one another. AlGaAs lasers are usually fabricated on highly conductive substrates. GaAs electronics, such as MESFETs (metal semiconductor field effect transistors), however, are fabricated on n-type layers which are formed on top of semi-insulating (SI) substrates. The use of the SI substrates reduces parasitic capacitances and also facilitates isolation between devices fabricated on a common substrate. It is therefore desirable for IOECs to fabricate lasers on SI substrates. One problem in fabricating lasers on SI substrates is that such lasers must be mounted on heat sinks with the substrate

side down, because of the requirement that both the P and N contacts be made to the top surface. Since the active layer is typically located about 1 micron beneath the top surface, the heat generated in the active layer can be removed more efficiently when the lasers are mounted substrate side up (active layer near the heat sink). For IOECs, it is therefore important to have lasers which have threshold currents as low as possible to minimize the heat dissipation of the devices. A second difficulty is the limitation on the size of the IOEC imposed by the laser cavity formed by the cleaved facets of the chip. Several methods of fabricating laser mirrors without cleaving through the substrate have been reported. Using techniques, such as that of microcleavage[14], which will be described in detail later in this thesis, lasers can be fabricated on substrates which are not restricted in size by the laser cavity length, which is typically 300 μm.

A second major area of application of semiconductor laser diodes is in the storage and retrieval of information from optical discs. In this application information stored on an optical disc is read out by a focused laser beam as illustrated in fig 1. Laser diodes are particularly well suited to this application because of their small size. Consumer electronics products in which audio and/or video information stored on a disc is read out by a laser diode have already been demonstrated. The digital audio disc, in which audio information is stored on the disc in a digital format, making possible nearly perfect sound reproduction, is expected to appear in the marketplace by late 1982.

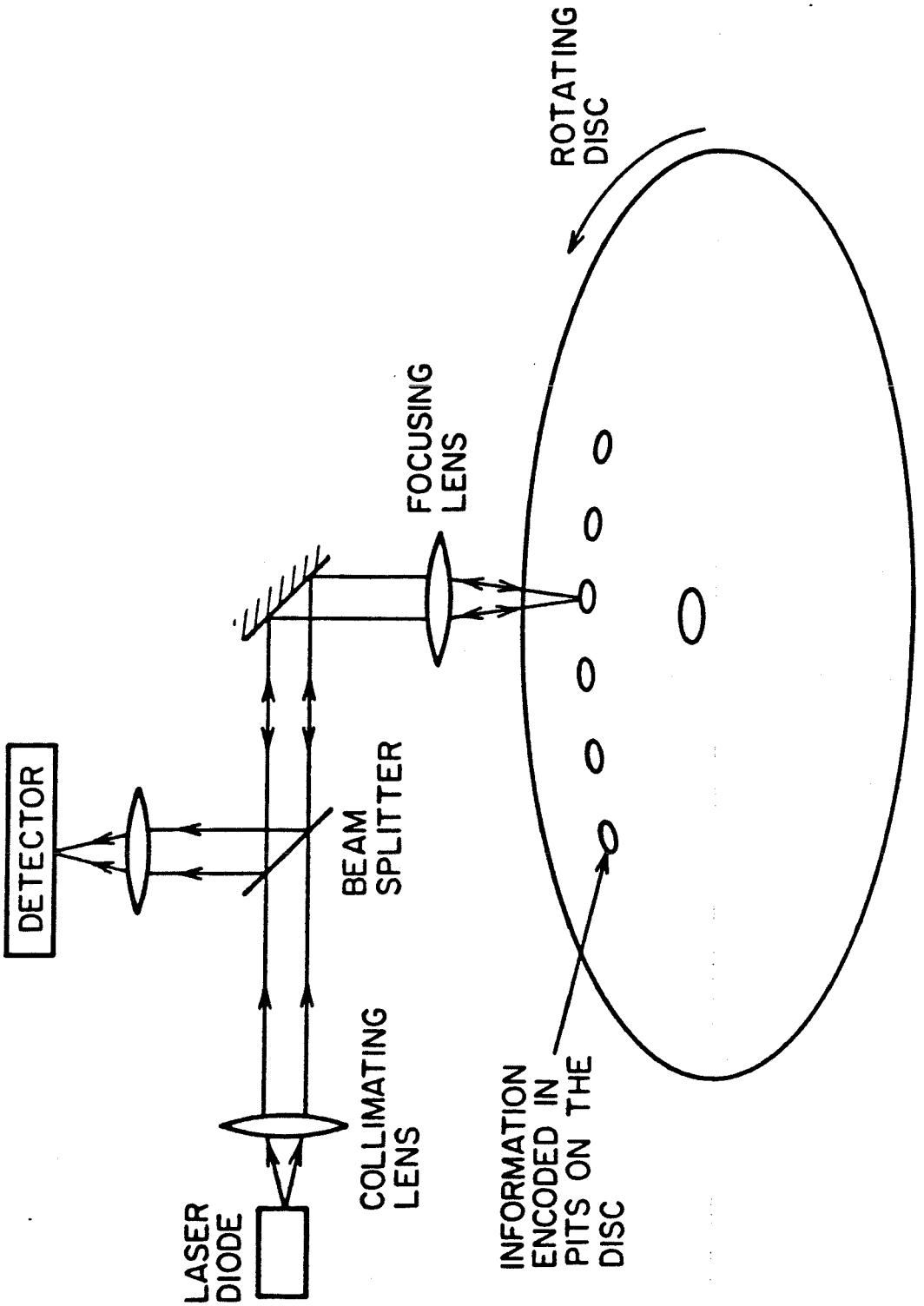

Fig. 1 Schematic representation of an optical disc information storage system

The first generation of optical disc recording systems are read only systems in which information can be encoded by using specialized and expensive equipment to evaporate pits in a metal film on the disc. These optical discs are analogous to conventional audio records in which prerecorded information can be played. Unlike audio and videotape, first generation optical disc systems do not have any provisions for recording information by the user. However, simple systems for recording information on discs using laser diodes has already been demonstrated[15] and recording capability can be expected in future generations of optical disc systems. The addition of a recording capability will make optical disc systems very attractive as an alternative to magnetic disc systems for computer memory.

For the reading of optical discs the most important laser characteristics are the laser beam quality and the emitting wavelength. High quality optical beams are essential for error free reading of the stored information. Since the minimum spot size of a focused laser beam is proportional to the wavelength, it is desirable to use lasers with as short a wavelength as possible. AlGaAs lasers emitting in the .7-.78 μm range have received the most attention for this application. The reading of information from optical discs requires relatively little laser output power, about 1 mW, which can be easily obtained from commercially available lasers. Optical recording of information requires substantially more power, about 30 mW. Although continuous power outputs of as high as 40 mW have been reported from lasers with good beam quality[6,7], reliable laser operation has not as yet been achieved for output powers greater than about 20 mW. The design and fabrication of high beam quality, high power lasers has been an area of intense research lately, and will be discussed in more detail later in this thesis.

1.2 Thesis Outline

Six subjects related to AlGaAs lasers will be discussed in this thesis in chapters II-VII. Chapter II describes a new technique for fabricating cleaved mirrors without cleaving through the substrate. This technique, called micro-cleavage, has potential applications for both opto-electronic integrated circuits and for the fabrication of short cavity length lasers. In this technique, cantilevers are formed by a sequence of etching steps. These cantilevers are subsequently cleaved using ultrasonic vibrations. This makes possible the fabrication of lasers with cleaved mirrors on a substrate which is not restricted in size to the laser cavity length. The fabrication and performance of oxide stripe lasers with micro-cleaved mirrors is discussed in detail in this chapter.

Chapter III is a theoretical chapter concerned with the spatial mode properties of semiconductor lasers and the closely related subject of high power single mode laser design. For most applications of laser diodes, it is highly desirable that the laser operates stably in the fundamental spatial mode. In chapter III, the factors which determine the spatial mode patterns of semiconductor lasers are examined. Spatial mode control of lasers actually involves two separate problems. First, the laser structure must be such that at low power levels the laser operates in the fundamental spatial mode. In addition, the laser structure must be such that as the power level of the laser is increased, the spatial mode pattern does not change. Both aspects of spatial mode control are discussed in chapter III. Calculations related to the mode gains and mode reflectivities of buried heterostructure lasers are presented. Predictions of the spatial mode properties of buried heterostructure lasers, based on these calculations are presented and compared with experimentally observed properties. The factors which limit the amount of single mode power

available from laser diodes are also discussed in detail in chapter III.

Chapter IV describes the fabrication and performance of buried heterostucture window lasers. The output power of semiconductor lasers, particularly during pulsed operation is limited by catastrophic mirror damage which occurs at power densities above a pulse width dependent damage threshold. The catastrophic damage thresholds are approximately 15 $mW/\mu m^2$ for continuous operation and 70 $mW/\mu m^2$ for 100 nsec pulses. The damage occurs due to local heating up to the melting point of the active region in the vicinity of the cleaved mirror facets. However, catastrophic mirror damage can be avoided by isolating the active layer from the cleaved mirrors. Chapter IV describes a variation on the buried heterostructure laser which has transparent "window" sections near the mirrors and is immune from catastrophic mirror damage at power levels up to three times the catastrophic damage limit of conventional buried heterostructure lasers.

Chapter V describes the fabrication and performance of Inverted Strip Buried Heterostructure (ISBH) lasers. ISBH lasers combine many of the best features of both the buried optical guide lasers developed by Chinone *et al.*[16] and the strip buried heterostructure (SBH) lasers developed by Tsang and Logan[17]. These lasers have significantly better beam quality than buried optical guide lasers and can be operated in the fundamental spatial mode for active layer widths up to 4 μm. These spatial mode characteristics are similar to those of strip buried heterostructure lasers. However, ISBH lasers have lower threshold currents and better thermal characteristics than SBH lasers. ISBH laser fabrication is also simpler and therefore of potentially higher yield than SBH laser fabrication.

Chapter VI describes a variation of a buried heterostructure laser which applies some of the concepts discussed in chapter III. In the narrow injection

buried heterostructure lasers the injected current is confined to a narrow section in the center of the active layer. The optical gain is therefore also confined to a narrow section in the center of the active layer. By doing so the fundamental mode is much better matched to the optical gain than the higher order spatial modes. The result is that fundamental mode operation is possible for buried heterostructure lasers with active layer widths up to 8 μm. When the current is injected uniformly into the active layer, fundamental mode operation is possible only for active layer widths less than 2 μm. The fabrication and performance of these lasers is discussed in detail in chapter VI.

Chapter VII describes a single liquid phase epitaxial growth laser structure in which the current is restricted to flow between two narrow stripes located above and below the active layer. This structure, which is fabricated using a meltback-growth technique allows the current injection to be restricted to a very narrow section of the active layer. The primary emphasis in this chapter will be simply to explain the structure and the properties of lasers with very narrow injection. Among the more significant characteristics are far field patterns characteristic of leaky mode waveguides and operation in a very large number of longitudinal modes. In addition, the properties of the lasers suggest that the laser structure may result in useful applications and potential applications, such as low threshold laser structures and arrays of optically coupled lasers are discussed briefly

Chapter VIII describes a multilayer avalanche photodetector (APD) which has been proposed for low noise applications. The noise generated by an APD is dependent on the statistics of the carrier multiplication process, since positive feedback effects, which exist when both electrons and holes produce secondary pairs, can greatly amplify any current fluctuations. Significantly more noise is generated if the electron and hole ionization rates (α,β) are equal than if only

one carrier produces secondary pairs. It is therefore highly desirable to have a detector in which the multiplication process is dominated by one carrier type. Unfortunately, most III-V materials have $\alpha \approx \beta$. The multilayer structure described and analyzed in this chapter is expected to have impact ionization which is dominated by electrons and therefore would be of importance for low noise applications.

References for Chapter 1

1. R.N. Hall, G.E. Fenner, J.D. Kingsley, T.J. Soltys, and R.O. Carlson "Coherent Light Emission from GaAs Junctions", Phys. Rev. Lett. **9** , pp366-368 (1962).

2. M.I. Nathan, W.P. Dumke, G. Burns, F.N. Dill, and G.J. Lasher "Stimulated Emission of Radiation from GaAs PN Junctions", Appl.Phys. Lett. **1** , pp 62-64 (1962).

3. M. Holonyak and S.F. Bevacqua "Coherent (Visible) Light Emission from $Ga(As_{1-x}P_x)$ Junctions", Appl. Phys. Lett. **1** , pp 82-83 (1962).

4. T.M. Quist, R.H. Rediker, R.J. Keyes, W.E. Krag, B. Lax, A.L. McWhorter, and H.J. Zeigler "Semiconductor Masers of GaAs" Appl. Phys. Lett. **1** , pp 91-92 (1962).

5. K. Saito, N. Shige, T Kajimura, T. Tsukada, M. Maeda, and R. Ito "Buried Heterostructure Lasers as Light Sources in Fiber Optic Communications", Technical Digest Integrated Optics and Optical Communications (IOOC Tokyo 1977) p 65.

6. D. Botez "CW High Power Single Mode Operation of Constricted Double Heterojunction AlGaAs Lasers with a Large Optical Cavity", Appl. Phys. Lett. **36** , pp190-192 (1980).

7. M. Nakamura, K. Aiki, N. Chinone, R. Ito, and J. Umeda, "Longitudinal-Mode Behaviors of Mode Stabilized $Al_xGa_{1-x}As$ Injection Lasers", J. Appl. Phys. **49** , pp 4644-4648 (1978).

8. H.C. Casey, and M.B. Panish *Heterostructure Lasers* Academic Press, New York 1978.

9. H. Kressel and J.K. Butler *Semiconductor Lasers* and *Heterojunction LEDs* Academic Press, New York, 1977.

10. G.H.B. Thompson *Physics of Semiconductor Laser Devices* John Wiley and Sons, Chichester, England 1980.

11. D. Botez and G.J. Herskowitz "Components for Optical Communications Systems: A Review" Proc. IEEE **68** , pp 689-731 (1980).

12. T. Miya, Y. Terunuma, T. Hosaka, and T. Miyashita "Ultimate Low-Loss Single Mode Fibers at 1.55 μm" Electron. Lett. **15** , pp 106-108 (1979).

13. A. Yariv "Active Integrated Optics" Proc. Esfahan Symposium on Fundamental and Applied Laser Physics" M.S. Feld, A. Javan, and N.A. Kurnit Eds. Wiley Interscience, New York, 1973 pp 897-919.

14. H. Blauvelt, N. Bar-Chaim, D. Fekete, S. Margalit, and A. Yariv "AlGaAs Lasers with Micro-cleaved Mirrors Suitable for Monolithic Integration" Appl. Phys. Lett. **40** , pp 289-290 (1982).

15. R. Bartolini, A. Bell, and F. Spong "Diode Laser Optical Recording Using Trilayer Structures" IEEE J. Quantum Electron. **QE-17** , pp 69-77 (1981).

16. N. Chinone, K. Saito, K. Aiki, and N. Shige "Highly Efficient (GaAl)As Buried Heterostructure Lasers with Buried Optical Guide", Appl. Phys. Lett. **35** , pp 513-516 (1979).

17. W.T. Tsang, and R. Logan, "GaAs-$Al_xGa_{1-x}As$ Strip Buried Heterostructure Lasers", IEEE J. Quantum Electron. **QE-15** , pp 451-469 (1979).

Chapter II

Lasers with Micro-cleaved Mirrors

2.1 Introduction

The conventional method of obtaining optical feedback in a semiconductor laser is to cleave opposite facets of the substrate. Although this provides nearly perfect mirror surfaces, this method is undesirable for many applications. For the fabrication of optoelectronic integrated circuits (OEICs), it is necessary to be able to fabricate lasers on relatively large substrates so that there is sufficient area for fabricating other optoelectronic devices. If opposite cleaved facets of the substrate are used as mirrors then the number of optoelectronic devices that can be integrated onto the chip with the laser is severely restricted by the laser cavity length, which is typically 300 μm. For other applications, it is desirable to fabricate lasers with very short cavity lengths. However, it is difficult to fabricate lasers with cavity lengths less than 100 μm by cleaving through the substrate.

In this chapter, a new fabrication process is described in which laser mirrors are cleaved without cleaving through the substrate. These lasers, which will be referred to as having micro-cleaved mirrors, have threshold currents and differential quantum efficiencies which are essentially identical to those of lasers with conventionally cleaved mirrors. However, this process makes possible the fabrication of lasers on substrates which are not limited by the laser cavity length. These lasers can therefore be fabricated on large area substrates which makes possible the integration of many electronic devices onto the same chip for applications such the integrated optical repeater[1]. Short cavity length lasers can also easily be fabricated using this process.

Many other techniques for fabricating lasers that do not rely upon opposite cleaved facets of the substrate for mirrors have been previously reported. The techniques which have received the most attention are mirrors formed by etching[2] and the use of distributed Bragg reflectors[3]. The difficulty with etched mirrors is due to the fact that any irregularities in the mirror surface must be much smaller than the wavelength of the laser light to obtain a high quality mirror. Using chemical etching it is both difficult to obtain vertical surfaces and almost impossible to reduce the irregularities to sizes small compared to the wavelength of light, due to limitations in the photolithographic processes involved. Reactive ion etching[4] is an alternative which gives vertical surfaces, but the irregularities tend to be even larger than is the case for chemical etching. Similar technical problems are involved in the fabrication of lasers with distributed Bragg reflectors. Irregularities in the reflectors result in unwanted scattering of the laser light. Other techniques for fabricating lasers that do not rely upon opposite cleaved facets of the substrate for mirrors include lasers with grown mirrors[5], lasers with ion milled mirrors[6], and lasers with curved cavities having mirrors on the same cleaved facet or on a cleaved corner[7]. For all of these approaches, the resulting lasers have been found to have significantly higher threshold currents and significantly lower quantum efficiencies than lasers with conventionally cleaved mirrors.

2.2 Fabrication of Lasers with Micro-cleaved Mirrors

The basic approach to obtaining micro-cleaved mirrors is to selectively etch underneath the double heterostructure, leaving a cantilever structure as is shown in figure 1. This thin cantilever of GaAs-AlGaAs is quite fragile and will easily break when subjected to mechanical stress. The idea of micro-cleavage is to break this cantilever in such a way as to produce a high quality cleaved

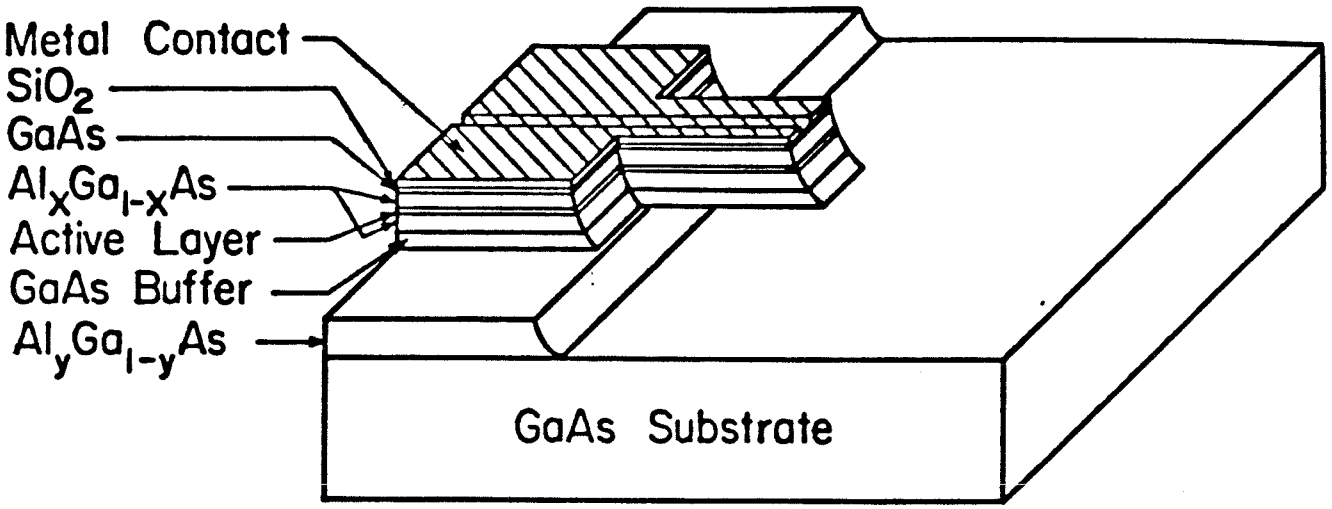

Fig. 1 Schematic diagram of a cantilever prior to micro-cleavage

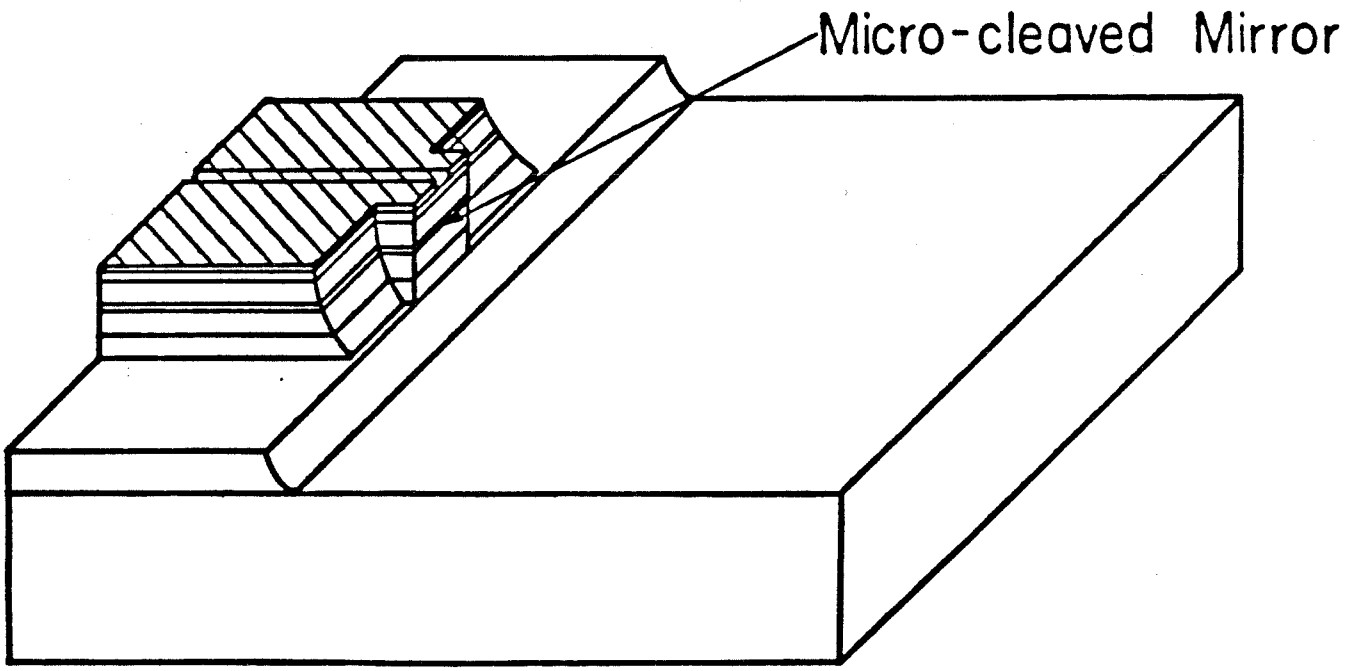

Fig. 2 Schematic diagram of a laser with a micro-cleaved mirror

mirror. It was found that ultrasonic vibrations were a particularly convenient way in which to cleave the cantilevers. By using ultrasonic vibrations, all the mirrors on a wafer can be cleaved simultaneously, making the process of micro-cleavage well suited to batch processing. Microcleavage enables the fabrication of lasers with cleaved mirrors on a chip which is not restricted in size by the laser cavity length, as is shown in fig. 2. The remaining area of the chip can then contain other optoelectronic devices.

The method used to fabricate the lasers described in this chapter was to grow the double heterostructure on top of a layer of $Al_yGa_{1-y}As$ of high aluminum content and to subsequently selectively etch this layer. The etchant that was used to etch the high aluminum content layer was concentrated HCl. Concentrated HCl at room temperature will etch layers with aluminum concentrations greater than 0.6 without significantly attacking the other AlGaAs layers. For y=0.8 the etch rate was approximately 1.5μm/min. To obtain the structure shown in fig. 1, 25 μm wide channels were first etched down to the $Al_yGa_{1-y}As$ layer using a nonselective etch H_2SO_4:H_2O_2:H_2O (1:8:8). The high aluminum content layer was then selectively etched in HCl until the double heterostructure was undercut by 20-25 μm. Next 1:8:8 was used to form a series of 20 μm cantilevers from the overhanging double heterostructure. This sequence of etching steps is illustrated in fig. 3. Figure 4 shows a scanning electron microscope (SEM) photograph of a cantilever prior to micro-cleavage. The cantilevers were then cleaved using ultrasonic vibrations. Figure 5 is an SEM photograph of a micro-cleaved mirror. Micro-cleavages were typically found to have small terraces (< 100 Å), but these terraces did not significantly affect the performance of the lasers.

Oxide stripe lasers with 7 μm wide stripes were fabricated with micro-cleaved mirrors. For 150 μm laser cavity lengths, threshold currents for devices with

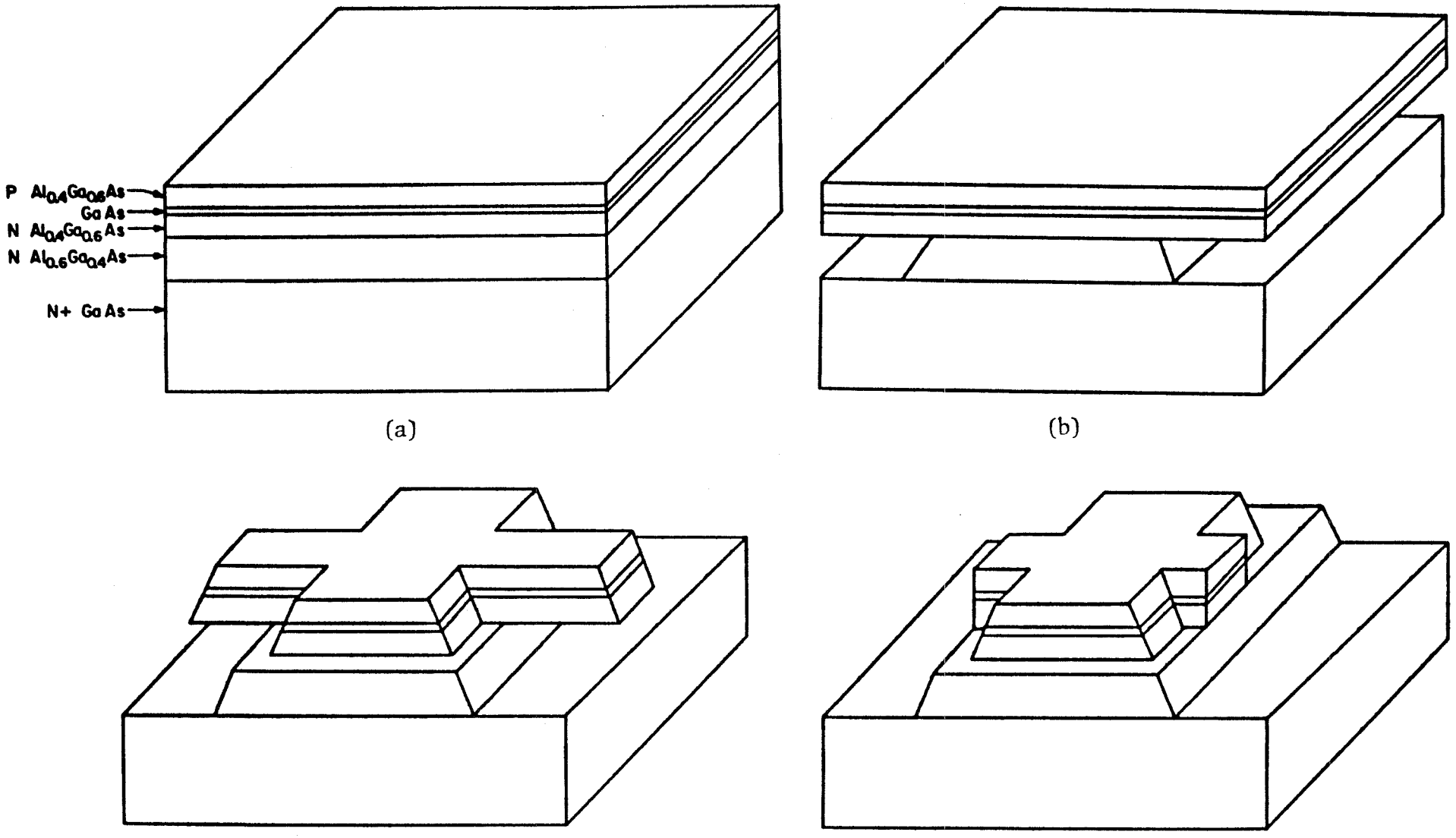

Fig. 3 Processing steps in the fabrication of micro-cleaved mirrors
a) Layers grown for lasers with micro-cleaved mirrors
b) Structure after selective etching of high aluminum content layer
c) Structure after etching of cantilevers
d) Structure after cantilevers have been micro-cleaved

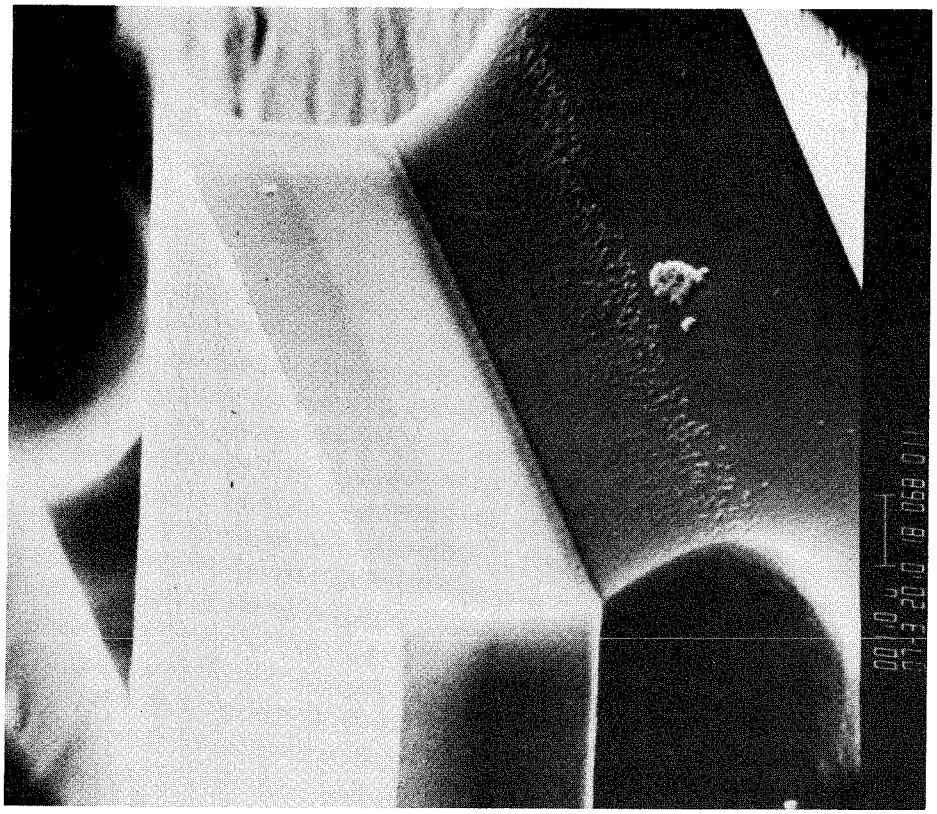

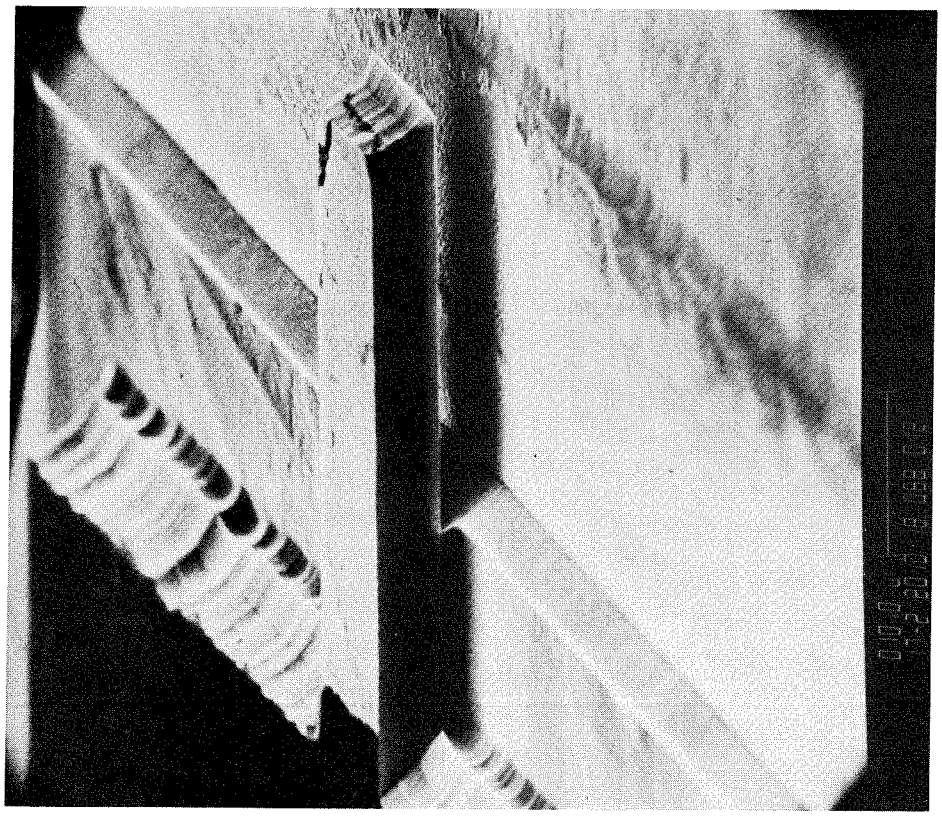

either two micro-cleaved mirrors or one micro-cleaved and one conventionally cleaved mirror were 80-120 mA. The differential quantum efficiencies were typically 15-20% per facet. Results obtained for lasers having micro-cleaved mirrors were no different from the results obtained for lasers of identical structure having conventionally cleaved mirrors.

After being subjected to ultrasonic vibrations, approximately 50% of the cantilevers cleaved properly. The main reason for failure of some of the cantilevers to cleave satisfactorily can be attributed to irregularities in the undercut edge. When the edge of an undercut was parallel to the cleavage plane, the cantilevers almost always cleaved properly.

There are undoubtedly many other approaches to obtaining micro-cleaved mirrors. For instance the position of the cleave can probably be determined by scribing the top surface of the cantilever rather than relying on the edge of the undercut. It is also possible to form double heterostructure cantilevers without growing an AlGaAs layer of high aluminum content. In this case the double heterostructure is undercut by selectively etching the GaAs substrate with H_2O_2 (pH=7). Micro-cleaved mirrors have also been fabricated in this case although the yield was not as good as the case in which a high aluminum content layer was used.

2.3 Optoelectronic Integrated Circuits

One of the major areas of application of lasers with micro-cleaved mirrors is for optoelectronic integrated circuits (OEICs), because micro-cleavage eliminates the restriction of the chip size to the laser cavity length. The fundamental requirements of OEICs are a material system and fabrication technology capable of integrating light sources, detectors, and electronic devices onto a single chip. The ternary system (AlGa)As best meets these requirements,

at the present time. This system has the following properties:

1. The ternary (AlGa)As is very nearly lattice matched to GaAs over the entire alloy composition range.

2. The alloy has a direct bandgap over the range from GaAs (E_g=1.43eV) to $Al_{.45}Ga_{.55}As$ (E_g=1.95eV). Properties 1 and 2 are essential requirements for the fabrication of efficient light sources and matching detectors for the wavelength range of 0.7 μm to 0.88 μm.

3. Semi-insulating substrates, which are doped with Cr are readily available. This facilitates isolation of electronic devices and reduces parasitic capacitances in integrated electronic circuits improving the high frequency characteristics.

Because of these properties well developed technologies have evolved for the fabrication of electronic and optical devices in this material system. However, they have evolved almost completely independent of one another and are therefore in many instances not compatible with one another. Micro-cleavage enables the elimination of one of the major areas of imcompatibility, namely the restriction of the chip size to the laser cavity length for lasers with conventionally cleaved mirrors. Elimination of this restriction enables OEICs such as the hypothetical chip shown in figure 6. In this chip a detector has been integrated with the laser to monitor the light output of the laser, a V-groove has been etched to align a fiber to the laser, and space remains for electronic circuits such as a multiplexor and laser driving circuitry.

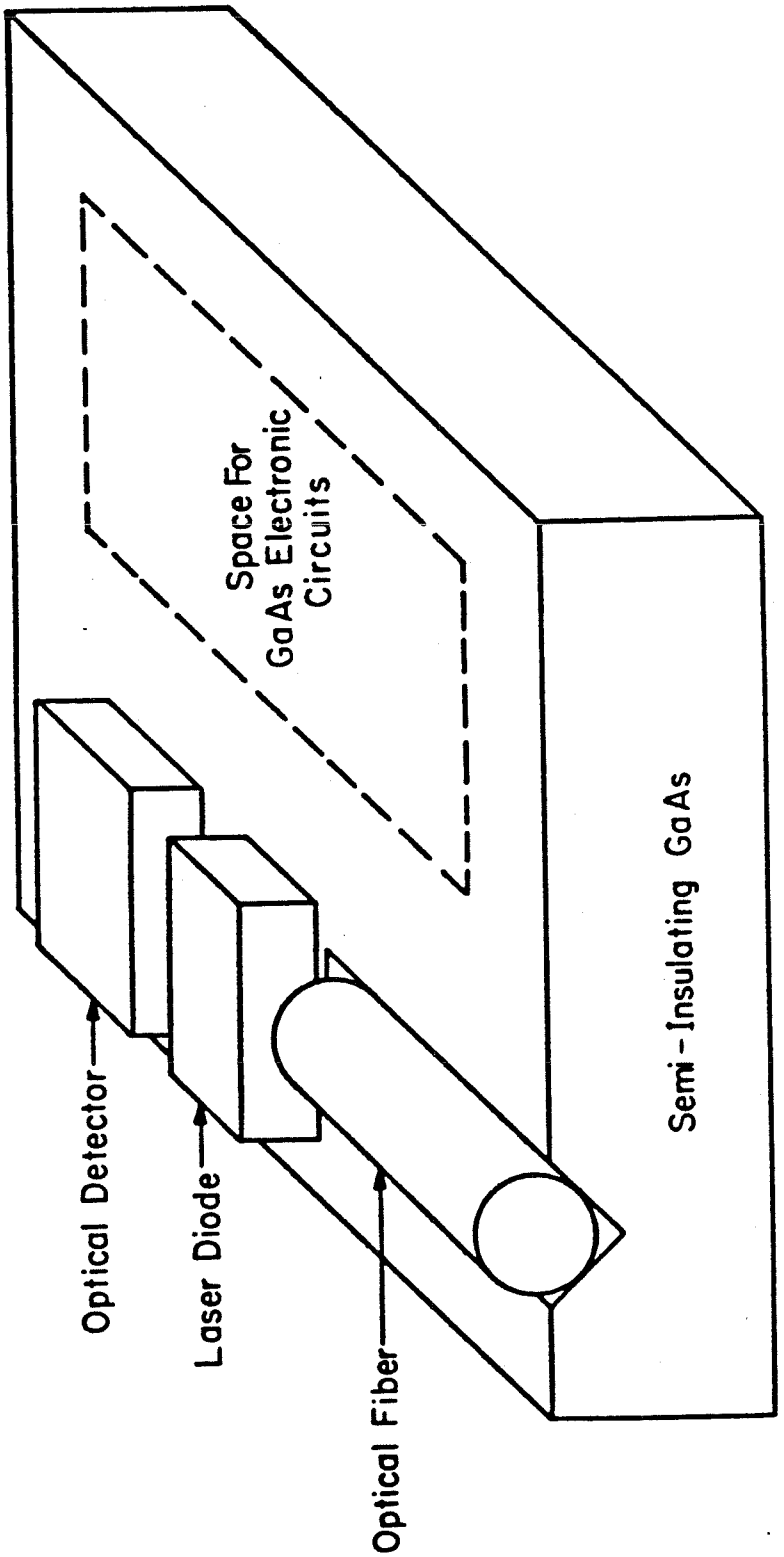

Fig. 6 Hypothetical optoelectronic integrated circuit incorporating a laser with a micro-cleaved mirror.

2.4 Short Cavity Lasers

When laser mirrors are fabricated by the conventional method of cleaving through the substrate it is difficult to fabricate lasers with cavity lengths less than 100 μm. Chips of such small dimension are also very difficult to handle for mounting on heat sinks. However, using micro-cleavage very short cavity lengths can be easily obtained without encountering the difficulties associated with small chips. Laser cavity lengths as short as a few microns should be possible using micro-cleavage. Such short cavity lengths are of interest for the fabrication of extremely low threshold lasers and for the fabrication of single frequency lasers.

For some applications of semiconductor laser diodes it is desirable to have the laser operate in a single longitudinal mode. Many index guided laser structures such as the buried heterostructure[8] and the transverse junction stripe[9] lasers operate in a single longitudinal mode for intermediate power levels. However, at both low and high power output levels and during high frequency modulation most lasers tend to exhibit multi-longitudinal mode operation. The number of longitudinal modes is usually small, even in extreme operating conditions, with the total bandwidth generally being less than 10 Å. The spacing between longitudinal modes of a laser diode is given by

$$\delta\lambda = \frac{\lambda}{2L\left[\frac{n_{eff}}{\lambda} - \frac{dn_{eff}}{d\lambda}\right]} \qquad (6.1)$$

where n_{eff} is the effective index of the transverse mode and L is the laser cavity length. For GaAs active layers with λ=8800 Å , reducing the cavity length to 50 μm will increase the longitudinal mode spacing to $\delta\lambda \approx$ 15Å. With such large mode spacings longitudinal mode operation might be expected even for extreme operating conditions.

The second area of application for short cavity length lasers is low threshold current lasers. The threshold current density of a GaAs laser diode[10] can be expressed as:

$$J_{th}(A/cm^2)=4.5x10^3 d/\eta+(20d/\eta\Gamma)[\alpha_i+(1/L)\ln(1/R)] \qquad (6.2)$$

where d is the active layer thickness in microns, η is the internal efficiency, Γ is the confinement factor, α_i is the sum of the internal losses, L is the laser cavity length, and R is the mirror reflectivity. The first term of (6.2) represents the current density which is required to pump the active layer to transparency and the second term is the additional current required to provide gain to compensate for the internal and mirror losses. The threshold current density versus laser cavity length is plotted in figure 7 for various mirror reflectivities. Uncoated laser facets have reflectivities of approximately 32%, but reflectivities as high as 81% have been reported for facets coated with a six layer Al_2O_3 /Si coating[11]. Recently, short cavity length buried heterostructure lasers with micro-cleaved lasers have been fabricated by Levine et al[12] at the Bell Laboratories following the technique just described, which was developed at Cal Tech. For laser cavity lengths of 40 μm threshold current as low as 7 mA were achieved. As can seen from fig. 7, for a laser cavity length of 40 μm, significant reductions in the threshold current can be expected by increasing the mirror reflectivity. Thus, much lower threshold currents, perhaps less than 1 mA, should be possible for micro-cleaved lasers. The lower limit to the threshold currents that are achievable with short cavity lasers will ultimately be determined by the mirror reflectivities that can be achieved. The threshold current of a GaAs laser will decrease in proportion to the cavity length, if the mirror reflectivity is adjusted so as to keep $(\frac{1}{L})\ln(\frac{1}{R})$ a constant. Short cavity length lasers with mirrror reflectivities of 80% ($\ln(\frac{1}{R}) = 0.22$) can therefore be

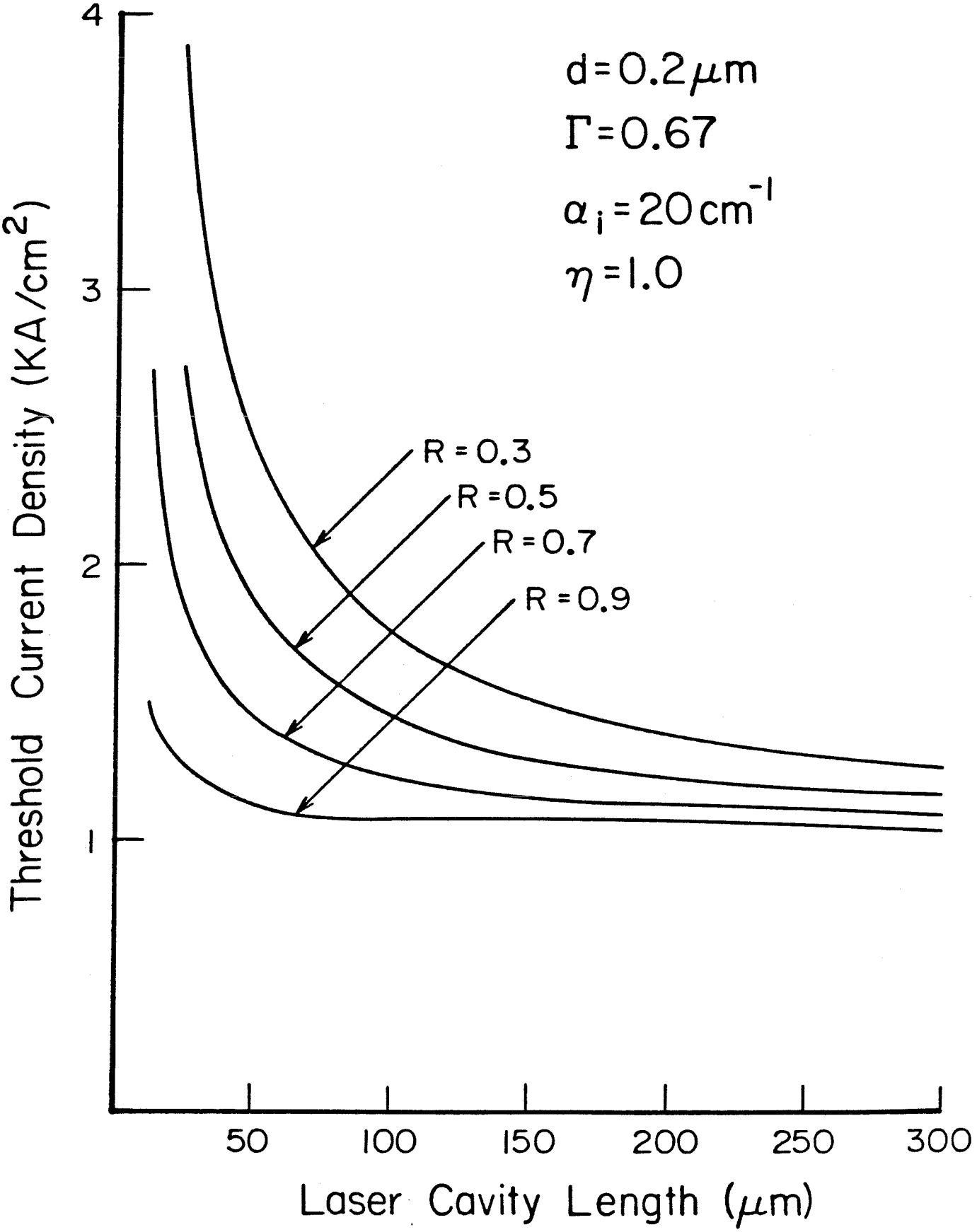

Fig. 7 Calculated threshold current vs. laser cavity length

expected to have threshold currents that are approximately 5 times lower than lasers with mirror reflectivities of 32% ($\ln(\frac{1}{R}) = 1.14$). Improvements in the fabrication of high reflectivity laser diode mirrors could result in even further reductions in the threshold currents.

In conclusion, lasers with micro-cleaved mirrors have been fabricated which have threshold currents and quantum efficiencies which are comparable to those of lasers with conventionally cleaved mirrors. The technique of micro-cleavage makes possible the fabrication of lasers on substrates which are not restricted in size to the laser cavity length. Very short cavity length lasers which have the potential for both very stable single longitudinal mode operation and very low threshold currents, can also be fabricated using the technique of micro-cleavage. Finally, the technique has the advantage of allowing the simultaneous formation of all of the mirrors on a wafer, making this technique desirable for the batch processing of lasers.

References for Chapter II

1. M. Yust, N. Bar-Chaim, S.H. Izadpanah, S. Margalit, I. Ury, D. Wilt, and A. Yariv, "A Monolithically Integrated Optical Repeater", Appl. Phys. Lett. **35** , pp 795-797 (1979).

2. J.L. Merz and R.A. Logan "Integrated GaAs-$Al_xGa_{1-x}As$ Injection Lasers and Detectors with Etched Reflectors", Appl. Phys. Lett. **30** , pp 530-533 (1977).

3. W. Ng, H.W. Yen, A. Katzir, I. Samid, and A. Yariv, "Room Temperature Operation of GaAs Bragg-Mirror Lasers", Appl. Phys. Lett. **29** , pp 684-686 (1976).

4. E.L. Hu and R.E. Howard "Reactive Ion Etching of GaAs and InP Using $CCl_2F_2/Ar/O_2$", Appl. Phys. Lett. **37** , pp 1022-1024 (1980).

5. F.A. Blum, K.L. Lawley, and W.C. Holton, "Monolithic $Ga_{1-x}In_xAs$ Mesa Lasers with Grown Optical Facets", J. Appl. Phys. **46** , pp 2605-2611 (1975).

6. Y. Suematsu, M. Yamada, and K. Hatashi, "A Multi-Hetero-AlGaAs Laser with Integrated Twin Guide", Proc. IEEE **63** , p 208 (1975).

7. I. Ury, S. Margalit, N. Barchaim, M. Yust, D. Wilt, and A. Yariv "Whispering Gallery Lasers on Semi-Insulating GaAs Substrates", Appl. Phys. Lett. **36** , pp 629-631 (1980).

8. K. Saito, R. Ito, "Buried Heterostructure AlGaAs Lasers" IEEE J. Quantum Electron. **JQE-16** ,pp 205-215 (1980).

9. H. Kumabe, T. Tanaka, H. Namizaki, M. Ishii, and W. Susaki, "High Temperature Single Mode CW Operation with a Junction Up TJS Laser", Appl.Phys. Lett. **33** , pp 38-40.

10. H.C. Casey, and M.B. Panish *Heterostructure Lasers*, chapter 7, Academic Press, New York 1978.

11. M. Ettenberg, D Botez, D. Gilbert, J. Connolly, H.V. Kowger, The Effect of Facet Reflectivity on the Spectrum of Single-Mode CW Constricted Double-Heterojunction Diode Lasers", IEEE J. Quantum Electron. **QE-17** , pp 2211-2214 (1981).

12. B. Levine, J.P. Van Der Ziel, R. Logan, C.G. Bethea, 'High Quantum Efficiency Low Threshold Micro-cleaved $Al_xGa_{1-x}As$ Lasers", Electron. Lett. **18** , pp 690-691 (1982).

Chapter III

High Power Single Mode AlGaAs Lasers

3.1 Introduction

Designing and fabricating high power single mode AlGaAs lasers consists primarily of identifying the factors that limit the output power of AlGaAs lasers, and when possible, altering the design to avoid these limitations. Many factors can influence the reliability of a laser in long term operation. However, for short term operation, the output power of an AlGaAs laser is usually limited by either catastrophic optical mirror damage (COMD) or heating.

The active layer of an AlGaAs laser is typically absorbing in the immediate vicinity of the mirrors due to non-radiative surface recombination of carriers at the mirrors. The interface between GaAs and air contains a large density of surface states at the cleaved mirror facets. Absorption of laser light by the end sections results in the heating of the active layer near the mirrors which makes these sections even more absorbing. Above a critical optical power density, thermal runaway results, causing the active layer to melt at the mirrors. The catastrophic optical mirror damage occurs at a threshold intensity of approximately 15 $mW/\mu m^2$ for CW operation and 70 $mW/\mu m^2$ for 100 nsec. pulses[1]. However, it is possible to avoid COMD by fabricating "window" lasers in which the active layers are terminated short of the mirror facets. These lasers have window sections located at the mirrors which are transparent to the laser light. A technique for fabricating window lasers, first demonstrated by Yonezu et al.[2] consists of diffusing zinc into the active layer everywhere except near the mirrors. The zinc diffusion reduces the bandgap of the active layer shifting the laser output to a longer wavelength which is not absorbed in the active layer near the mirrors, where no zinc diffusion takes place. Using this technique the available pulsed output power from a stripe geometry laser has been increased

by a factor of 10. A second technique, which was developed at Caltech involves eliminating, by selective etching, the active layer in the vicinity of the mirrors[3]. In this case, only transparent AlGaAs layers extend to the laser mirrors. These two types of window lasers are shown in fig. 1.

The selectively etched window laser structure, fabricated in the process of the research reported here, consists of a 200 μm long center active section, and two 25 μm long passive window sections in which the active layer has been removed by selective etching. The optical power is mostly contained in the $Al_{.22}Ga_{.78}As$ optical guide layer in both the active and window sections. This enables low loss coupling of the laser light between the sections. This approach has been used to fabricate buried heterostructure window lasers[3] which have threshold currents and quantum efficiencies which are nearly identical to those of conventional buried heterostructure lasers, but can be operated without degradation at pulsed power outputs up to three times the catastrophic damage threshold of otherwise identical lasers without windows. The power output was limited by heating of the laser during the pulse. By improving the thermal properties of these lasers, still higher power outputs can be expected. This laser will be discussed in more detail in chapter 4.

The second important factor for high power operation is designing lasers to minimize the heating of the laser under high power operation. The power dissipation of a laser can be expressed as follows

$$P_{dis} = I^2R_s + IV_j - P_{out} \qquad (3.1\text{-}1)$$

$$= I^2R_s + IV_j - \eta(I - I_{th})(E_g/q) \qquad (3.1\text{-}2)$$

where R_s is the series resistance(primarily contact resistance), V_j is the junction voltage, η is the differential quantum efficiency, I_{th} is the threshold current, E_g is

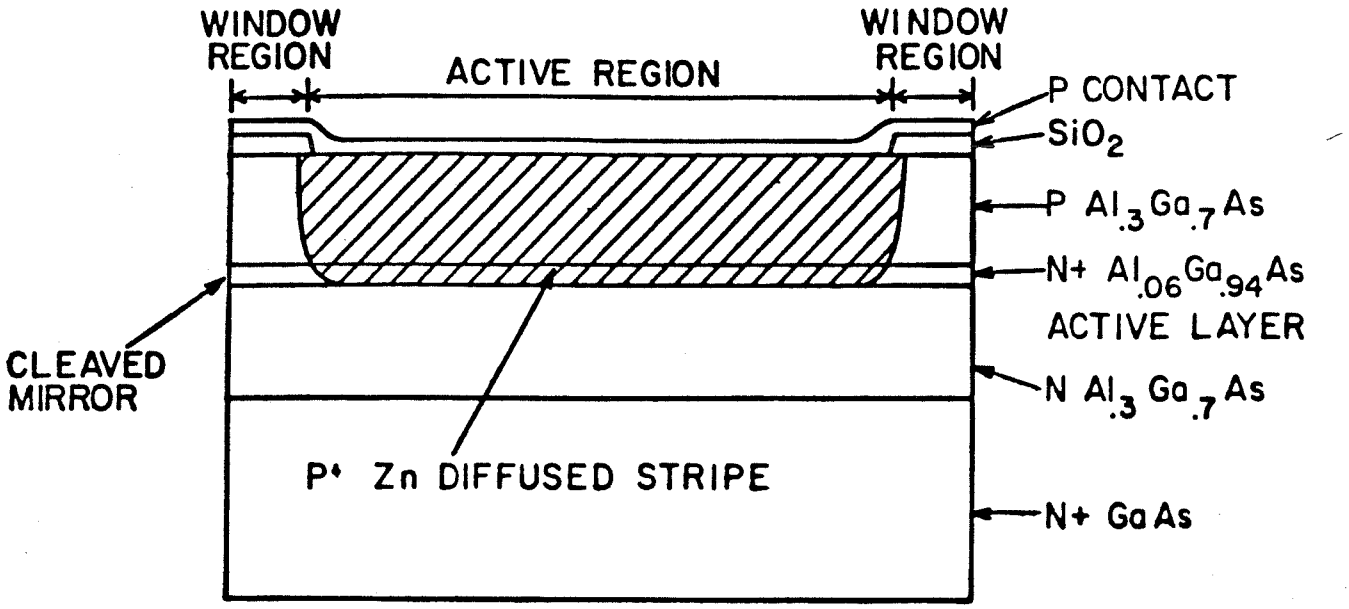

fig 1 a) Zinc diffused window laser

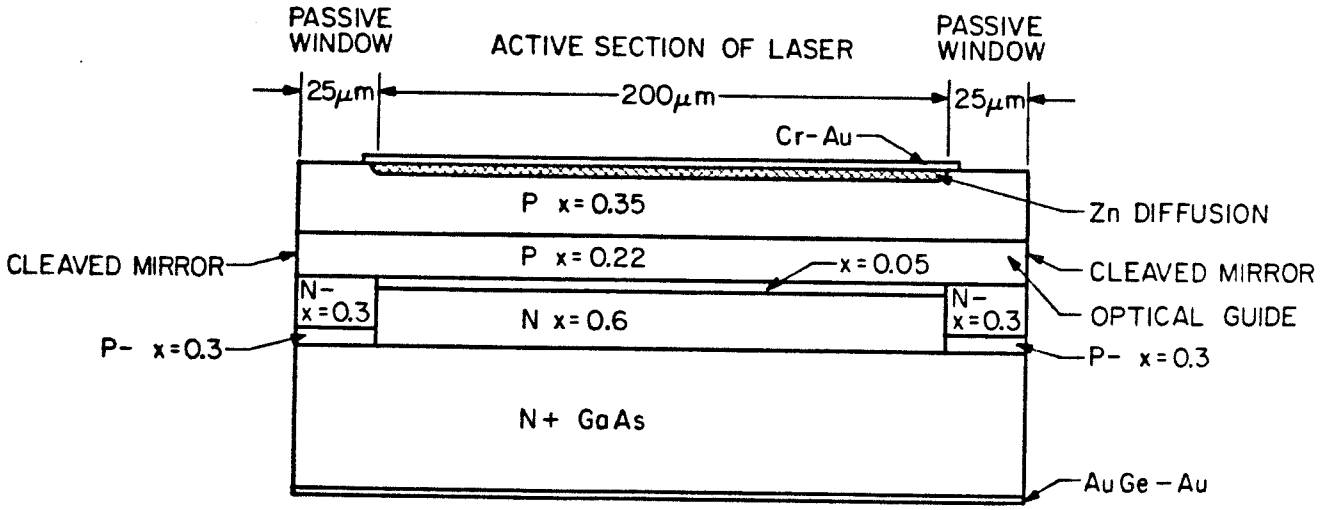

Fig. 1b Selectively etched window laser

the bandgap, and q is the electron charge. A more relevant property, especially for high power operation, where the temperature rise of the active layer is significant, is the power dissipation per unit area.

$$P_{dis}/Area = J^2R_c + JV_j - \eta(J-J_{th})(E_g/q) \qquad (3.1\text{-}3)$$

where R_c is the specific contact resistance in $\Omega - cm^2$ and J is the current density in A/cm^2. To minimize power dissipation per unit area a laser should have a low J_{th}, large η, and small R_c. The threshold current densities and quantum efficiencies of most laser structures are relatively insensitive to the stripe width. Increasing stripe width is therefore an effective way of increasing the power output of a laser without increasing the power dissipation per unit area. Increasing the stripe width also increases the catastrophic optical damage threshold. The difficulty is in obtaining stable fundamental mode operation for wide stripes, stable meaning that the beam profile does not change as the power level is increased.

3.2 Mode Control of Semiconductor Lasers

The spatial mode properties of semiconductor lasers can be divided into two categories:

I. Spatial Mode at Low Output Powers

II. Stability of the Spatial Mode as the Laser Power is Increased

For example consider the buried optical guide (BOG) laser developed by Chinone et al[4] which is shown in fig 2. This laser has the following spatial mode characteristics:

1. For stripe widths less than 2-3 μm the laser operates in the fundamental lateral spatial mode and the output is stable as the power is increased.

2. As the stripe width is increased up to 5 μm the lasers continue to operate

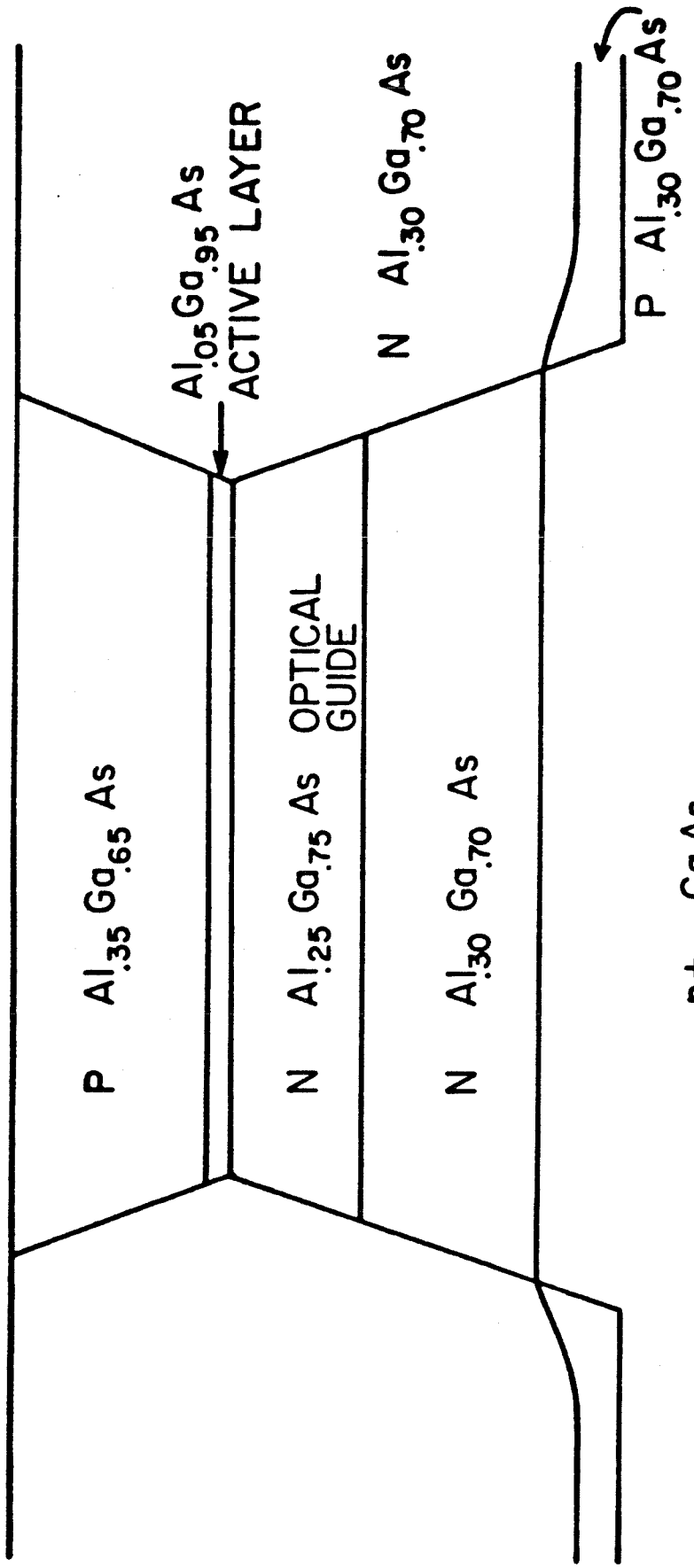

Fig. 2 Cross section of a buried optical guide laser

stably, but in successively higher order spatial modes.

3. Above 5 μm stripe widths the laser operates in higher order modes and the beam profile is not stable as the power is increased.

The spatial mode at the onset of lasing is the mode which reaches the threshold condition first, the threshold condition being that the round trip gain inside the cavity equals the round trip loss.

for

$$e^{-i\beta_m z} \qquad z \text{ dependence of the laser field}$$

the threshold condition can be written as

$$\text{Power gain of mode m} = 2\text{Im}\{\beta_m\} = \alpha_{im} + (\frac{1}{L})\ln(\frac{1}{R_m}) \qquad (3.2\text{-}1)$$

where

$$\text{Im}\{\beta_m\} = (\frac{k_o^2}{\beta_m}) \frac{\int \text{Im}\{n^2\}|E_m|^2}{\int |E_m|^2} \qquad (3.2\text{-}2)$$

α_{im}= internal losses of mode m

R_m= reflectivity of mode m

To obtain stable fundamental mode operation it is therefore necessary to have only the fundamental mode reach the threshold condition. Because the fundamental mode is best confined to the gain region, the mode gain of the fundamental mode is generally higher than any other spatial mode, at least at low output power levels. At high output power levels spatial hole burning[5,6] can distort the gain profile in such a way that higher order modes can have mode gains exceeding that of the fundamental mode. The simplest approach to mode control is to obtain a preference for the fundamental spatial mode by designing

the laser structure so that the fundamental mode has a significantly larger gain than the higher order modes. This is done by designing waveguides in which the fundamental mode is significantly better matched to the gain than are any of the other modes. The simplest way to do this is to have weak lateral waveguiding so that the there is only one guided spatial mode or if the waveguide supports more than one mode, so that the higher order modes have much lower confinement factors than that of the fundamental mode. The confinement factor of a semiconductor laser waveguide is defined to be the fraction of the optical power that is propagating in the active layer where there is gain. For instance the lateral waveguiding in a strip buried heterostructure laser is weaker than that of a conventional buried heterostructure laser. This is why the strip BH lasers developed by Tsang and Logan[7] can be operated in the fundamental mode for active layer widths up to 5 μm (see discussion in chapter 5). Inverted strip BH lasers which have been developed recently at Caltech[8] also are weakly guiding and fundamental mode operation has been achieved in this case for active layer widths up to 4 μm. The inverted strip BH laser structure which will be discussed in more detail in chapter 5 is shown in fig. 3

A slightly more complicated approach is to cause the gain to possess a nonuniform profile across the active layer. If there is only gain in the middle of the active layer, the fundamental mode will be preferred over the higher order modes since it has relatively more power in the center of the waveguide, and will thus exercise a larger gain. This has been achieved in a buried heterostructure laser to obtain fundamental mode operation for a laser with a 8 μm wide active layer. The structure studied is shown in fig. 4 and will be referred to as a narrow injection buried heterostructure (NIBH) laser. If the active layer of a NIBH laser is much wider than the injecting stripe width, then a NIBH laser is expected to behave like a gain guided stripe laser. If the active layer width is approximately

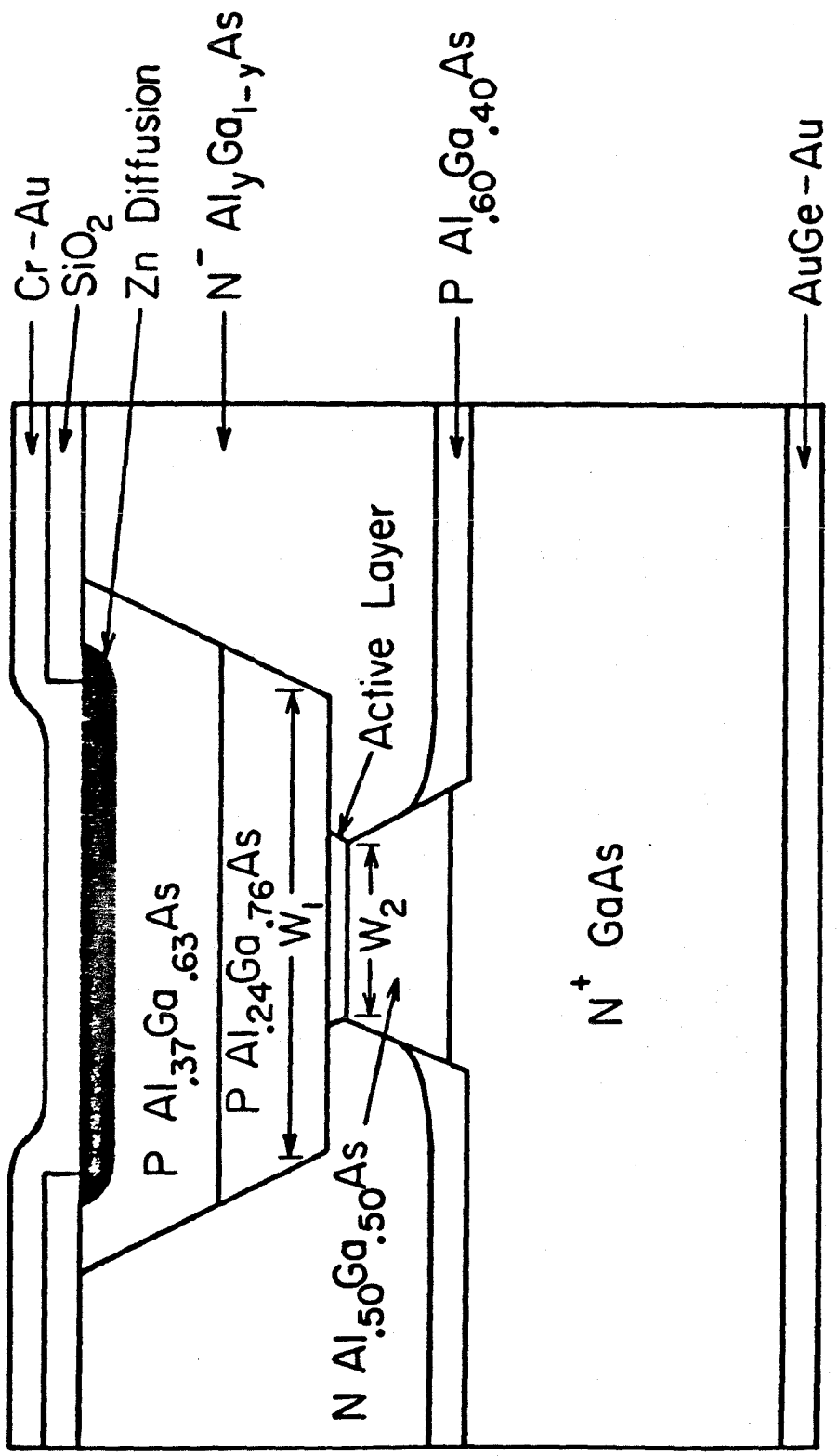

Fig. 3 Cross section of an inverted strip buried heterostructure laser

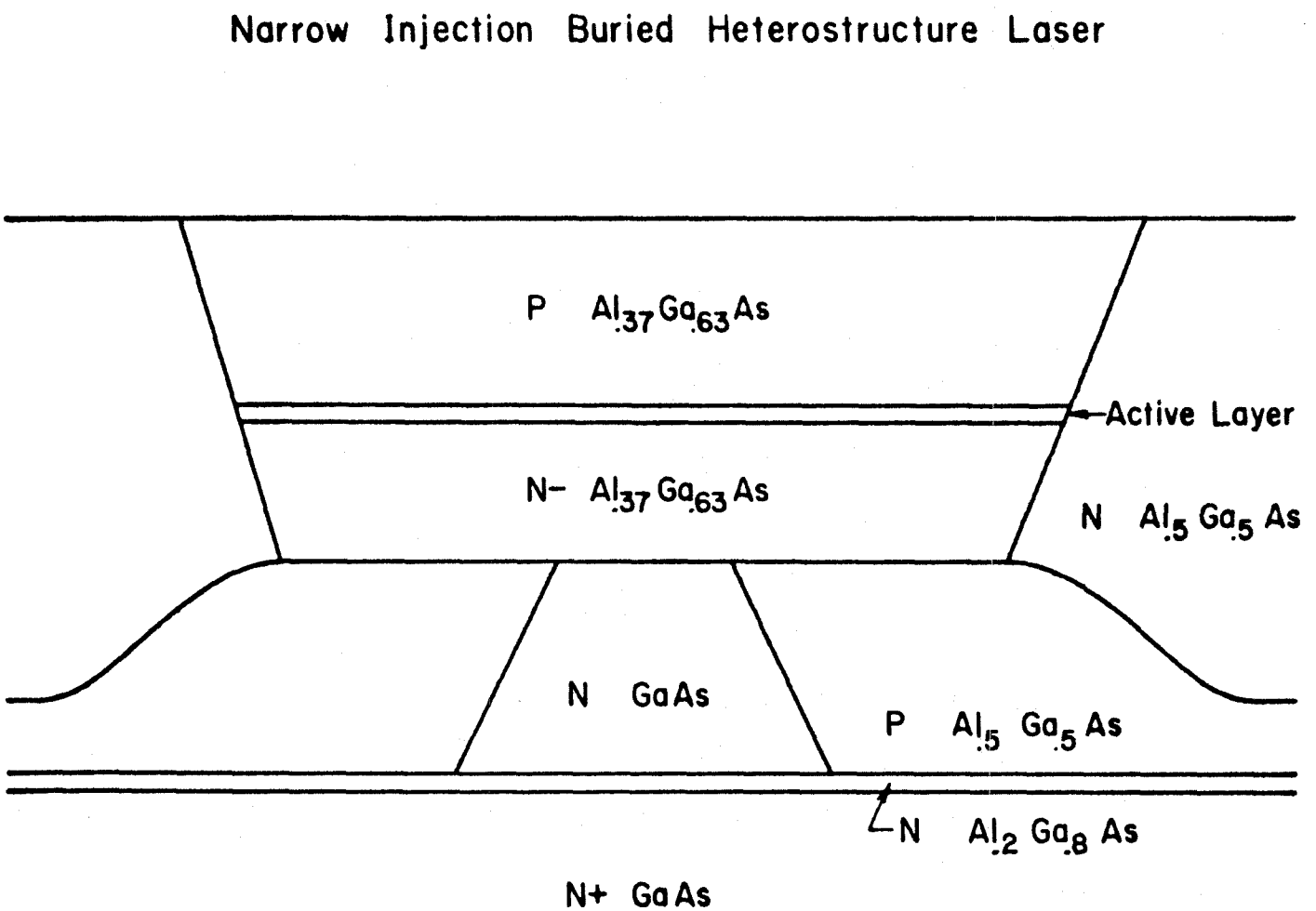

Fig. 4 Cross section of a narrow injection buried heterostructure laser

the same as the injecting stripe width then a NIBH laser should behave like a conventional BH laser. The intermediate case where the active layer is a few microns wider than the injecting stripe width is the most interesting case and will be discussed in more detail in chapter 6.

Mode control can also be achieved by making the internal losses of the higher order modes larger than that of the fundamental. One way to achieve this in semiconductor lasers is to fabricate a leaky wavguide in the lateral direction. Mode control in the high power constricted double heterostructure (CDH) lasers developed by Botez[9] is achieved by incorporating such a leaky waveguide. These lasers have been operated at higher single mode CW power levels than any other laser structure yet developed. The structure has been operated at CW single mode output powers of 40 mW. The output power of the high power CDH laser is limited by heating. The greatest amount of CW single mode power reported from a BH laser to date has been 25 mW[4]. However, the BH lasers are much more efficient than the CDH lasers and the power output has been limited not by heating, but rather by catastrophic mirror damage. Thus incorporation of passive window sections at the mirrors may enable greater single mode output powers from BH lasers than can be obtained from CDH lasers.

The final factor which determines the spatial mode that lases is the mirror reflectivity. Unfortunately, the mode reflectivities of the higher order TE-like modes generally are higher than the mode reflectivity of the fundamental mode. The problem of solving for the mode reflectivity and transmitted power distribution at the boundary between a dielectric slab waveguide and a uniform dielctric medium has been analyzed by several authors[10-14]. The basic approach to solving the problem involves matching the tangential electric and magnetic fields at the boundary. The geometry of the problem is shown below in fig. 5.

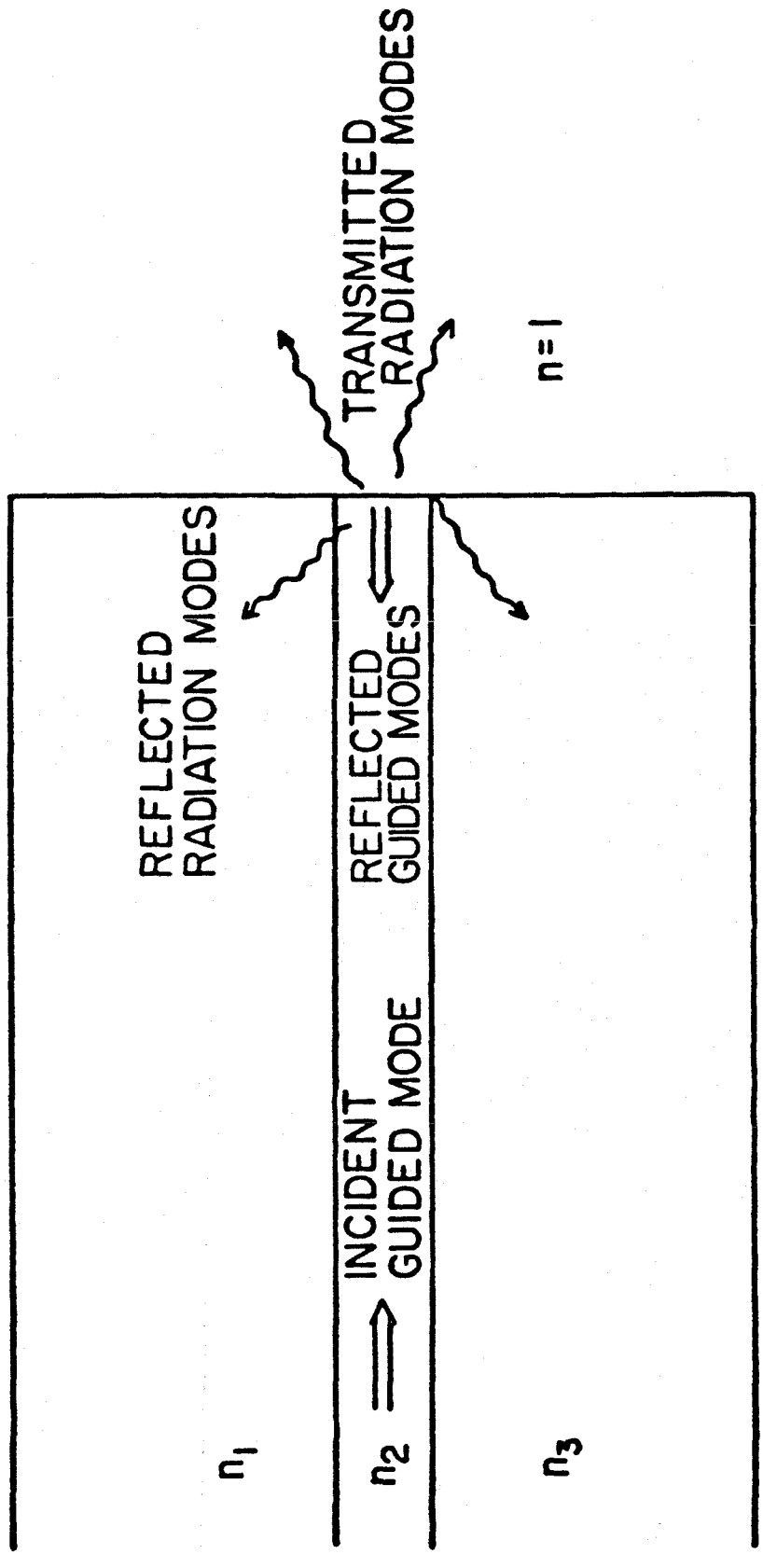

Fig. 5 Transmitted and reflected fields at a cleaved mirror facet

For the problem of calculating the mode reflectivities of laser modes, the solution method must be extended to two dimensional waveguides. Although this makes the calculation more complicated numerically, the extension to two dimensions does not introduce any fundamental difficulties. For simplicity, the spatial modes of the two dimensional waveguides were solved approximately using the effective index method[15-17]. If more precision is required the more rigorous vector variational method[18-20] or the finite element method[22,23] can be used. The effective index method and the vector variational technique will be described in more detail at the end of this chapter.

The mode reflectivities of BH lasers have been calculated following the method used by Gelin etal.[14] to analyze the reflectivities of dielectric slab waveguides. This method uses an iterative approach to converge on the solution for the mode reflectivities and transmitted power distribution. For TE-like modes the dominant field components are E_y and H_x. The requirement that these tangential field components be continuous across the interface can be written as follows.

$$a_i E_i + \sum b_n E_n = \int c(\rho) E(\rho) d\rho \qquad (3.2\text{-}3)$$

$$\beta_i a_i E_i - \sum \beta_n b_n E_n = \int \beta(\rho) c(\rho) E(\rho) d\rho \qquad (3.2\text{-}4)$$

where

a_i = amplitude of the incident mode

b_i = amplitudes of the reflected modes

$c(\rho)$ = amplitude of the transmitted radiation modes (plane waves in this calculation)

β_n = propagation constant of mode n

ρ=transverse propagation constant of the radiation modes

$\beta(\rho) = (k_o^2 - \rho^2)^{1/2}$

$k_o = 2\pi/\lambda$

λ= laser wavelength in free space

and the relation between the tangential electric and magnetic fields has been used.

$$H_x = \frac{-i}{\omega\mu}\frac{\partial E_y}{\partial z} \tag{3.2-5}$$

To calculate the mode reflectivities, zeroth order estimates of b_n are first made. Using these values of b_n, equation (3.2-3) is used to calculate $c(\rho)$. Next using equation (3.2-4) and $c(\rho)$, first order estimates of b_n can be calculated which are then used in equation (3.2-3) to obtain a refined estimate of $c(\rho)$. This process is continued until the desired accuracy is obtained. Typically, 5 iterations are sufficient. Some of the results obtained for BH lasers are shown in fig 6-9.

In fig 6-9, the structure on which the calculations are based is shown in part (a). Part (b) of the figures shows the calculated mirror reflectivities of the four lowest order transverse modes. Part (c) shows the lateral confinement factor of the modes which is defined as

$$\Gamma_{lat} = \frac{\int_{-W/2}^{W/2} |E|^2 dy}{\int_{-\infty}^{\infty} |E|^2 dy} \tag{3.2-6}$$

Assuming the internal losses of all the modes are the same, the spatial mode in which the laser oscillates is determined by the mode reflectivities and the mode confinement factors. Neglecting internal losses, the threshold gain is given by:

$$g_{mth} = \frac{1}{\Gamma_m L} \ln\left(\frac{1}{R_m}\right) \tag{3.2-7}$$

where

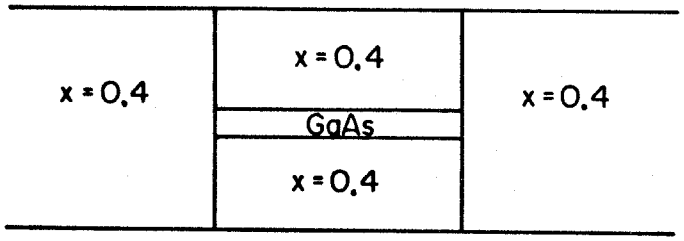

(a)

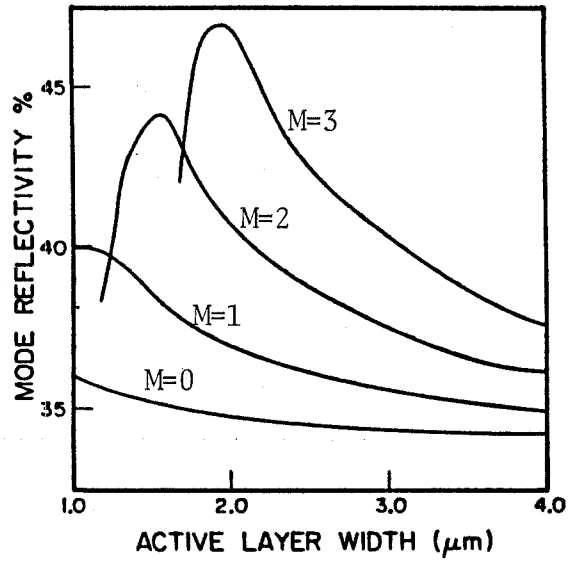

(b)

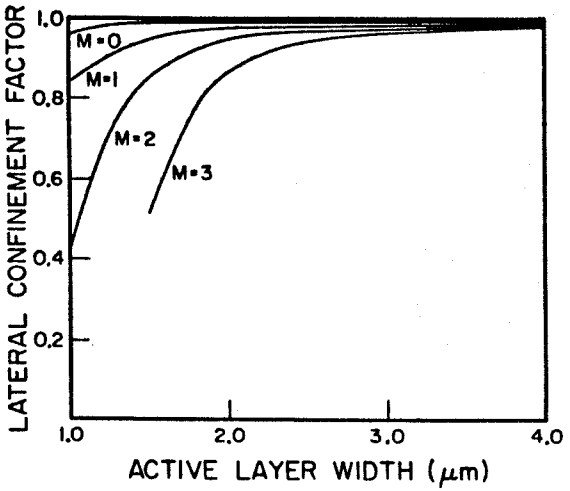

(c)

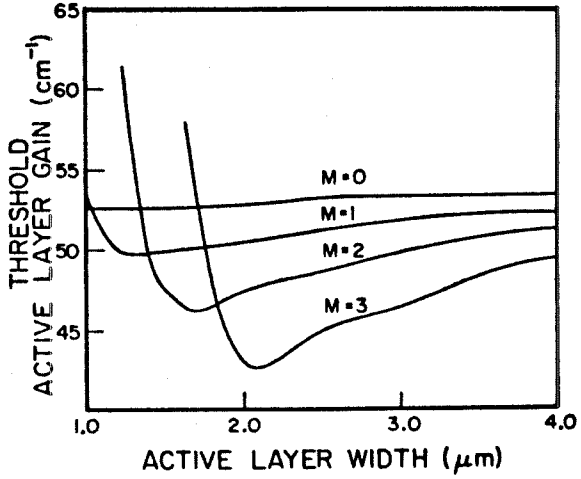

(d)

Fig. 6 a) Cross section of a buried heterostructure laser
b) Mode reflectivities of the transverse modes of a buried heterostructure laser
c) Lateral confinement factor of the transverse modes of a buried heterostructure laser
d) Active layer threshold gain of the transverse modes of a buried heterostructure laser

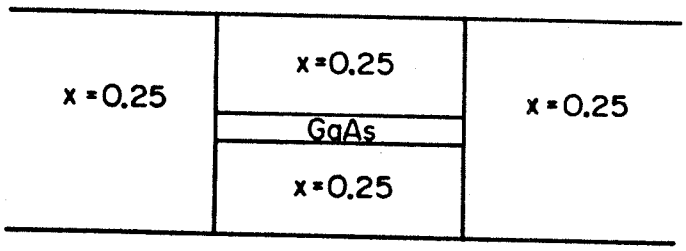

(a)

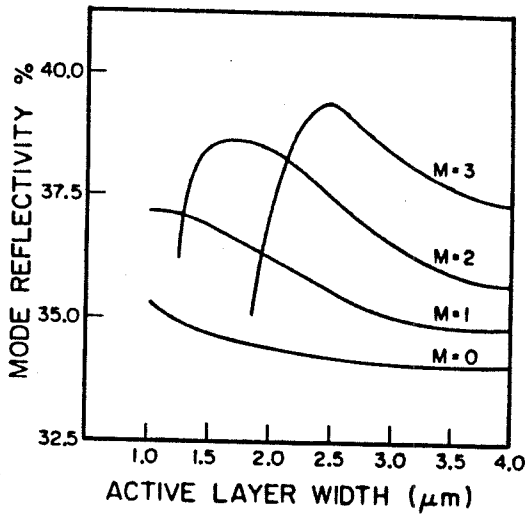

(b)

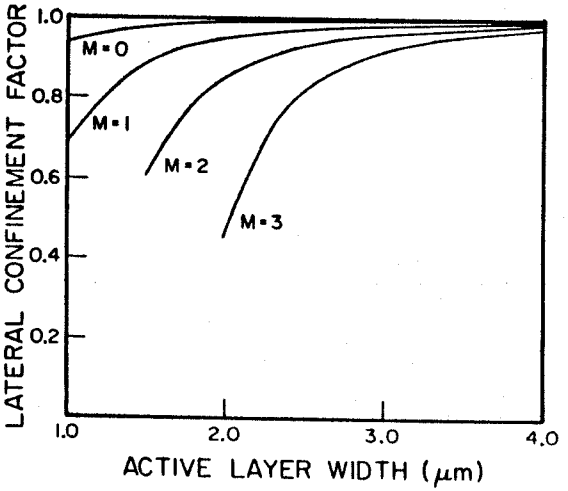

(c)

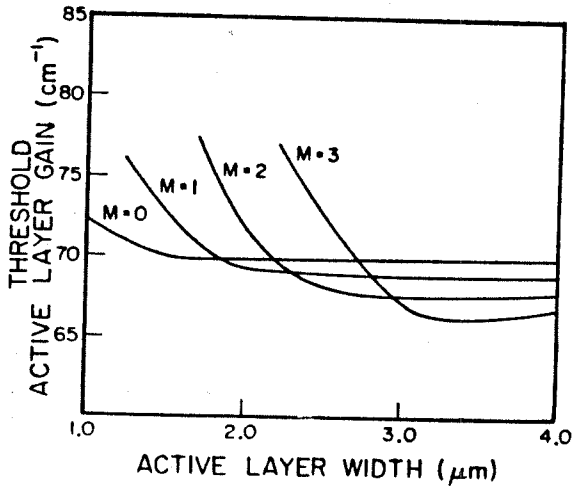

(d)

Fig. 7 a) Cross section of a buried heterostructure laser
b) Mode reflectivities of the transverse modes of a buried heterostructure laser
c) Lateral confinement factor of the transverse modes of a buried heterostructure laser
d) Active layer threshold gain of the transverse modes of a buried heterostructure laser

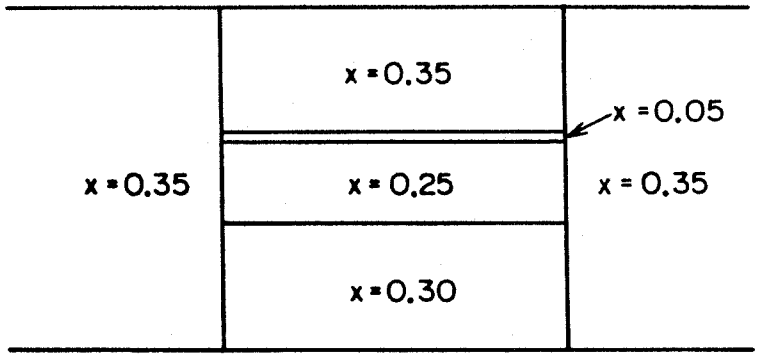

(a)

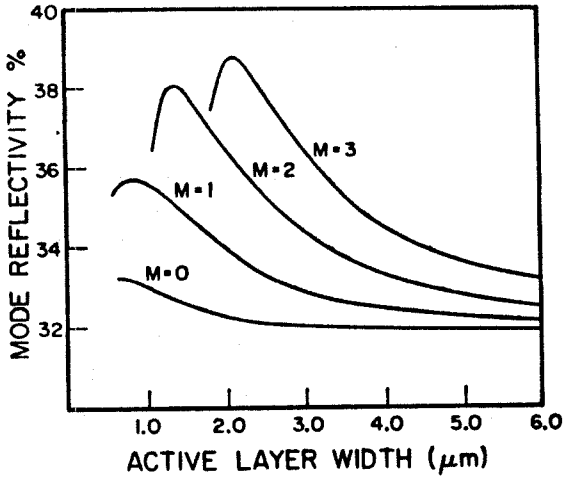

(b)

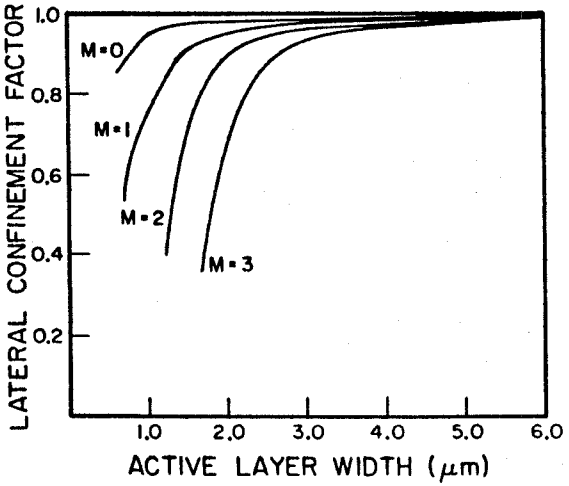

(c)

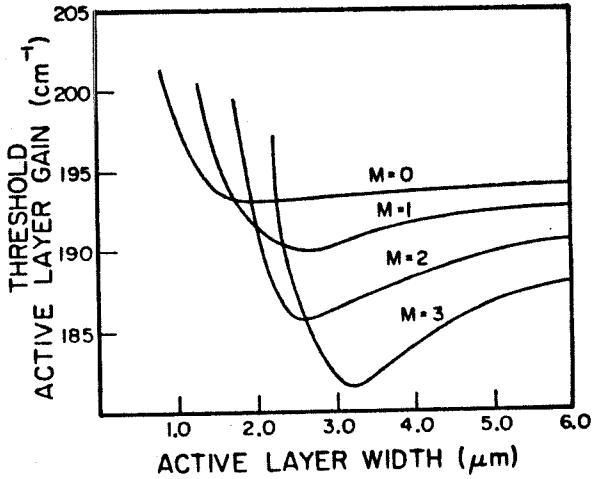

(d)

Fig. 8 a) Cross section of a buried optical guide laser
b) Mode reflectivities of the transverse modes of a buried optical guide laser
c) Lateral confinement factor of the transverse modes of a buried optical guide laser
d) Active layer threshold gain of the transverse modes of a buried optical guide laser

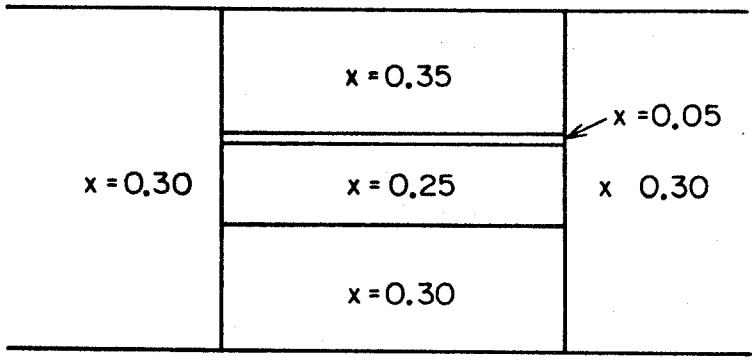

(a)

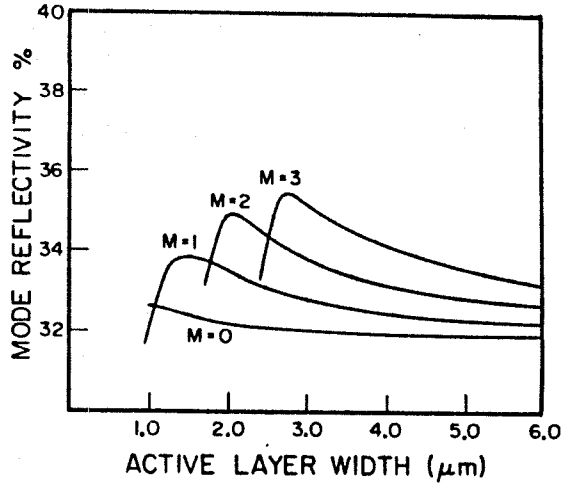

(b)

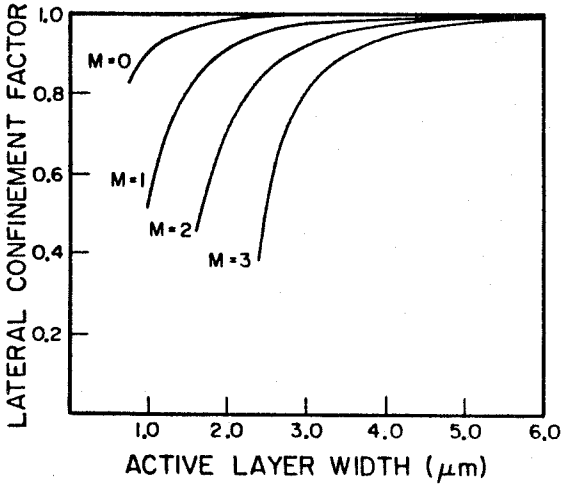

(c)

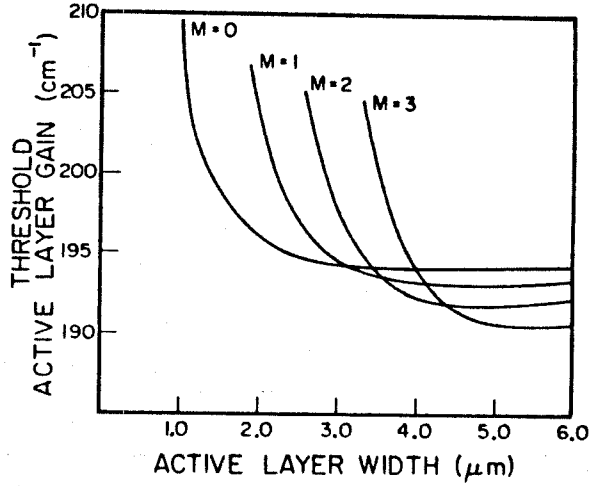

(d)

Fig. 9 a) Cross section of a buried optical guide laser
b) Mode reflectivities of the transverse modes of a buried optical guide laser
c) Lateral confinement factor of the transverse modes of a buried optical guide laser
d) Active layer threshold gain of the transverse modes of a buried optical guide laser

$$\Gamma_m = \frac{\int_{-W/2}^{W/2}\int_{-d/2}^{d/2} |E|^2 dxdy}{\int_{-\infty}^{\infty}\int_{-\infty}^{\infty} |E|^2 dxdy} \qquad (3.2\text{-}8)$$

where

W = Active layer width

d = Active layer thickness

g_{mth} = active layer gain at which mode m reaches threshold

The transverse mode that oscillates is the mode which reaches threshold at the lowest active layer gain. It is almost always desirable to have the laser oscillate in the fundamental mode. For many applications, such as those which require high output powers it is desirable to obtain fundamental mode operation for as wide an active layer (wide emitting area) as possible. In practice, fundamental mode operation is generally achievable in buried heterostructure lasers only for active layer widths less than 1.5-2 microns. Buried optical guide lasers are slightly better , but fundamental mode operation is still typically observed only for active layer widths less than 2-3 microns. This spatial mode behavior is consistent with the results shown in part (d) of fig. 6-9

There are several significant features of these calculated curves of mirror reflectivities. Most significant for understanding the operation of semiconductor lasers is that the higher order modes have greater mode reflectivities than the fundamental mode. Although it is necessary to use an approach such as that outlined above to calculate the mirror reflectivities accurately, these curves can be understood qualitatively by the following simple model. In this model the mirror reflectivities of the spatial modes are obtained by first decomposing the incident mode into plane waves. Each plane wave component is then assumed to be reflected at the laser mirror according to the Fresnel relations for the reflection and transmission of light at an interface between semi-infinite slabs

of uniform index of refraction. This then gives the Fourier transform of the reflected radiation. This in turn can be expanded in terms of the actual modes of the waveguide with the coefficients of this expansion giving the mode reflectivies. The spatial modes of a semiconductor laser structure can be classified as either TE-like (dominant fields E_y and H_x) or TM-like (dominant fields E_x and H_y). The TE-like modes are analogous to plane waves with the polarization perpendicular to the plane of incidence and the TM-like modes are analogous to plane waves with the polarization in the plane of incidence. For plane waves with the polarization perpendicular to the plane of incidence the reflectivity increases as the angle of incidence increases. Based on this result for plane waves, one would expect that the higher order TE-like modes of a semiconductor laser would have larger reflectivities than the lower order modes. This is because if the modes are decomposed into plane waves, a greater fraction of the power of the higher order modes are in the plane waves with large angles of incidence. For the polarization in the plane of incidence the reflectivity at first decreases as the angle of incidence increases, reaching 0 at the Brewster's angle. The reflectivity of plane waves polarized in the plane of incidence is less than or equal to that of the other polarization for all angles of incidence. One would then also expect from this model that semiconductor lasers would oscillate in the TE-like modes because these modes would be expected to have greater reflectivities. This is in fact what is observed.

A second interesting feature of the curves shown in fig 6-9 is the fact that the reflectivity advantage of the higher order modes is more pronounced when the lateral waveguiding is stronger. This can be seen by comparing fig 8 and 9 which are for structures which are otherwise identical except for the aluminum content of the burying layer. The greater the aluminum content the greater is the difference between the index of refraction of the active layer and the

burying layer, and the stronger the lateral waveguiding. In addition, the reflectivities of the four lowest order modes approach one another asymptotically as the stripe width is increased. This would tend to indicate that fundamental mode operation in very wide stripe structures may be possible if the gain is matched best to the fundamental mode, such as was done in the narrow injection buried heterostructure laser (see chapter 6).

3.3 High Power Single Mode Buried Heterostructure Lasers

Buried heterostructure lasers have many characteristics which are desirable for high power single mode lasers. They have low threshold currents, are very efficient, and operate in a single longitudinal mode even at high output power levels and when being modulated. However, until now the power output of BH lasers has been relatively low due to the small emitting area of most BH lasers. In this section, the factors limiting the output power of BH lasers will be examined and some projections will be made as to the ultimate power capabilities of single mode BH lasers.

As mentioned in the beginning of this chapter, the power output of a semiconductor laser during short term operation is limited by either catastrophic mirror damage or heating of the device. Conventional BH lasers, being small emitting area devices, are generally limited by catastrophic mirror damage. For the structure shown in fig. 10, the active layer width typically is less than 2 μm so that fundamental spatial mode operation can be achieved. The vertical size of the mode is typically about 0.3 μm. This gives an emitting area of only about 0.6 μm^2. For the structure shown in fig. 10 with a 0.2 μm thick active layer the peak intensity inside the active layer reaches the CW catastrophic damage threshold intensity of 15 mW/μm^2 at a power output of only 5 mW. A significant advancement in the power capabilities of BH lasers was made when

the buried optical guide lasers were developed by Chinone et al[4]. This structure is shown in fig. 11. The most significant change is the incorporation of a four layer large optical cavity waveguide which increased the vertical size of the optical mode to approximately 1 μm. Fundamental mode operation in this structure can be reproducibly obtained for active layer widths up to approximately 3 μm. For an optical guide layer thickness of 1 μm and an active layer thickness of 0.08 μm, the peak intensity inside the active layer reaches the CW catastrophic damage limit at a power output of approximately 25 mW.

To further improve the power handling capabilities of BH lasers, it is desirable to further increase the emitting area and possibly to incorporate a window structure. Strip buried heterostructure lasers, such as the inverted strip buried heterostructure laser[8] shown in fig. 3 are capable of fundamental mode operation for active layer widths up to 4 μm. Further refinements could probably consistently enable fundamental mode operation for stripe widths up to approximately 5 μm. In addition, the thickness of the optical guide layer can probably be increased to approximately 1.5 μm while still maintaining fundamental mode operation in the vertical direction. For the structure shown in fig. 12 with a 0.08 μm thick active layer, the peak intensity in the active layer reaches the catastrophic damage limit at a power output of approximately 50 mW. Further increases in the stripe width, while maintaining fundamental mode operation may be possible using techniques such as narrow injection of current into the active layer, but the effect of this on the spectral characteristics of the lasers is unclear.

From the preceding analysis it appears that CW power outputs up to 50 mW should be possible from BH lasers, without using a window laser structure. To further increase the power output, transparent window sections at the mirrors will probably be necessary. The incorporation of window sections will most likely

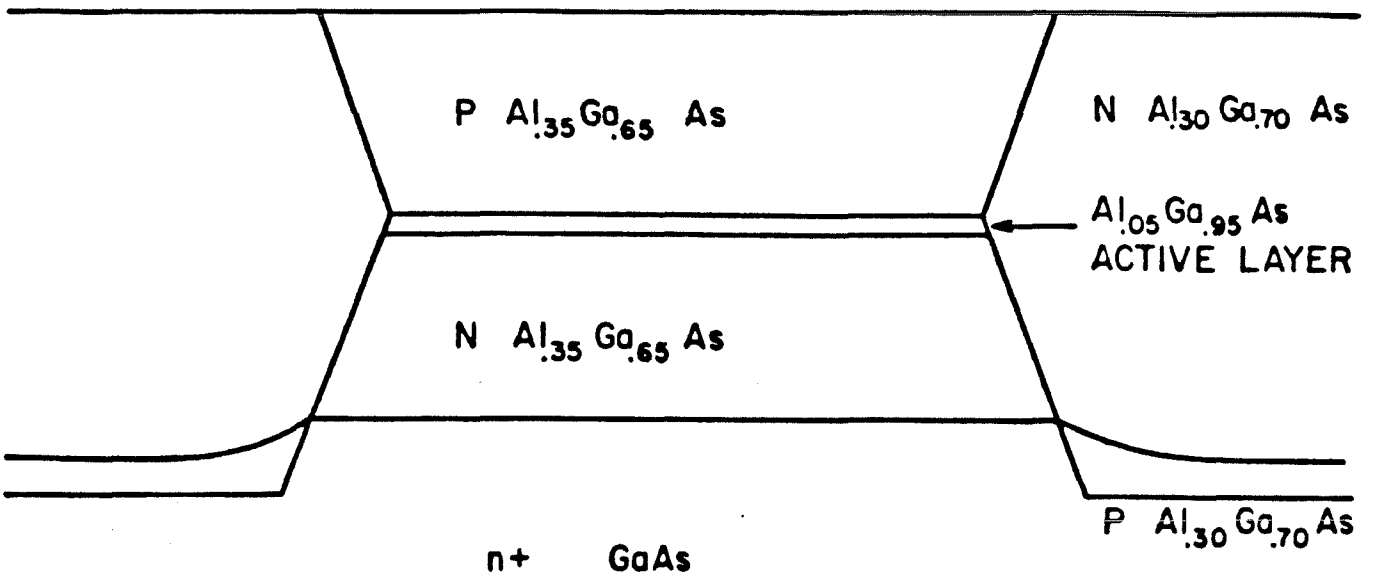

Fig. 10 Cross section of a buried heterostructure laser

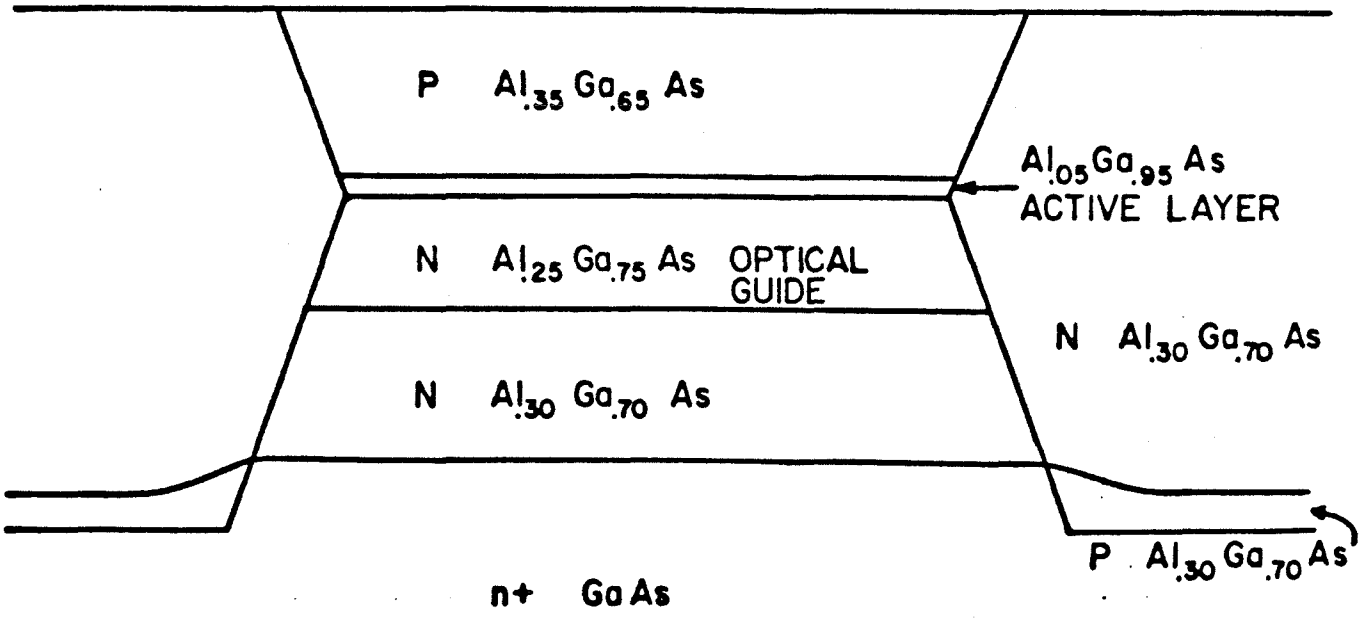

Fig. 11 Cross section of a buried optical guide laser

eliminate optical damage as the limiting factor for short term operation. More likely, the power output of window lasers will be limited by heating of the device. The power level can then be expected to saturate above a certain current density. In the high power CDH lasers[9] fabricated by RCA and the channeled substrate planar[24] lasers of Hitachi, the power saturates at a current density of approximately $2x10^4$ A/cm^2. For a laser stripe width of 5 μm and a laser cavity length of 300 μm this corresponds to a current of 300 mA. A laser of these dimensions can be expected to have a threshold current of approximately 50 mA and a differential power output of 0.4-0.5 mW/mA per facet. If one mirror is coated for high reflectivity the differential power output from the other mirror can be increased by nearly a factor of two to 0.8-1 mW/mA. Based on these estimates, heating can be expected to limit the power output to

$$(1mW/mA)(300mA-50mA)=250\ mW$$

Since the BH lasers are more efficient than the CDH lasers, operation to even higher current densities should be possible for a BH laser with the same series resistance and thermal resistance as the CDH lasers. For a series resistance-stripe area product of $4x10^{-5}\ \Omega-cm^2$, which is the value for the RCA lasers, the power from BH lasers can be expected to saturate at a current density of 22 kA/cm^2 rather than the 20 kA/cm^2 of the CDH laser. This increases the limit on the power due to heating slightly to approximately 280 mW. This figure should be viewed as an upper limit on the short term CW single mode power capabilities of BH lasers. Since this is an order of magnitude greater power than has been thus far achieved from BH lasers, it is difficult to predict the maximum power level at which BH lasers can be operated at reliably. One problem with the window BH lasers, such as shown in fig 1b, is that the optical guide layer is above the active layer. This increases the distance between the active layer and the heat sink, which in turn increases the thermal resistance of the laser. It would

be preferable for high power applications to have the active layer on top of the optical guide layer. However, window laser structures may result in an improvement in the reliability of BH lasers. In a conventional laser, even at power levels below the catastrophic damage threshold, defects are generated at a fast rate in the active layer near the mirrors. Window structures enable the passivation of the end of the active layer and may result in a decrease in the rate of defect generation.

Appendix 3.1 Optical Waveguide Theory

An understanding of the optical modes of the dielectric waveguides of various laser structures is essential to design lasers for high power operation. In this section some basic concepts related to optical waveguide theory are reviewed and two numerical methods for calculating the modes of optical waveguides are described.

The starting point for optical waveguide theory is Maxwell's equations. It is convenient to resolve the fields into transverse and longitudinal components

$$\mathbf{E}=(\mathbf{E_t}+\mathbf{k}E_z)e^{i(\omega t-\beta z)} \tag{A3.1-1}$$

$$\mathbf{H}=(\mathbf{H_t}+\mathbf{k}H_z)e^{i(\omega t-\beta z)} \tag{A3.1-2}$$

where $\mathbf{k}$ is a unit vector in the longitudinal direction and β is the propagation constant. Substituting these expressions into Maxwell's equations

$$\nabla\times\mathbf{E} = -i\omega\mu\mathbf{H}, \qquad \nabla\times\mathbf{H} = i\omega\varepsilon\mathbf{E} \tag{A3.1-3}$$

gives the following four equations:

$$\nabla\times\mathbf{E}_t = -i\omega\mu\mathbf{k}H_z \tag{A3.1-4}$$

$$\nabla\times\mathbf{H}_t = i\omega\mu\mathbf{k}E_z \tag{A3.1-5}$$

$$i\beta\mathbf{k}\times\mathbf{E}_t + \mathbf{k}\times\nabla E_z = i\omega\mu\mathbf{H}_t \tag{A3.1-6}$$

$$i\beta\mathbf{k}\times\mathbf{H}_t + \mathbf{k}\times\nabla H_z = -i\omega\mu\mathbf{E}_t \tag{A3.1-7}$$

substituting (A3.1-1) and (A3.1-2) into the equations:

$$\nabla\cdot\varepsilon\mathbf{E} = 0, \qquad \nabla\cdot\mu\mathbf{H} = 0 \tag{A3.1-8}$$

gives the equations:

$$\nabla\cdot\varepsilon\mathbf{E}_t = i\beta\varepsilon E_z, \quad \nabla\cdot\mu\mathbf{H}_t = i\beta\mu H_z \tag{A3.1-9}$$

Using these expressions the wave equation for the transverse E fields can be obtained

$$\mu\nabla\times\frac{1}{\mu}\nabla\times\mathbf{E}_t-\nabla\frac{1}{\varepsilon}\nabla\cdot\varepsilon\mathbf{E}_t-(\omega^2\varepsilon\mu-\beta^2)\mathbf{E}_t=0 \qquad \text{(A3.1-10)}$$

a similar expression holds for the transverse H fields

$$\varepsilon\nabla\times\frac{1}{\varepsilon}\nabla\times\mathbf{H}_t-\nabla\frac{1}{\mu}\nabla\cdot\mu\mathbf{H}_t-(\omega^2\varepsilon\mu-\beta^2)\mathbf{H}_t=0 \qquad \text{(A3.1-11)}$$

Optical waveguide theory consists of methods of obtaining solutions to these wave equations. Unfortunately, there are relatively few waveguides for which an exact solution is known. Therefore, waveguide theory is comprised primarily of numerical methods for obtaining approximate solutions. In the following section, the effective index method, and the vector variational method will be described and the approximations included in these techniques will be analyzed.

Appendix 3.2 Effective Index Method

The effective index method is an extremely useful method for obtaining approximate solutions to optical waveguide problems. The effective index method is useful primarily because it is very simple. However, because of the many simplifying approximations that are made, the technique should not be used when great accuracy is required. Nonetheless for most optical waveguide problems associated with laser structures, the effective index method provides sufficient accuracy and this method is the most widely used approximation method for laser waveguide problems.

The effective index method is best applied to waveguides in which there is strong optical guiding in one direction and weak optical guiding in the other direction. This is generally true for laser structures, which typically have strong guiding in the vertical, x, direction and relatively weak guiding in the lateral, y,

direction. In general, all six field components ($E_{x,y,z}H_{x,y,z}$) of the modes of a two dimensional waveguide will be nonvanishing. However, for the case of strong guiding in one direction and weak guiding in the other, the solutions can be classified as pseudo-TE and pseudo-TM. Pseudo-TE modes have dominant field components E_y,H_x, and H_z and pseudo-TM modes have dominant field components H_y,E_x, and E_z. Semiconductor lasers generally oscillate in pseudo-TE modes because of the larger modal reflectivities of the pseudo-TE modes. With the assumption of only one dominant electric field component the wave equation can be significantly simplified. Using

$$\nabla \cdot \varepsilon \mathbf{E}_t = i\beta\varepsilon E_z = 0 \qquad \text{(A3.2-1)}$$

The wave equation for E_y can be written as

$$\mu\nabla \times \frac{1}{\mu}\nabla \times \mathbf{E}_y - (\omega^2\varepsilon\mu - \beta^2)\mathbf{E}_y = 0 \qquad \text{(A3.2-2)}$$

Making the further assumption that μ is constant and using the vector identity

$$\nabla \times \nabla \times \mathbf{A} = \nabla(\nabla \cdot \mathbf{A}) - \nabla^2\mathbf{A} \qquad \text{(A3.2-3)}$$

the wave equation can be written as

$$-\nabla(\nabla \cdot \mathbf{E}_y) + \nabla^2\mathbf{E}_y + (\omega^2\varepsilon\mu - \beta^2)\mathbf{E}_y = 0 \qquad \text{(A3.2-4)}$$

where $\mathbf{E}_y$ here refers to a vector directed along the y-axis. this can be further simplified using the relation

$$\nabla \cdot \mathbf{E}_y = \frac{1}{\varepsilon}\nabla \cdot \varepsilon\mathbf{E}_y - \frac{1}{\varepsilon}\mathbf{E}_y \cdot \nabla\varepsilon \qquad \text{(A3.2-5)}$$

but

$$\nabla \cdot \varepsilon\mathbf{E}_y = 0 \qquad \text{(A3.2-6)}$$

so the wave equation becomes

$$\nabla^2 \mathbf{E}_y + (\omega^2 \varepsilon \mu - \beta^2)\mathbf{E}_y = -\nabla \left(\frac{1}{\varepsilon} \mathbf{E}_y \cdot \nabla \varepsilon\right) \qquad \text{(A3.2-7)}$$

Generally, laser structures are made up of layers which have uniform ε. In this case the right hand side of (A3.2-7) is zero and we arrive at the form of the wave equation that is generally used to analyze laser waveguide problems

$$\nabla^2 E_y + (\omega^2 \varepsilon \mu - \beta^2) E_y = 0 \qquad \text{(A3.2-8)}$$

In the effective index method, the solutions are taken to be of the form

$$E_y(x,y) = F(x,y)G(y) \qquad \text{(A3.2-9)}$$

where F is a slowly varying function of y. Substituting this into (A3.2-8) gives

$$G\frac{\partial^2 F}{\partial x^2} + \frac{\partial^2 (FG)}{\partial y^2} + k_o^2 n^2(x,y)FG - \beta^2 FG = 0 \qquad \text{(A3.2-10)}$$

The next step in the effective index method is to solve

$$\frac{d^2 F(x,y)}{dx^2} + (k_o^2 n^2(x,y) - \beta^2{}_x(y))F(x,y) = 0 \qquad \text{(A3.2-11)}$$

for $F(x,y)$ and $\beta_x(y)$ for all values of y, where $F(x,y)$ and $\beta(y)$ are the solutions of a dielectric slab waveguide (infinite in the $\hat{y}$ direction) with an index of refraction $n(x,y)$. The values of $\beta_x(y)$ thus obtained are used to obtain an equation for the y variation.

$$\frac{d^2 G(y)}{dy^2} + (\beta^2{}_x(y) - \beta^2)G = 0 \qquad \text{(A3.2-12)}$$

F and G thus satisfy

$$G\frac{\partial^2 F}{\partial x^2} + F\frac{\partial^2 G}{\partial y^2} + k_o^2 n^2(x,y)FG - \beta^2 FG = 0 \qquad \text{(A3.2-13)}$$

Comparing this to (A3.2-11), we can see that the effective index method makes the approximation:

$$\frac{\partial^2(FG)}{\partial y^2} = F\frac{\partial^2 G}{\partial y^2} \qquad \text{(A3.2-14)}$$

which is an approximation which is good if F(x,y) is slowly varying in y. This, in turn is true when n(x,y) is slowly varying in y. The entire procedure is best explained by means of an example.

Fig 12 shows a strip buried heterostructure laser. To apply the effective index method, the modes and effective indices of dielectric slab waveguides of infinite width corresponding to the layers of sections I and II are first calculated. Then the shape of the modes in the lateral direction are determined approximately by solving for the modes of an infinite slab waveguide having indices of refraction equal to the effective indices of sections I and II. Fig 13 illustrates this procedure.

In this case, n(x,y) is actually not slowly varying in y, but changes abruptly. The use of the effective index is therefore not completely justified for this type of waveguide. However for most purposes the effective index method will provide solutions of sufficient accuracy. For laser waveguide problems, the uncertainty associated with difficulties in precisely controlling the layers that are grown is generally larger than the error made by using the effective index method. However, it is sometimes desirable to solve waveguide problems with more accuracy than is possible with the effective index method. In such cases, methods such as the vector variational method or the finite element method can be used. These methods unfortunately require orders of magnitude more computer time and are therefore not practical for calculations where the modes of many waveguides need to be determined.

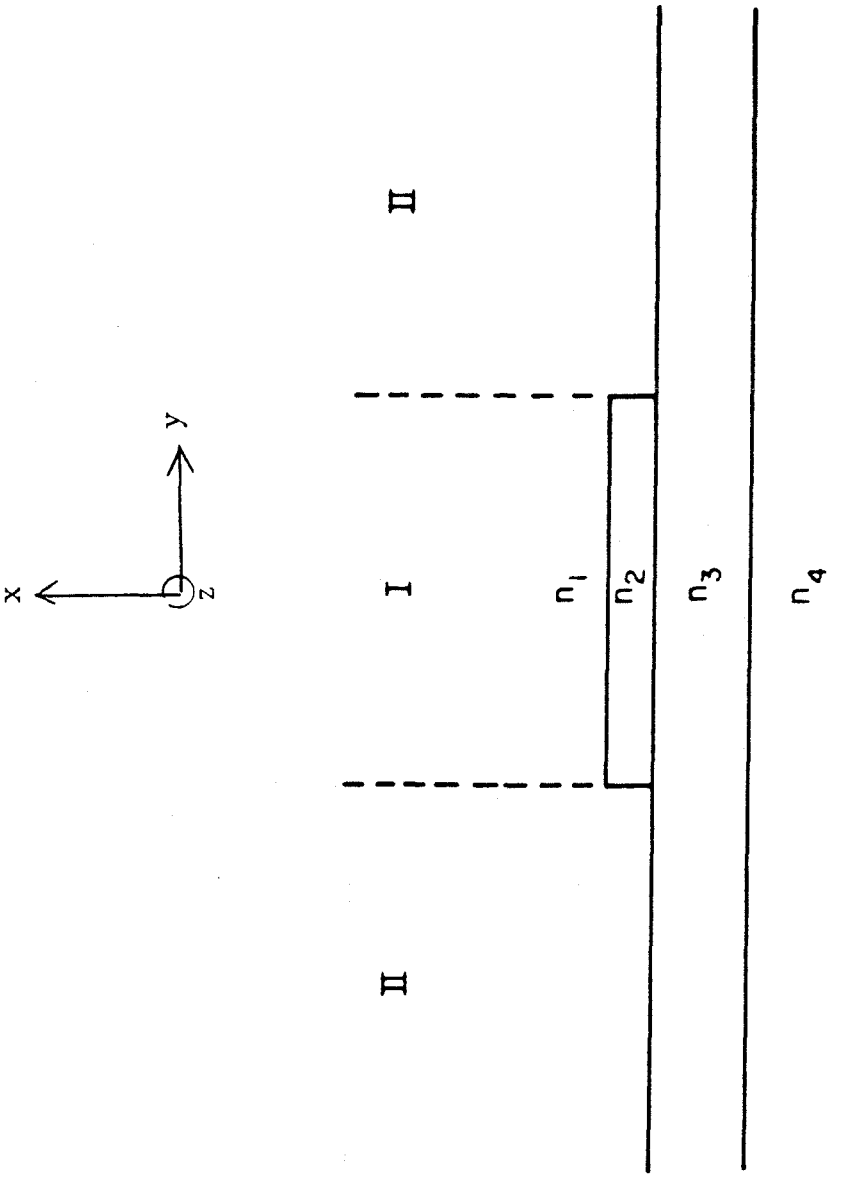

Fig. 12 Cross section of a strip buried heterostructure laser

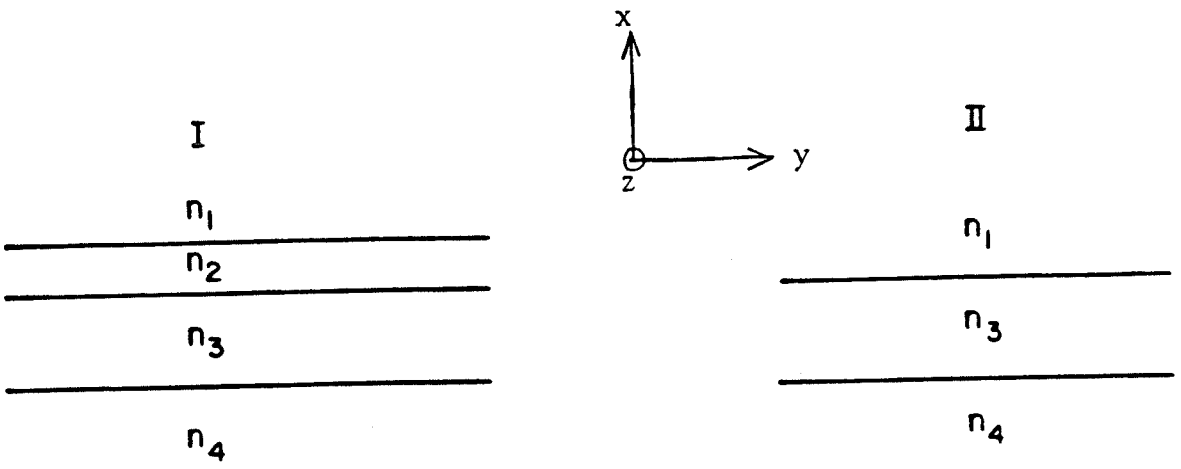

a) The first step in the effective index method is to solve for the modes ,$F^{I,II}(x)$, and the effective indices, $n_{eff}^{I,II}$, of dielectric slab waveguides corresponding to sections I and II of fig 12. These slab waveguides are made up of the layers of sections I and II, but are infinite in the y direction.

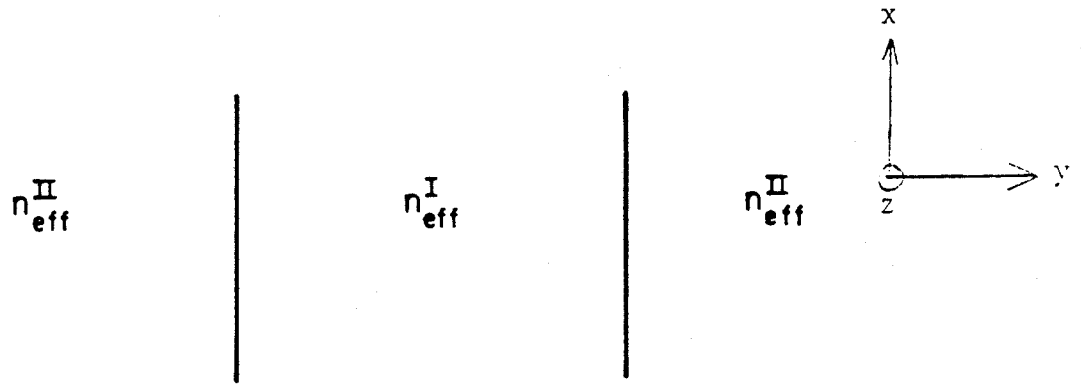

b) Having solve for n_{eff}^{I} and n_{eff}^{II}, the dielectric slab waveguide shown below is now solved for the lateral mode variation G(y) and the waveguide propagation constant β. In this case, the waveguide is taken to be infinite in the x direction

Fig. 13 Application of the effective index method to a strip buried heterostructure laser

Appendix 3.3 Vector Variational Method

The vector variational method is an extremely powerful technique for obtaining accurate solutions to optical waveguide problems. It is, however, considerably more complex computationally, and the vector variational method is used only when a high degree of accuracy is required. For the research described in this thesis, this method was only used to check the accuracy of the application of the effective index method to laser waveguide problems. The method is based on the variational expression for the propagation constant, which in a lossless dielectric waveguide is given by[17]:

$$\beta^2 = N/D \tag{A3.3-1}$$

where

$$N = \int\left[\varepsilon(\omega^2\mu H_t - \nabla\times\frac{1}{\varepsilon}\nabla\times H_t)^2 - \omega^2\frac{1}{\mu}(\nabla\cdot\mu H_t)^2\right]dS \tag{A3.3-2}$$

$$+ 2\int\left[\left(\frac{1}{\mu}\nabla\cdot\mu H_t\right)\mathbf{n}\cdot(\omega^2\mu H_t - \nabla\times\frac{1}{\varepsilon}\nabla\times H_t)\right]dl$$

and

$$D = \int\left[\omega^2\mu H_t - \frac{1}{\varepsilon}(\nabla\times H_t)^2\right]dS + 2\int\left[\left(\frac{1}{\varepsilon}\nabla\times H_t\right)\cdot(\mathbf{n}\times H_t)\right]dl \tag{A3.3-3}$$

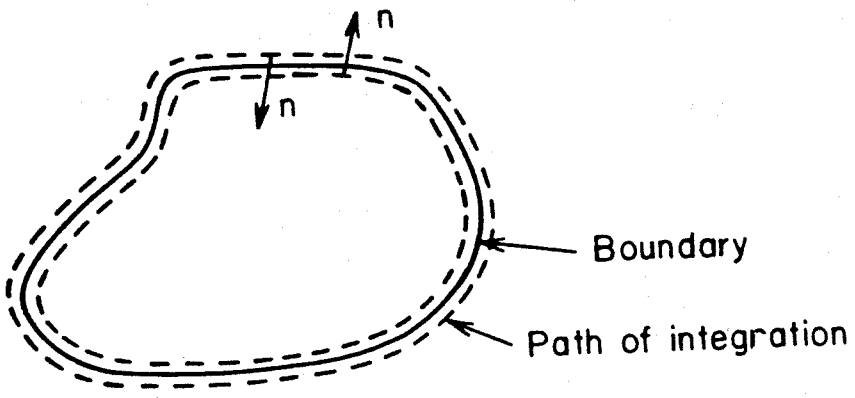

The surface integrals are carried out over the whole cross section of the waveguide and the line integrals are carried out over all the boundaries at which the material constants μ,ε change discontinuously. $\mathbf{n}$ is a unit vector normal to the boundary and directed as shown in fig 14. If trial functions are chosen such that $(1/\mu)\nabla\cdot\mu\mathbf{H}_t$ and $\mathbf{k}\cdot(\mathbf{n}\times\mathbf{H}_t)$ are continuous across the boundaries between the media then the variational expression is stationary for trial functions which satisfy the wave equation and the boundary conditions that the tangential H fields are continuous. This method does not yield solutions which satisfy the boundary conditions related to the derivatives of the H fields at the boundaries.

It is most convenient to take trial functions to be of the form:

$$\mathbf{H}_t = \sum a_n \mathbf{u}_n \qquad \text{(A3.3-4)}$$

then the variational expression can be written as

$$\beta^2 = \frac{\sum a_n a_m N_{nm}}{\sum a_n a_m D_{nm}} \qquad \text{(A3.3-5)}$$

this can be written in matrix form as follows:

$$\beta^2 = \frac{\mathbf{a}^t\mathbf{N}\mathbf{a}}{\mathbf{a}^t\mathbf{D}\mathbf{a}} \qquad \text{(A3.3-6)}$$

The condition that β^2 is stationary is equivalent to the condition[22]

$$\mathbf{N}\mathbf{a} = \beta^2\mathbf{D}\mathbf{a} \qquad \text{(A3.3-7)}$$

Thus the problem of finding solutions to the optical waveguide problem is reduced to an eigenvalue problem which can be easily solved using standard numerical techniques.

References for Chapter 3

1. T. Kamejima and H. Yonezu, "Catastrophic Optical Damage Generation Mechanism in (AlGa)As DH Lasers", Japan. J. Appl. Phys. supplement **19-1** , pp 425-429 (1978).

2. H. Yonezu, M. Ueno, T. Kamejima, and I. Hayashi, "An AlGaAs Window Structure Laser", IEEE J. Quantum Electronics **QE-15** , pp 775-781 (1979).

3. H. Blauvelt, S. Margalit, and A. Yariv, "Large Optical Cavity AlGaAs Buried Heterostructure Window Lasers" Appl. Phys. Lett. **40** ,pp 1029-1031, (1982).

4. N. Chinone, K. Saito, R. Ito, K. Aiki, N. Shige, "Highly Efficient (GaAl)As Buried Heterostructure Lasers with Buried Optical Guide", Appl. Phys. Lett. **35** , pp 513-516 (1979).

5. R. Lang, "Lateral Transverse Mode Instability and Its Stabilization in Stripe Geometry Injection Lasers", IEEE J. Quantum Electron. **QE-15** , pp 718-726 (1979).

6. S. Wang, C. Chen, A. Liao, and L. Figueroa, "Control of Mode Behavior in Semiconductor Lasers", IEEE J. Quantum Electron. **QE-17** , pp 453-468 (1981).

7. W.T. Tsang and R. Logan, "GaAs-$Al_xGa_{1-x}As$ Strip Buried Heterostructure Lasers", IEEE J. Quantum Electron. **QE-15** ,pp 451-469, (1979).

8. H. Blauvelt, S. Margalit, and A. Yariv "AlGaAs Inverted Strip Buried Heterostructure Lasers", Appl. Phys. Lett. **41** ,1982

9. D. Botez, "Constricted Double-Heterojunction AlGaAs Diode Lasers: Structures and Electrooptical Characteristics", IEEE J. Quantum Electron. **QE-17** ,pp 2290-2309, (1981).

10. F.K. Reinhart, I. Hayashi, and M.B. Panish, "Mode Reflectivity and Waveguide Properties of Double-Heterostructure Injection Lasers" J. Appl. Phys. **42** ,pp

4466-4479, (1971).

11. T. Ikegami, "Reflectivity of Mode at Facet and Oscillation Mode in Double Heterostructure Injection Lasers", IEEE J. Quantum Electron. **QE-8** ,pp 470-476, (1972).

12. L. Lewin, "A Method for the Calculation of the Radiation Pattern and Mode Conversion Properties of a Solid State Heterojunction Laser", IEEE Trans. Microwave Theory and Tech., **MTT-23** ,pp 576-585, (1975).

13. T. Rozzi, and G. in't Veld "Variational Treatment of the Diffraction at the Facet of D.H. Lasers and of Dielectric Millimeter Wave Antennas", IEEE Trans. Microwave Theory and Tech., **MTT-28** ,pp 61-73, (1980).

14. P. Gelin, M. Petenzi, and J. Citerne, "Rigorous Analysis of the Scattering of Surface Waves in an Abruptly Ended Slab Dielectric Waveguide", IEEE Trans. Microwave Theory and Tech., **MTT-29** ,pp 107-114 (1981).

15. W. McLevige, T. Itoh, and R. Mittra, "New Waveguide Structures for Millimeter Wave and Optical Integrated Circuits", IEEE Trans. Microwave Theory and Tech., **MTT-23** ,p788, (1975).

16. P. Kirkby, and G.H.B. Thompson, "Channeled Substrate Buried Heterostructure GaAs-(GaAl)As Injection Lasers", J. Appl. Phys. **47** , p4578, (1976).

17. W. Streifer, and E. Kapon, "Application of the Equivalent Index Method to DH Diode Lasers", Appl.Opt. **18** ,p 3724, (1979).

18. K. Kurokawa, "Electromagnetic Waves in Waveguides with Wall Impedance" IEEE Trans. Microwave Theory and Tech., **MTT-10** ,pp 314-320, (1962).

19. M. Matsuhara, and N. Kumagai, "Theory of Coupled Open Transmission Lines and Its Application",IEEE Trans. Microwave Theory and Tech., **MTT-22** ,pp 378-382, (1974).

20. K. Morishita, and N. Kumagai, "Unified Approach to the Derivation of Variational Expression for Electromagnetic Fields", IEEE Trans. Microwave Theory and Tech., **MTT-25** ,pp 34-40, (1977).

21. M. Ohtaka, M. Matsuhara, and N. Kumagai, "Analysis of the Guided Modes in Slab Coupled Waveguides Using a Variational Method",IEEE J. Quantum Electron. **QE-12** ,pp 378-382, 1976.

22. C. Yeh, "Optical Waveguide Theory",IEEE Trans. Circuits and Systems, **CAS-26** ,pp 1011-1019, (1979).

23. C. Yeh, K. Ha, S. Dong, and W. Brown, "Single Mode Optical Waveguides" Applied Optics, **18** ,pp 1490-1505, (1979).

24. K. Aiki, M. Nakamura, T. Kuroda, J. Umeda, R. Ito, N. Chinone, and M. Maeda, "Transverse Mode Stabilized $Al_xGa_{1-x}As$ Injection Lasers with Channeled Substrate Planar Structure", IEEE J. Quantum Electron. **QE-14** , pp 89-94 (1978).

25. see for example P. Morse and H. Feshbach, *Methods of Theoretical Physics* , McGraw-Hill Book Co. New York, 1953.

Chapter IV

Large Optical Cavity AlGaAs Buried Heterostructure Window Lasers

4.1 Introduction

Many failure mechanisms of AlGaAs lasers can be attributed to the presence of the active layer at the laser mirrors. Local heating due to optical absorption in the active layer near the mirrors can result in catastrophic mirror damage[1] at high output powers. At somewhat lower output powers, facet erosion due to oxidation of the active layer can occur[2,3]. Even at low output powers, defects are generated at a fast rate in the active region in the vicinity of the mirrors[4]. Catastrophic mirror damage can be avoided by making the laser structure transparent to the light output in the vicinity of the mirrors. This has been accomplished previously by selective Zn diffusion in stripe lasers and results in an order of magnitude increase in the available pulsed optical power[5]. The power output of Zn diffused window lasers is limited by catastrophic damage due to local heating in the bulk rather than at the laser mirrors. There is also evidence that laser degradation due to facet oxidation is greatly reduced in lasers with transparent AlGaAs mirrors[6]. This has been attributed to the greater stability of the native oxide of AlGaAs compared to the native oxide of GaAs.

Although many factors can influence the long term reliability of AlGaAs lasers, for short term operation, the power output is generally limited either by catastrophic mirror damage or heating. The active layer of an AlGaAs laser is typically absorbing in the immediate vicinity of the mirrors due to surface recombination of carriers at the mirrors. The cleaved GaAs facet contains a high density of surface states. Absorption of laser light by the end sections results in the heating of the active layer near the mirrors which makes these sections even more absorbing. Above a critical optical power density, thermal runaway results, causing the active layer to melt at the mirrors. The catastrophic optical mirror damage occurs at a threshold

intensity of approximately 15 mW/μm^2 for CW operation and 70 mW/μm^2 for 100 nsec. pulses[7].

Buried heterostructure lasers have many characteristics which are desirable for high power single mode lasers. They have low threshold currents, are very efficient, and operate in a single longitudinal mode even at high output power levels and when modulated. However, until now the power output of BH lasers has been relatively low due to the small emitting area of most BH lasers. A conventional BH laser (without a large optical cavity) reaches the catastrophic optical damage threshold at a power output of only 5 mW. Large optical cavity BH lasers are better primarily because the vertical size of the mode is substantially increased. Because fundamental mode operation can be obtained for slightly wider stripe widths in LOC BH lasers the lateral size of the mode is also increased. Still the CW power output is limited by catastrophic mirror damage to approximately 25 mW. If the catastrophic damage can be avoided then it may be possible to increase the CW power of a BH laser by as much as a factor of 10 (see chapter 3).

In this chapter large optical cavity (LOC) buried heterostructure (BH) window lasers are described in which only the transparent AlGaAs layers, and not the active layer, extend to the laser mirrors. These lasers have threshold currents and quantum efficiencies comparable to those of LOC BH lasers without transparent end sections and have been operated, without degradation at up to three times the power at which regular LOC BH lasers degrade by catastrophic mirror damage. Window LOC BH lasers also appear to be more resistant to degradation due to mirror oxidation.

The window LOC BH laser structure is illustrated in fig. 1. The laser actually consists of two separate structures, a 200 μm central section which is a regular LOC BH structure[8] grown by liquid phase epitaxy (LPE) and 25μm transparent window

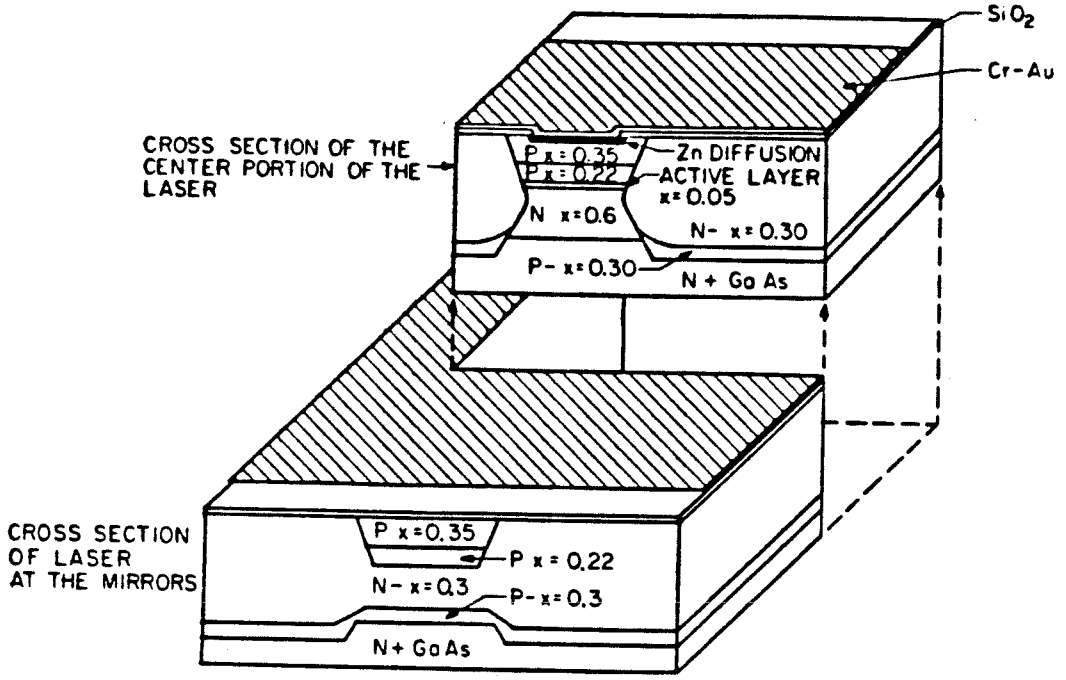

Figure 1a. Schematic diagram of a window LOC BH laser structure

x=Aluminum content of the layers

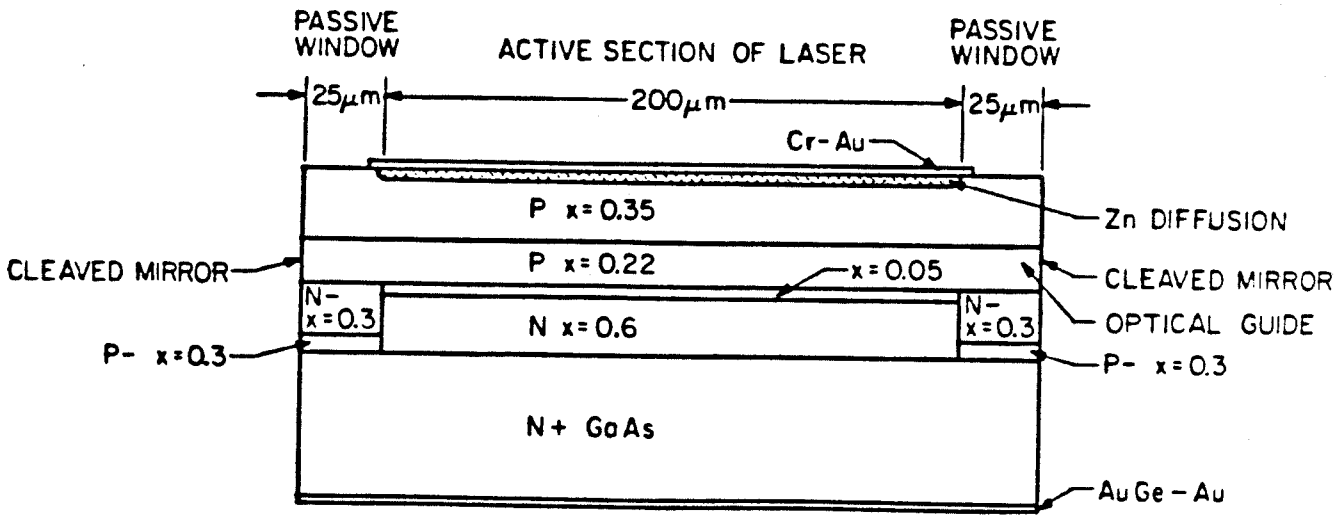

Figure 1b. Side view of a window LOC BH laser

sections from which the active layer and lower cladding layers have been removed after the first growth and replaced by transparent AlGaAs layers that are added during a second LPE growth. The optical mode is mostly confined to the $Al_{0.22}Ga_{0.78}As$ guide layer in both the center and window sections, which results in low loss coupling of the laser mode between the waveguides in the center and window sections.

The problem of determining the coupling loss between the center and window sections is similar to the problem of calculating mode reflectivities that was discussed in chapter 2. In general there will be one forward traveling incident guided mode, reflected guided and radiation modes, and transmitted radiation and guided modes. The geometry is shown in fig 2.

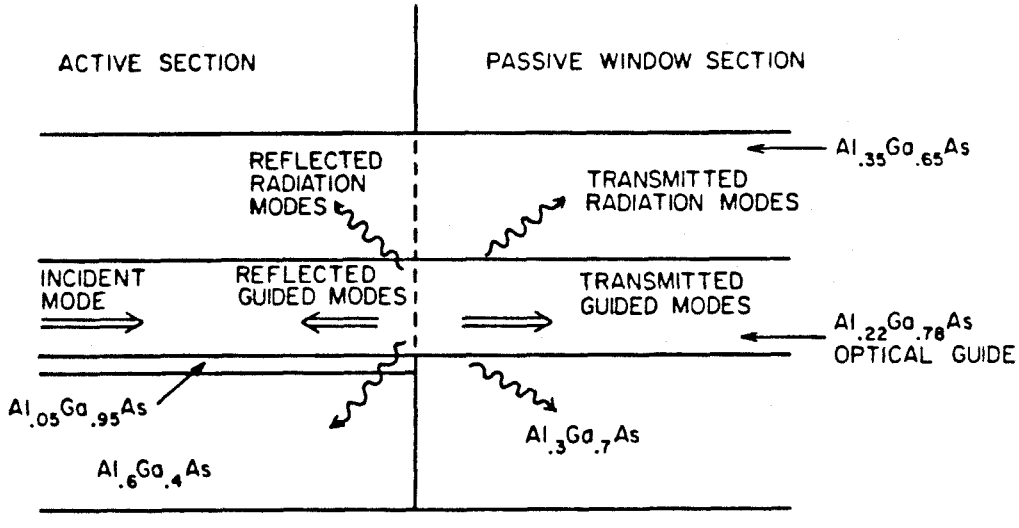

Figure 2. Coupling of power between the center and window sections

In general this problem has to be solved by techniques such as the iterative technique described in chapter two. However, for the case where the waveguides which are coupled together are well matched, the radiation modes and the reflected modes other than than the incident mode can be neglected to a first approximation.

As is the case in determining mirror reflectivities the coupling problem is solved by matching the tangential E and H fields at the boundary between the two regions. For TE-like modes the dominant field components are E_x and H_y. The requirement that these tangential components be continuous across the boundary can be written as follows:

$$E_i^{(1)}(1+r_i) = \Sigma t_n E_n^{(2)} \tag{4.1}$$

$$\beta_i^{(1)} E_i^{(1)}(1-r_i) = \Sigma \beta_n^{(2)} t_n E_n^{(2)} \tag{4.2}$$

where

$E_n^{(1,2)}$ = Guided mode n in region 1,2

r_i = amplitude of reflected mode i

t_n = amplitudes of the transmitted modes

$\beta_n^{(1,2)}$ = propagation constant of mode n in region 1,2

using the orthogonality relation for guided modes, the transmitted and reflected amplitudes can be expressed as follows:

$$r_i = \frac{\beta_i^{(1)} - \beta_i^{(2)}}{\beta_i^{(1)} + \beta_i^{(2)}} \tag{4.3}$$

$$t_m = \frac{2\beta_i^{(1)}}{\beta_i^{(1)} + \beta_m^{(2)}} \int E_i^{(1)} E_m^{(2)} ds \tag{4.4}$$

where the modes have been normalized to satisfy

$$\int E_m^{(1,2)} E_n^{(1,2)} ds = \delta_{nm} \tag{4.5}$$

For the laser structure shown in fig. 1 with a 0.8 μm thick optical guide layer, a 0.1 μm thick active layer, a 2 μm wide active layer, and an incident fundamental mode the reflection and transmission coefficients are listed below. The modes which the waveguide can support are labeled according to the order of the mode in the vertical and horizontal directions, respectively. Because of symmetry there is no coupling of

the fundamental mode to modes of odd order in the lateral direction.

Mode	% Total Power
transmitted 00	95.2
transmitted 10	1.8
all other transmitted and reflected guided modes	< .01
transmitted forward radiation modes	3.0

4.2 Fabrication of Buried Heterostructure Window Lasers

The fabrication of the window LOC BH laser requires two LPE growths. The layers grown in the first growth are N $Al_{0.6}Ga_{0.4}As$ (1.5μm Te doped), undoped $Al_{0.05}Ga_{0.95}As$ (0.12μm), P $Al_{0.22}Ga_{0.78}As$ (0.7μm Ge doped), and P $Al_{0.35}Ga_{0.65}As$ (1.0μm Ge doped). Next, mesas are etched as is done for a regular BH laser. These first two fabrication steps are illustrated in fig. 3. The mesas are then masked by photoresist, except for 50μm sections, which will eventually be the window sections of the laser. The $Al_{0.6}Ga_{0.4}As$ layer in the unmasked sections is then removed by selective etching in HF. This is followed by a brief nonselective etch to remove the active region as well in the unmasked sections. Fig. 4 shows scanning electron microscope (SEM) photographs of mesas prior to the second LPE growth showing the selective removal of the bottom cladding layer in the window section. After this, a thin P– $Al_{0.3}Ga_{0.7}As$ layer and an N- $Al_{0.3}Ga_{0.7}As$ layer are grown in the second LPE growth. These layers grow on the sides of the unetched sections of the mesas, and both underneath and on the sides of the selectively etched sections. Fig. 5 is a scanning electron micrograph of a cross section of a window section of the laser, after the second growth.

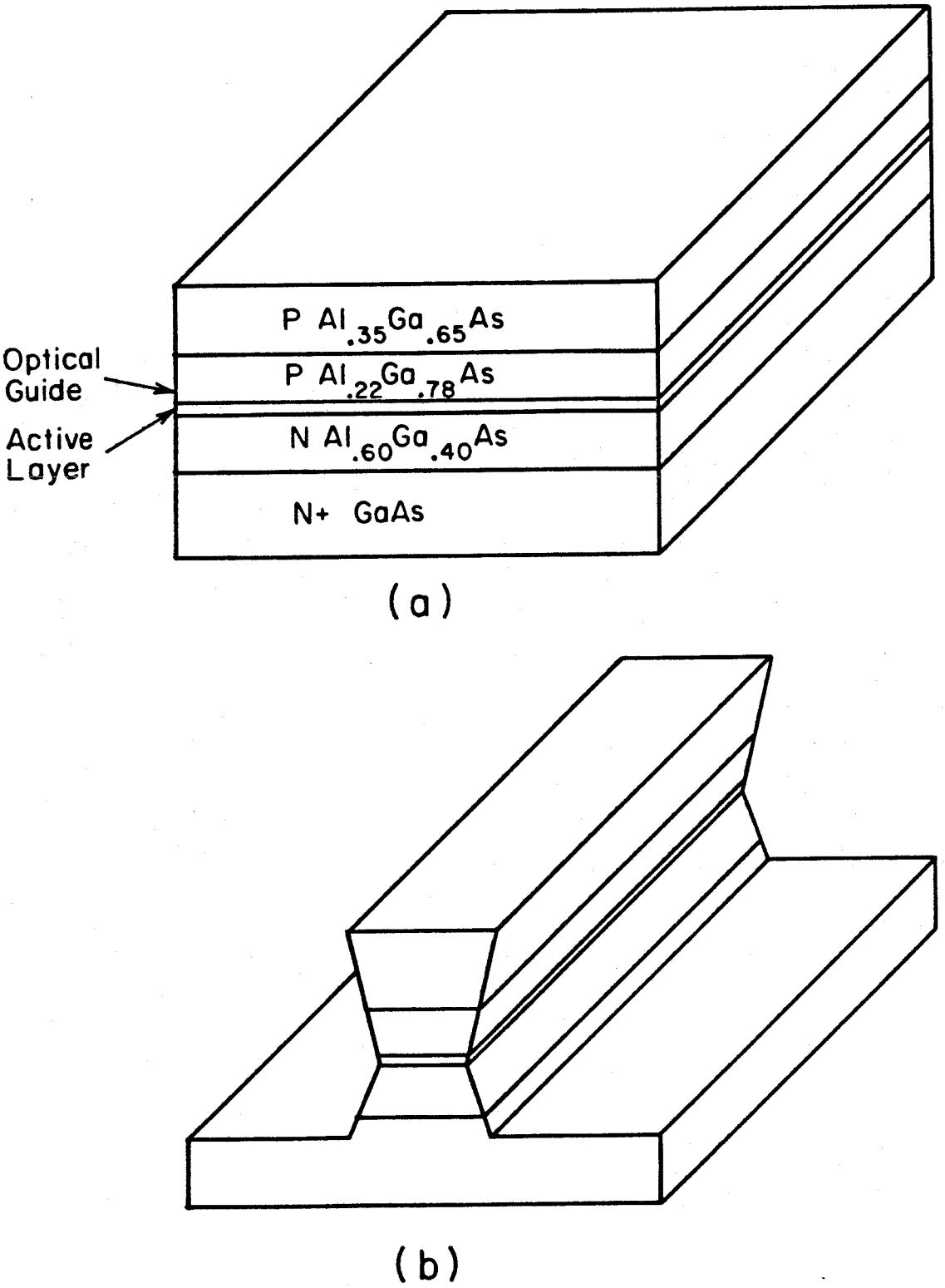

Figure 3. Fabrication steps for a buried heterostructure laser

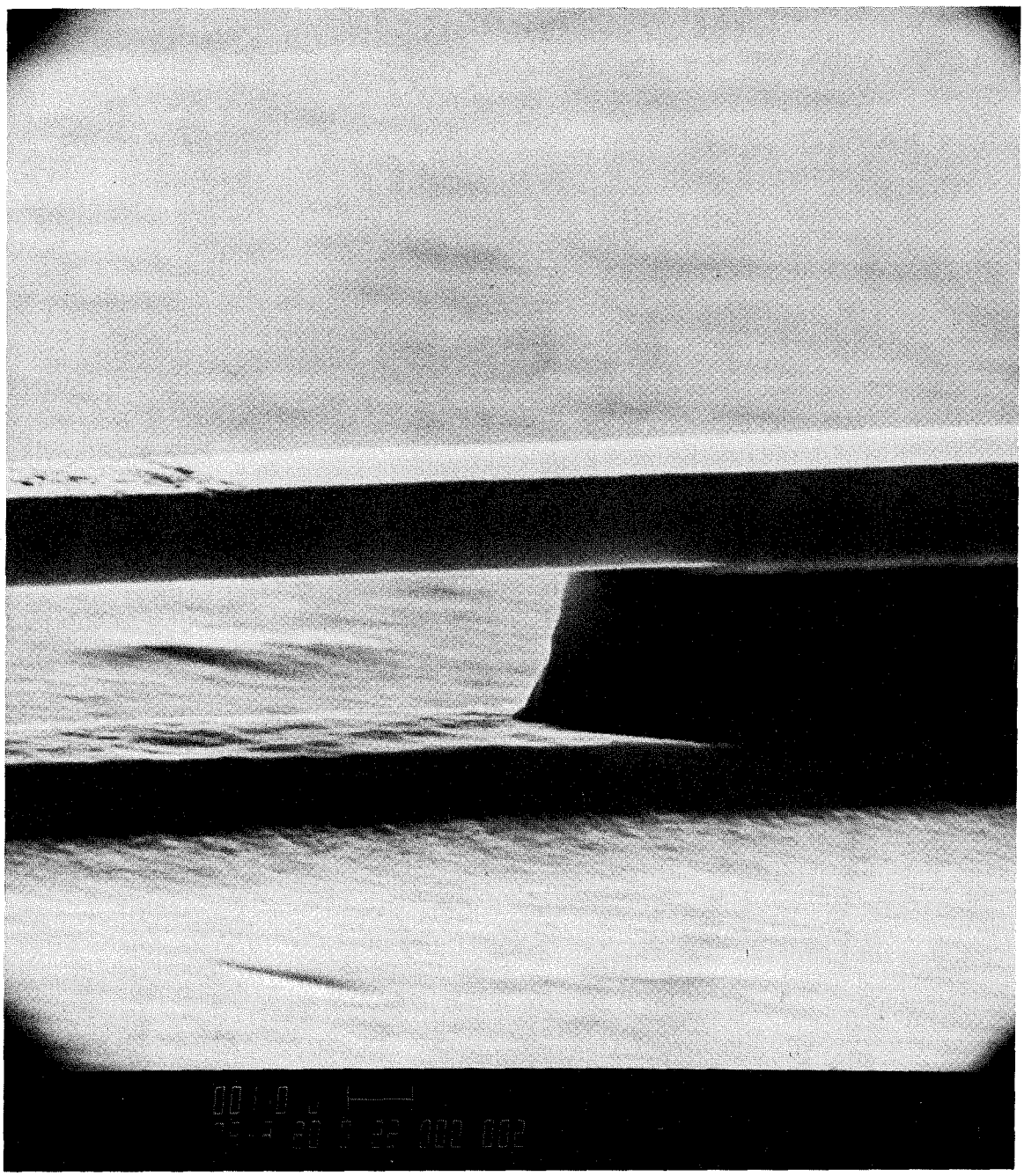

Fig. 4

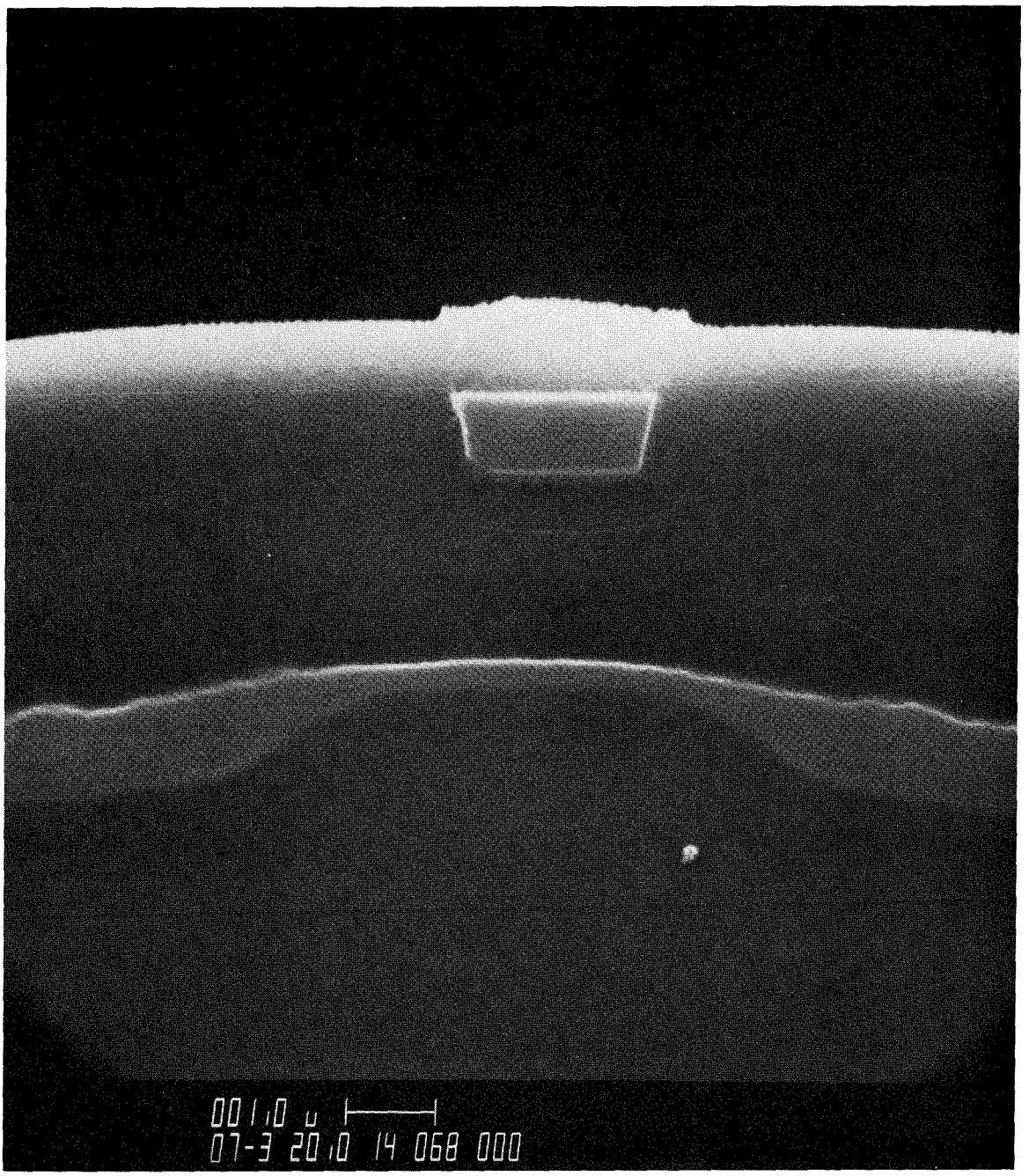

Fig. 5

Normally, LOC BH lasers are grown with N type optical guide layers to minimize electron leakage. For a double heterostructure with a given difference in the aluminum contents of the active and cladding layers, the leakage of electrons into the P cladding layer will be greater than the leakage of holes into the N cladding layer. If a relatively low aluminum content optical guide layer is incorporated into the laser structure, it is therefore desirable that it be N type. When n type GaAs substrates are used this means the active layer is on top of the guide layer. However, it is difficult to fabricate these lasers with the active layer on top of the guide layer, since this would require growing over the AlGaAs guide layer in the second LPE growth. Having the active layer underneath the optical guide layer, enables the layers of the second growth to be grown starting from the GaAs substrate. ISBH lasers can still have N type optical guide layers if p type GaAs substrates are used.

4.3 Properties of Buried Heterostructure Window Lasers

Since the transparent $Al_{0.22}Ga_{0.78}As$ guide layer, to which most most of the optical power is confined, extends from mirror to mirror, there is very little coupling loss between the center and window sections of the laser. Typically, our window LOC BH lasers have threshold currents of 8-10 mA per μm stripe width of the lasers for pulsed operation and 9-12 mA per μm for CW operation and differential quantum efficiencies of 20-30% per facet. The best results obtained for 2 μm wide stripes were pulsed and CW threshold currents of 15 mA and 18 mA, respectively, and a differential quantum efficiency of 35% per facet. These results are nearly identical to those of regular LOC BH lasers fabricated from the same wafer. The most significant difference between the window and regular LOC BH lasers was the ability of the window lasers to operate at high pulsed output powers without catastrophic mirror damage. Fig. 6 shows the light vs. current characteristics of a LOC BH laser and a window LOC BH laser for 2 μm wide devices driven by 75 nsec. pulses at a repetition rate of 1 KHz. Window LOC BH lasers were operated up to 130 mW/μm stripe width,

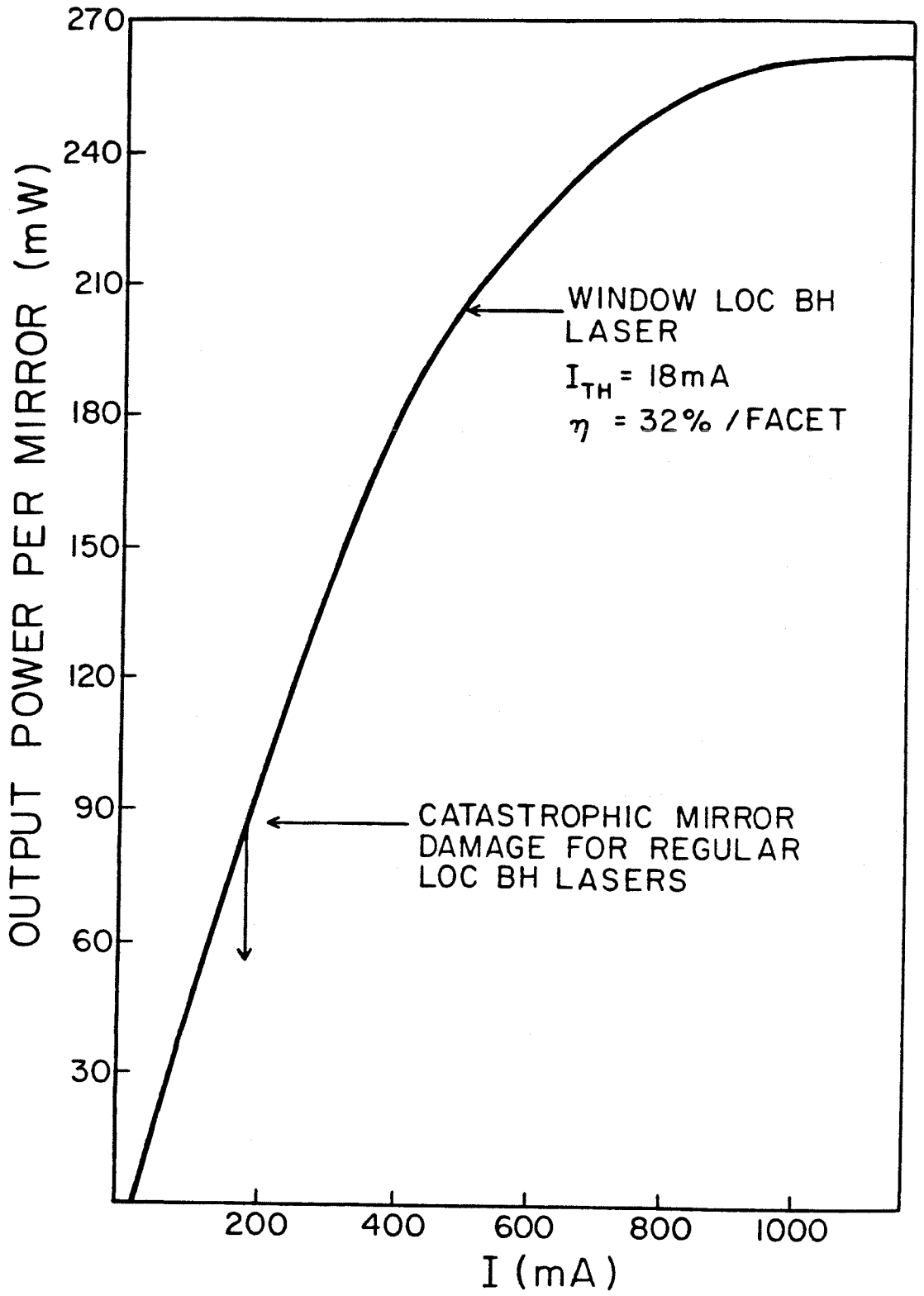

Figure 6. Light vs. current characteristics of a regular and window LOC BH laser

which is three times the power at which regular LOC BH lasers fabricated from the same wafer failed due to catastrophic mirror damage. The output power of the window lasers was limited by heating and not by mirror damage.

To further increase the output power of window BH lasers it would be desirable to both increase the laser stripe width and improve the thermal characteristics of the laser. By going to a strip BH structure (see for instance chapter 5) the stripe width can be roughly doubled while maintaining fundamental mode operation. Much more important, however, for increasing the power output would be to decrease the series resistance of the devices which results primarily from the contact resistance. Since BH lasers have in the past been primarily low current devices, the contacts have been relatively unimportant. The usual fabrication procedure results in the P contact being made to the upper cladding layer which typically has an aluminum content of 0.35. Much lower contact resistances are possible for contacts made to GaAs layers. Therefore, significant reductions in the power dissipation of the lasers can be expected if the fabrication process is modified to allow GaAs contacts. Such a modification should be possible with only a slight increase in the fabrication complexity. The main difficulty is that it is normally undesirable to have growth on top of the mesa during the second growth and growth will occur on top of GaAs, but not on $Al_{.35}Ga_{.65}As$.

For stripe widths of less than 2 μm , operation of the window LOC BH lasers in the fundamental transverse mode can be obtained. The far fields typically had irregularities due to scattered light as is shown in fig 7. Irregularities in the far field typically are present in regular BH lasers as well due to scattering from the sidewalls of the laser[6]. In window LOC BH lasers scattered light can also result from losses in the coupling of the laser light between the center and window sections. However, it could not be determined whether coupling losses were significantly affecting the beam quality. The inverted strip BH lasers which will be described in the next

chapter have significantly improved beam quality and are compatible with this window laser technology.

The effect of mirror oxidation on the laser performance has also been examined by oxidizing the mirrors in boiling water. At regular intervals during this accelerated mirror oxidation test the pulsed laser characteristics were measured. Lasers without windows were found to degrade approximately four times as fast as window lasers, as is shown in fig. 8. One possible explanation for this is that the oxide that is grown on the AlGaAs window sections is more stable than the oxide grown on the active layer of lasers without windows.

In conclusion window LOC BH lasers with transparent waveguides at the mirrors have been fabricated. These lasers have threshold currents and quantum efficiencies that are nearly identical to those of regular LOC BH lasers, but have been operated at pulsed power outputs which are three times the level at which regular LOC BH lasers degrade by catastrophic mirror damage. Even greater output powers may be possible since the power is currently limited by heating of the window LOC BH lasers rather than catastrophic damage. The window lasers also appear to be less susceptible to damage due to facet oxidation.

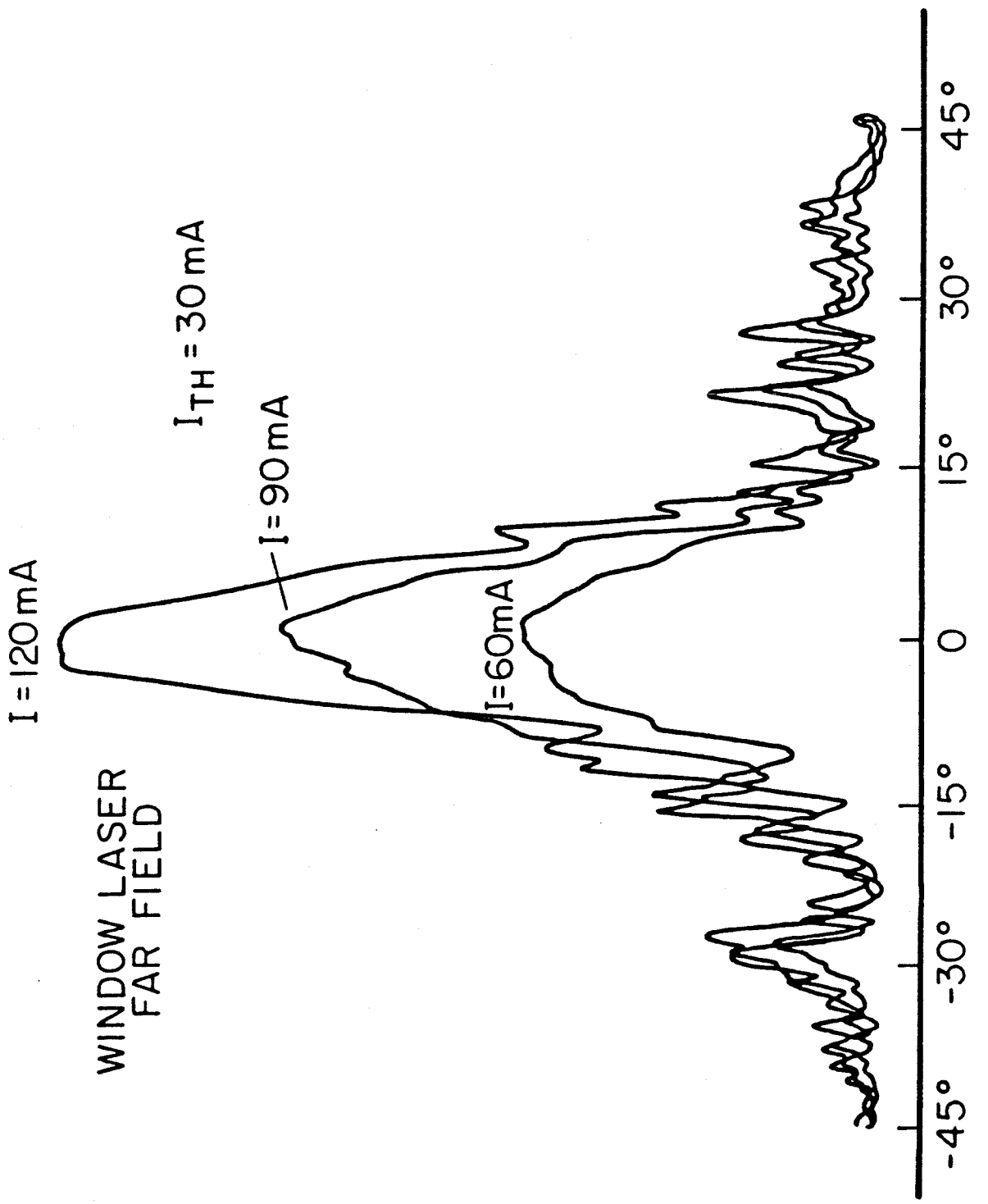

Figure 7. Far field pattern of a window LOC BH laser

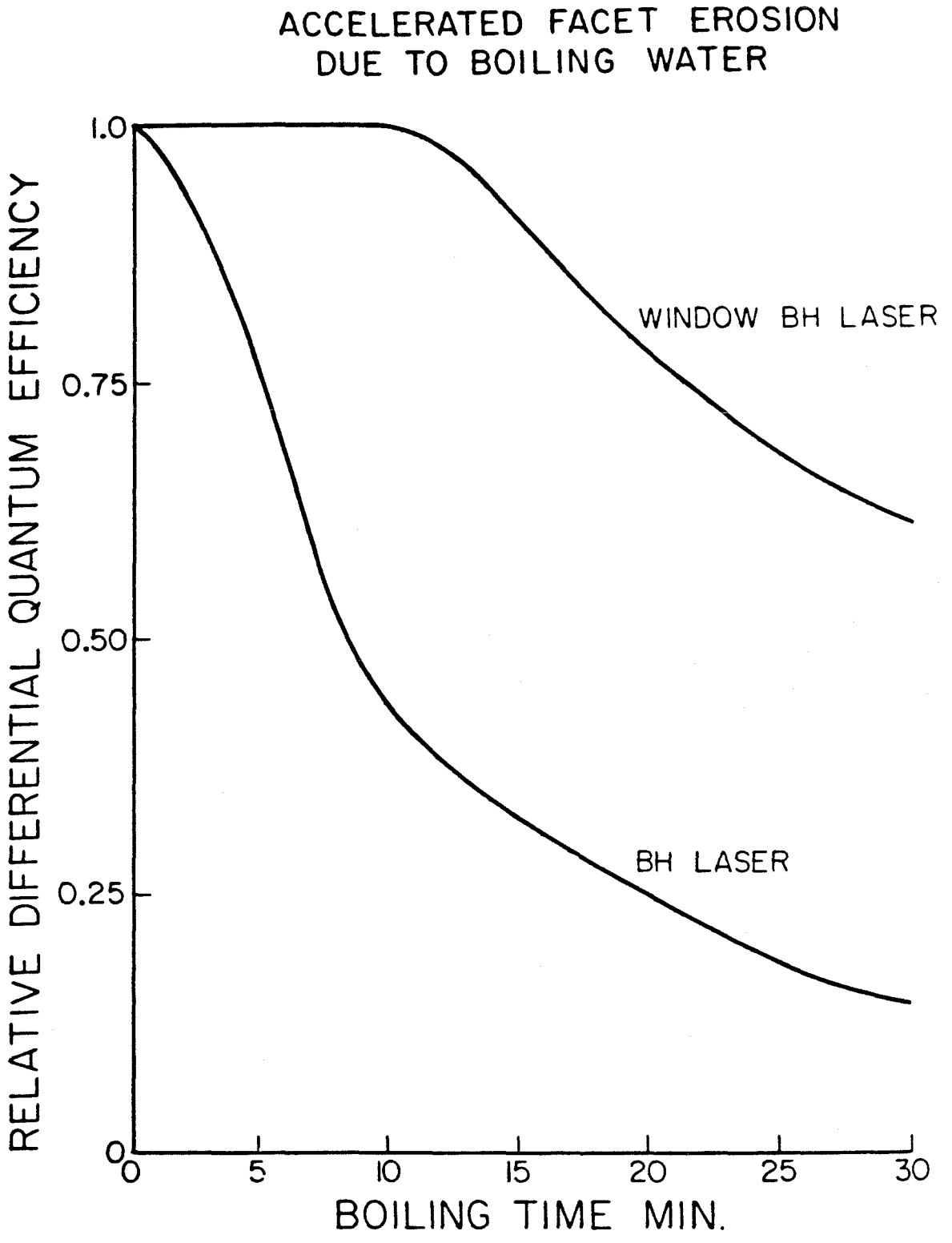

Figure 8. Degradation due to accelerated mirror oxidation

References for Chapter 4

1. T. Kamejima and H. Yonezu, "Catastrophic Optical Damage Generation Mechanism in (AlGa)As DH Lasers", Japan. J. Appl. Phys. supplement **19-1** , pp 425-429 (1978).

2. T. Yuasa, M. Ogawa, K. Endo, and H. Yonezu, "Degradation of (AlGa)As DH Lasers Due to Facet Oxidation" Appl. Phys. Lett. **32** , pp 119-121 (1978).

3. Y. Shima, N. Chinone, and R. Ito, "Effects of Facet Coatings on the Degradation Characteristics of GaAs-$Ga_{1-x}Al_xAs$ DH Lasers" Appl. Phys. Lett. **31** , pp 625-627 (1977).

4. F. R. Nash, R.L. Hartman, N.M. Denkin, and R.W. Dixon "GaAs Laser Reliability and Protective Facet Coatings" J. Appl. Phys. **50** , pp 3123-3132 (1979).

5. H. Yonezu, M. Ueno, T. Kamejima, and I. Hayashi, "An AlGaAs Window Structure Laser", IEEE J. Quantum Electronics **QE-15** , pp 775-781 (1979).

6. S. Takahashi, T. Kobayashi, H. Saito, and Y. Furakawa, "GaAs-AlGaAs DH Lasers with Buried Facet", Japan J. Appl. Phys. **17** , pp 865-870 (1978).

7. N. Chinone, K. Saito, R. Ito, K. Aiki, N. Shige, "Highly Efficient (GaAl)As Buried Heterostructure Lasers with Buried Optical Guide", Appl. Phys. Lett. **35** , pp 513-516 (1979).

8. K. Saito and R. Ito "Buried Heterostructure AlGaAs Lasers" IEEE J. Quantum Electron. **QE-16** ,pp 205-215 (1980).

Chapter V

AlGaAs Inverted Strip Buried Heterostructure Lasers

5.1 Introduction

Large optical cavity buried heterostructure (LOC BH) lasers have recently been developed by Chinone *et al.*[1] which have many highly desirable characteristics. These lasers have low threshold currents (8-10 mA/μm stripe width), high differential quantum efficiencies (60-80%), and operate stably in a single transverse and longitudinal mode. However, fundamental transverse mode operation is achievable only for relatively narrow stripe widths. The maximum allowable stripe width is typically between 2 and 3 microns depending on the exact composition of the layers. As a result the power output of these lasers is limited by catastrophic mirror damage to approximately 20 mW CW and 80 mW for 100 nsec pulses. Scattering of light by irregularities in the sidewalls of the waveguide can also result in a significant degradation of beam quality. This is of particular importance for lasers with stripe widths less than 2 microns[2]. A second important type of buried heterostructure laser is the strip buried heterostructure (SBH) laser developed by Tsang *et al.*[3] These lasers can be operated in a stable fundamental mode for strip widths up to 5 microns and are much less susceptible to degradation of beam quality due to scattered light. However, fabrication of this laser requires epitaxial growth on top of an $Al_xGa_{1-x}As$ guide layer. Initiation of growth on air exposed AlGaAs layers of aluminum content greater than 0.1 is very difficult due to the formation of an oxide layer on the exposed AlGaAs surface. To obtain good growth on top of the guide layer requires a precisely controlled meltback prior to the second liquid phase epitaxial (LPE) growth. By comparison the layers of the second LPE

growth of the LOC BH lasers are grown starting from the GaAs substrate and can be simply and reliably grown without a meltback. In this chapter the fabrication of inverted strip buried heterostructure lasers (ISBH), which combine many of the desirable features of the LOC BH and SBH lasers, is described. A detailed comparison between the fabrication steps of the ISBH and SBH lasers is also included.

The ISBH laser structure is shown schematically in fig. 1. The structure resembles that of the LOC BH laser except the active and the lower cladding layers are narrower in width than the $Al_{.24}Ga_{.76}As$ optical guide layer. This results in two significant changes in the modal characteristics of the laser. First, the laser mode is isolated from the sidewalls of the optical guide layer, in which most of the power propagates. This greatly reduces irregularities in the far field patterns of the lasers due to scattered light. The lateral near field intensity of an ISBH laser, calculated using the effective index method (see chapter 3) is shown in fig. 2. As can be seen most of the power is confined within the width of the optical guide. Second, the confinement of the mode in the lateral direction by a weakly guiding strip loaded waveguide makes possible operation of these lasers in the fundamental transverse mode for wider stripe widths than can be achieved for LOC BH lasers. The reason for this is that the higher order modes are less well confined to the active layer and therefore have significantly lower modal gains than the fundamental mode.

As was mentioned in chapter 3, the transverse spatial mode in which the laser operates is determined primarily by the mode reflectivities and the mode confinement factors. Fig. 3b shows the mode reflectivities of the 4 lowest order lateral spatial modes of an ISBH laser. In this case the aluminum contents of the burying layers were taken to be 0.35. The mode reflectivities were calculated

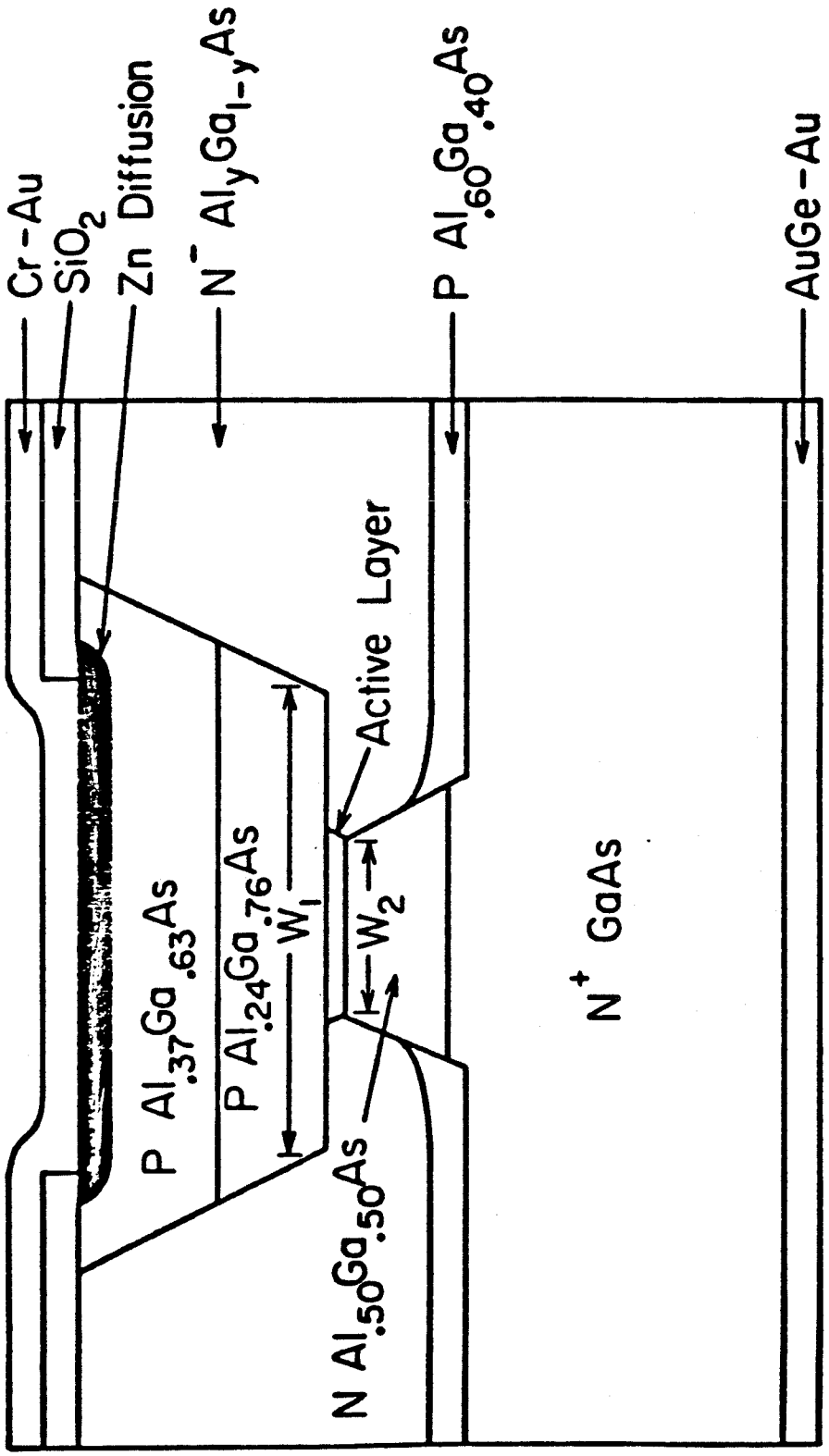

Fig. 1 Cross section of an ISBH laser

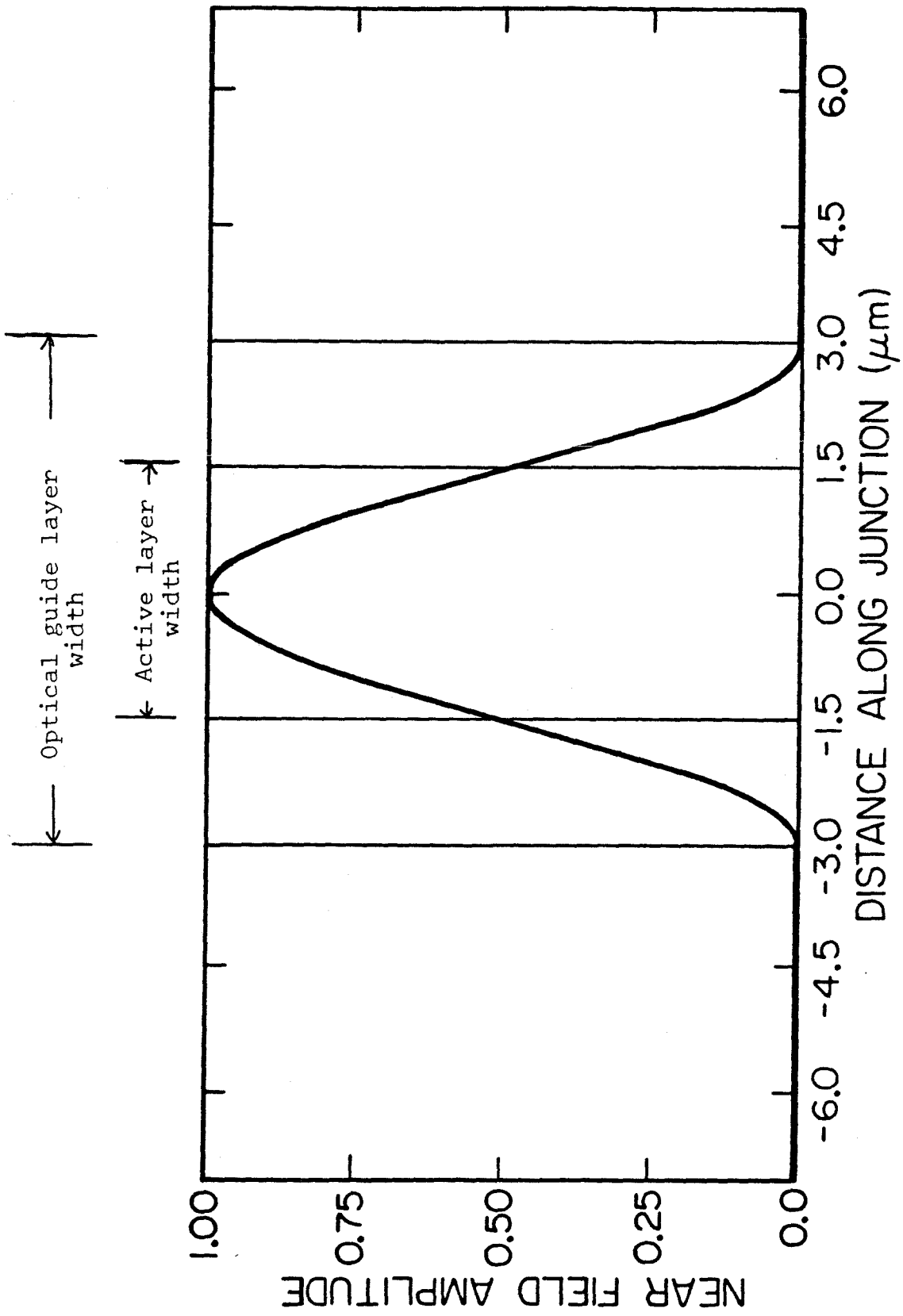

Fig. 2 Mode profile in the lateral direction of the fundamental mode of an ISBH laser

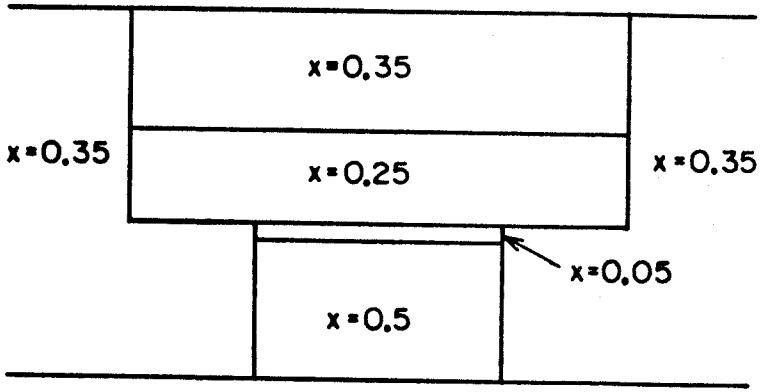

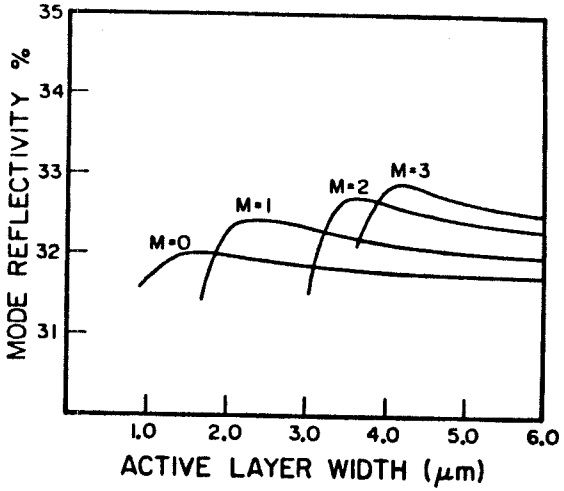

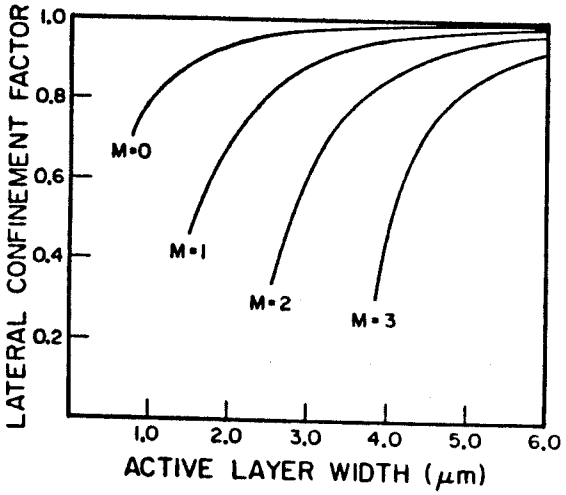

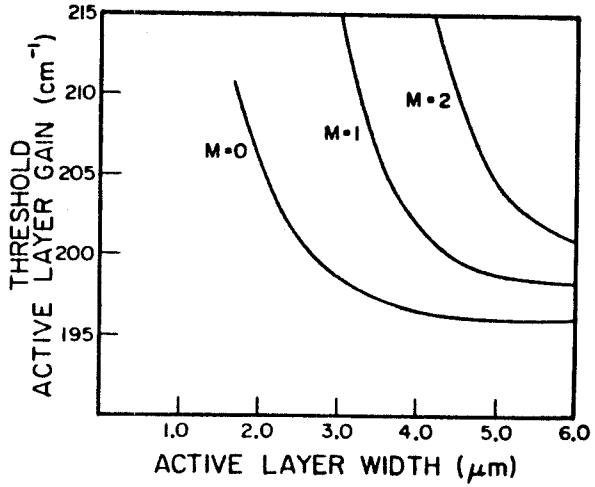

Fig. 3 a) Cross section of an ISBH laser
b) Reflectivity of the modes of an ISBH laser
c) Lateral confinement factors of the modes of an ISBH laser
d) Active layer threshold gains of the modes of an ISBH laser

using the method described in chapter 3. Fig. 3c shows the confinement factors calculated by the effective index method of the same 4 lowest order modes vs. stripe width. If these confinement factors are compared to the lateral confinement factors of a LOC BH laser with the same aluminum content in the burying layers (see chapter 3), it can be seen that the ISBH laser has a significantly stronger preference for the lowest order mode due to the difference in confinement factors. This is because the strip BH laser structure provides weaker lateral optical guiding than does the LOC BH laser structure. Combining the results shown in fig. 3b and 3c the active layer gain required for each mode to reached threshold is plotted in fig. 3d vs stripe width. For the calculation shown in fig. 3d it is assumed that there are no internal losses, such as from free carrier absorption or optical scattering. In this case, the threshold gain is given by:

$$g_{mth} = \frac{1}{\Gamma_m L} \ln\left(\frac{1}{R_m}\right) \tag{5.1}$$

where

$$\Gamma_m = \frac{\int_{-W/2}^{W/2}\int_{-d/2}^{d/2} |E|^2 dxdy}{\int_{-\infty}^{\infty}\int_{-\infty}^{\infty} |E|^2 dxdy} \tag{5.2}$$

where

W = Active layer width

d = Active layer thickness

g_{mth} = active layer gain at which mode m reaches threshold

The transverse mode that oscillates is the mode which reaches threshold at the lowest active layer gain. It is almost always desirable to have the laser oscillate in the fundamental mode. For many applications, such as those which require high output powers it is desirable to obtain fundamental mode operation for as

wide an active layer (wide emitting area) as possible. In practice, fundamental mode operation is generally achievable in buried heterostructure lasers only for active layer widths less than 1.5-2 microns. The results shown in fig. 3 predict that the ISBH laser will operate in the fundamental mode for active layer widths up to 6 microns, which was the maximum stripe width calculated. In practice, fundamental mode operation was achieved only for active layer widths up to 4 microns. The discrepancy is most likely due to inaccuracies introduced by the use of the effective index method, which probably resulted in an overstating of the confinement factor advantage of the fundamental mode.

5.2 Fabrication of ISBH Lasers

The steps involved in the fabrication of ISBH lasers are illustrated in fig. 4. The fabrication of ISBH lasers requires two LPE growths. The layers grown in the first growth are an N $Al_{.5}Ga_{.5}As$ bottom cladding layer (1.5 μm thick, Te doped), an $Al_{.05}Ga_{.95}As$ active layer (.10 μm thick, undoped), a P $Al_{.24}Ga_{.76}As$ optical guide layer (0.8 μm thick, Ge doped), and a P $Al_{.37}Ga_{.63}As$ top cladding layer (1.0 μm thick, Ge doped). After the first growth, mesas are formed by etching down to the GaAs substrate using H_2SO_4:H_2O_2:H_2O 1:8:8. The width of the guide layer after the mesa etch, W_1, is typically 5-7 microns. Next the bottom cladding layer is selectively etched in an HF etch until the top of the mesa is undercut by 1-1.5 microns. The portion of the active layer which is exposed after the HF etch is then selectively removed using H_2O_2 (pH=7.0). The width of the remaining portion of the active layer, W_2, is typically 2.5-4 microns. Next a thin P $Al_{0.6}Ga_{0.4}As$ layer and an N $Al_yGa_{1-y}As$ layer are grown in the second LPE growth. As in the case of the LOC BH lasers, these layers are grown starting from the GaAs substrate. A meltback step is not required, nor are there any limitations on the aluminum content of the optical guide layer. Fig. 5 is a scanning electron microscope photograph of a cleaved cross section of an ISBH laser. For

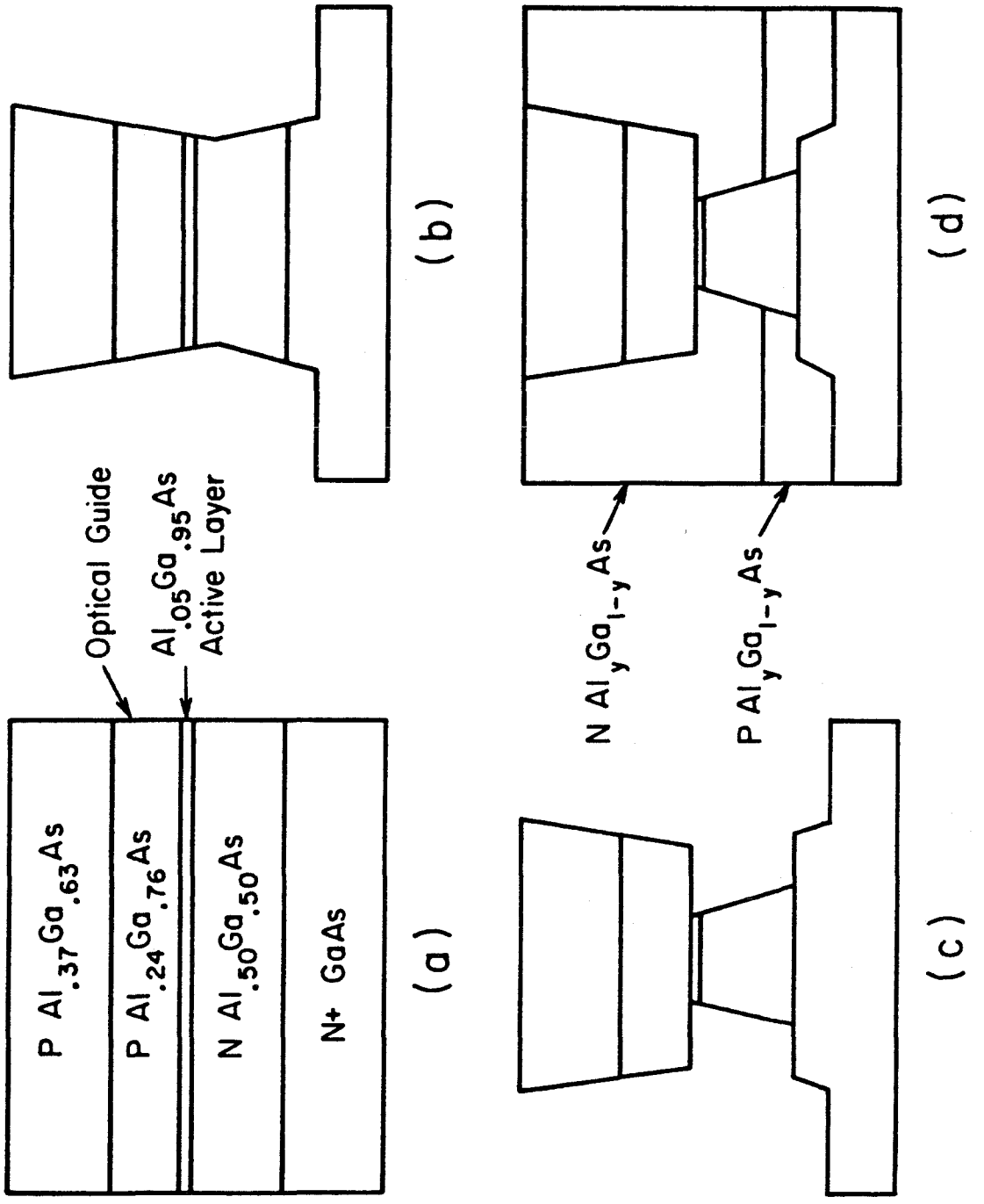

Fig. 4 Steps in the fabrication of ISBH lasers

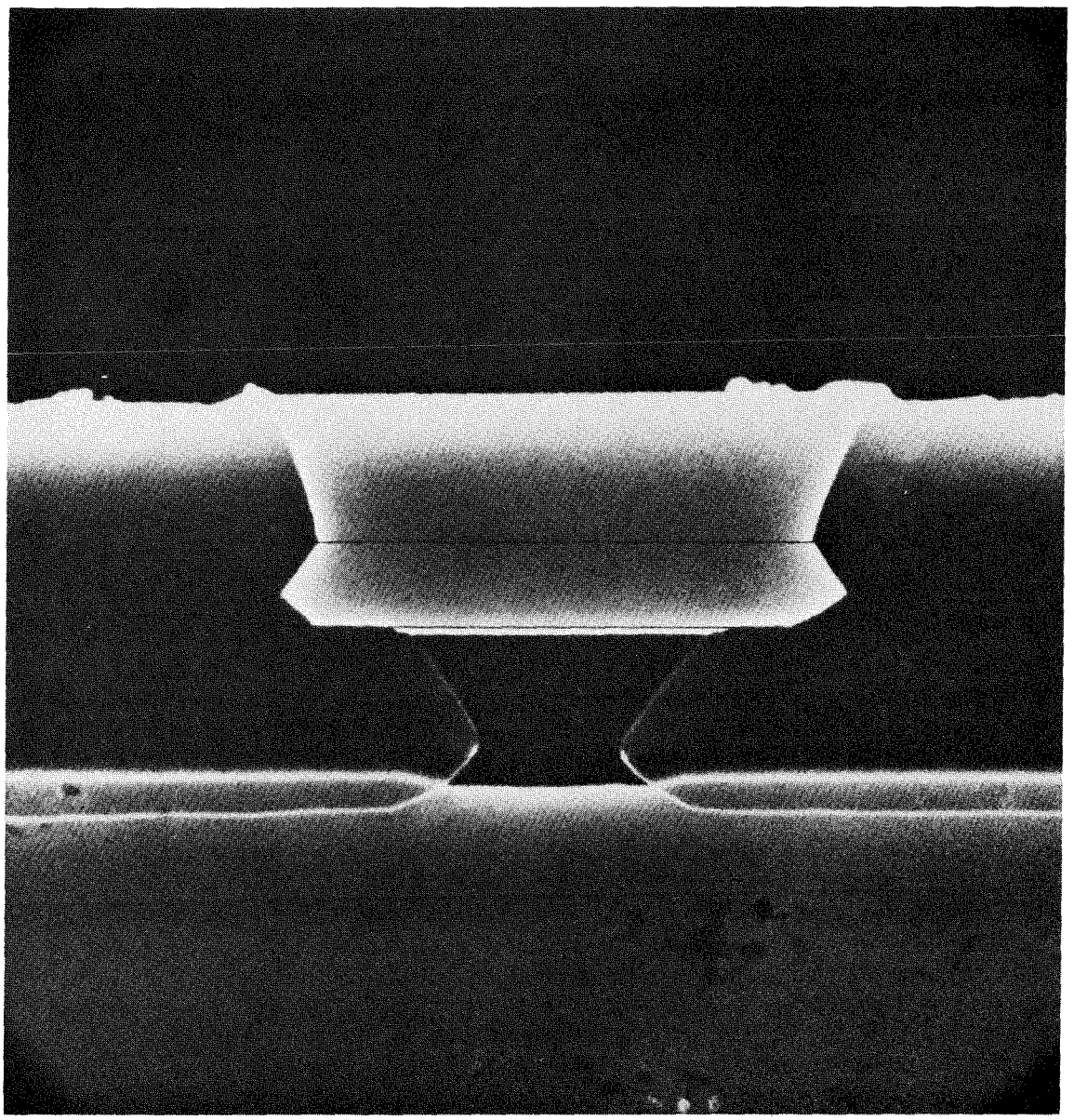

Fig. 5

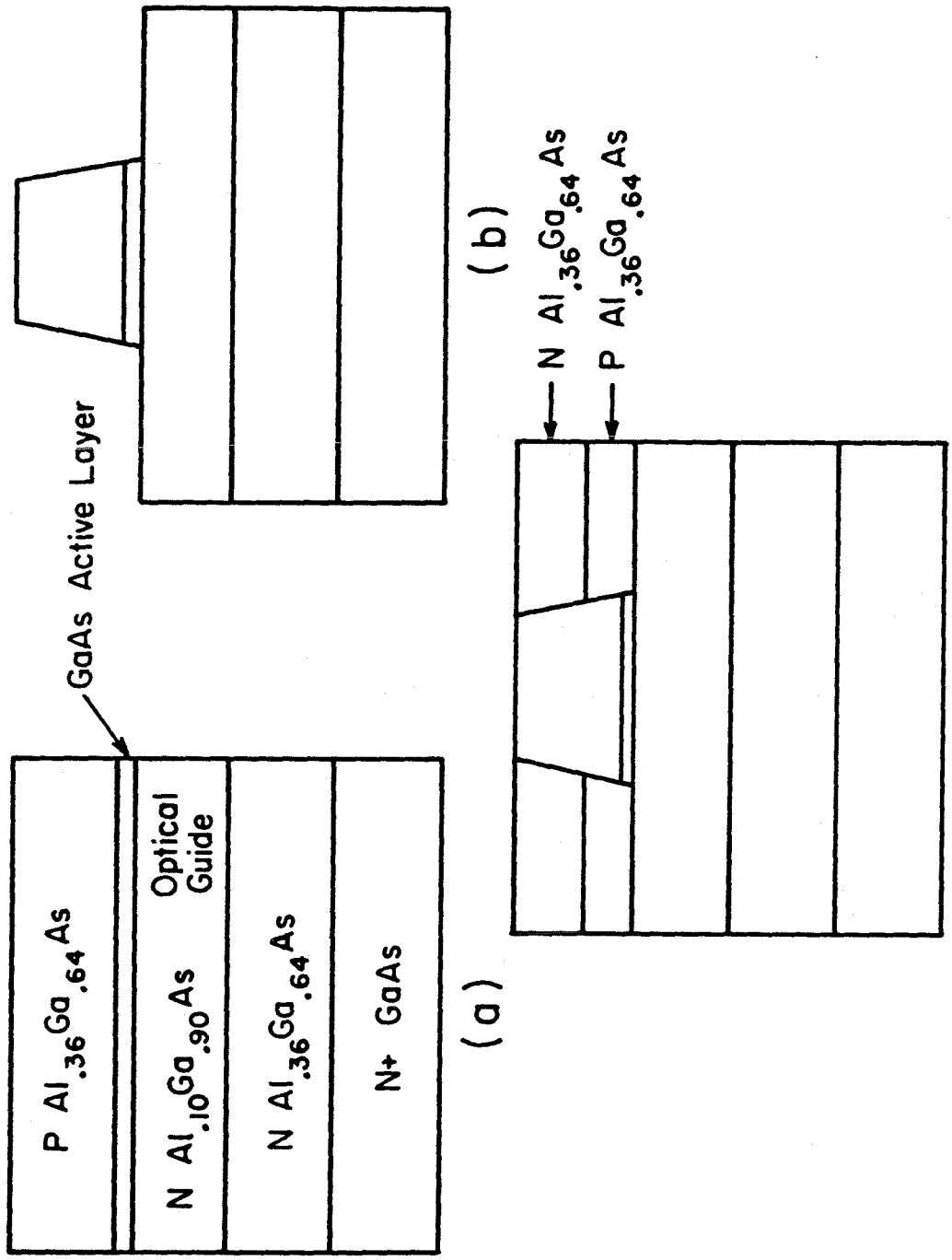

Fig. 6 Steps in the fabrication of strip buried heterostructure lasers

purposes of comparison, the steps involved in the fabrication of strip buried heterostructure lasers are shown in fig. 6. The main disadvantage of the SBH laser is that it requires an LPE growth initiated on top of the optical guide layer. Initiation of growth on air exposed AlGaAs layers of aluminum content greater than 0.1 is very difficult due to the formation of an oxide layer on the exposed AlGaAs surface.

Normally, LOC BH lasers are grown with N type optical guide layers to minimize electron leakage. For a double heterostructure with a given difference in the aluminum contents of the active and cladding layers, the leakage of electrons into the P cladding layer will be greater than the leakage of holes into the N cladding layer[4]. If a relatively low aluminum content optical guide layer is incorporated into the laser structure, it is therefore desirable that it be N type. The use of N type GaAs substrates causes the active layer to be on top of the guide layer. However, it is difficult to fabricate these lasers with the active layer on top of the guide layer, since this would require growing over the AlGaAs guide layer in the second LPE growth. Having the active layer underneath the optical guide layer, makes it possible to grow the layers in the second growth starting from the GaAs substrate. ISBH lasers can still have N type optical guide layers if p type GaAs substrates are used.

5.3 Properties of ISBH Lasers

ISBH lasers were found to have threshold currents and differential quantum efficiencies that were nearly identical to those of LOC BH lasers fabricated in our lab. For 300 μm cavity lengths, pulsed threshold currents were typically 25-30 mA for 2.5 μm wide active layers and 35-40 mA for 4 μm wide active layers. CW thresholds were approximately 10% higher. Differential quantum efficiencies were generally 50-60%, and exceeded 70% in a few devices. ISBH lasers operated

stably in a single transverse and longitudinal mode. For lasers with $Al_{.3}Ga_{.7}As$ burying layers ISBH lasers operated predominantly in the fundamental transverse mode for active layer widths, W_2, up to 4 microns. By comparison, LOC BH lasers fabricated *in our lab* operated predominantly in the fundamental mode only for active layer widths less than 2 microns. Since fundamental mode operation of LOC BH lasers for stripe widths greater than 2 microns has been achieved elsewhere[2], it is possible that predominantly fundamental mode operation of ISBH lasers with stripe widths greater than 4 microns can also be achieved by optimizing this structure. A second important characteristic of ISBH lasers was that irregularities in the far field patterns of the lasers were greatly reduced as compared to LOC BH lasers that we have fabricated. Fig. 7 shows lateral far field patterns for ISBH lasers with active widths of 2.5 and 4 microns. Although the LOC waveguide structure can support two modes in the direction perpendicular to the junction, ISBH lasers typically operated in the fundamental mode in the direction perpendicular to the junction. The full width half maximum of the far field in this direction was typically 30–35°.

The effect of varying the aluminum content of the $Al_yGa_{1-y}As$ burying layer has also been investigated. The modal characteristics were found to be much less sensitive to the aluminum content of the burying layers than were conventional LOC BH lasers, although increasing the aluminum content, y, of the burying layer from 0.3 to 0.6 decreased the maximum stripe width for which fundamental mode operation was obtained from 4 μm to 3 μm. However, the lasers with y=0.6 had significantly improved thermal characteristics. Similar results have recently been reported for conventional BH lasers with high aluminum content burying layers[5]. Lasers with y=0.6 operated CW at output powers up to the catastrophic optical damage limit even when mounted junction up. The temperature dependence of the pulsed threshold current for ISBH

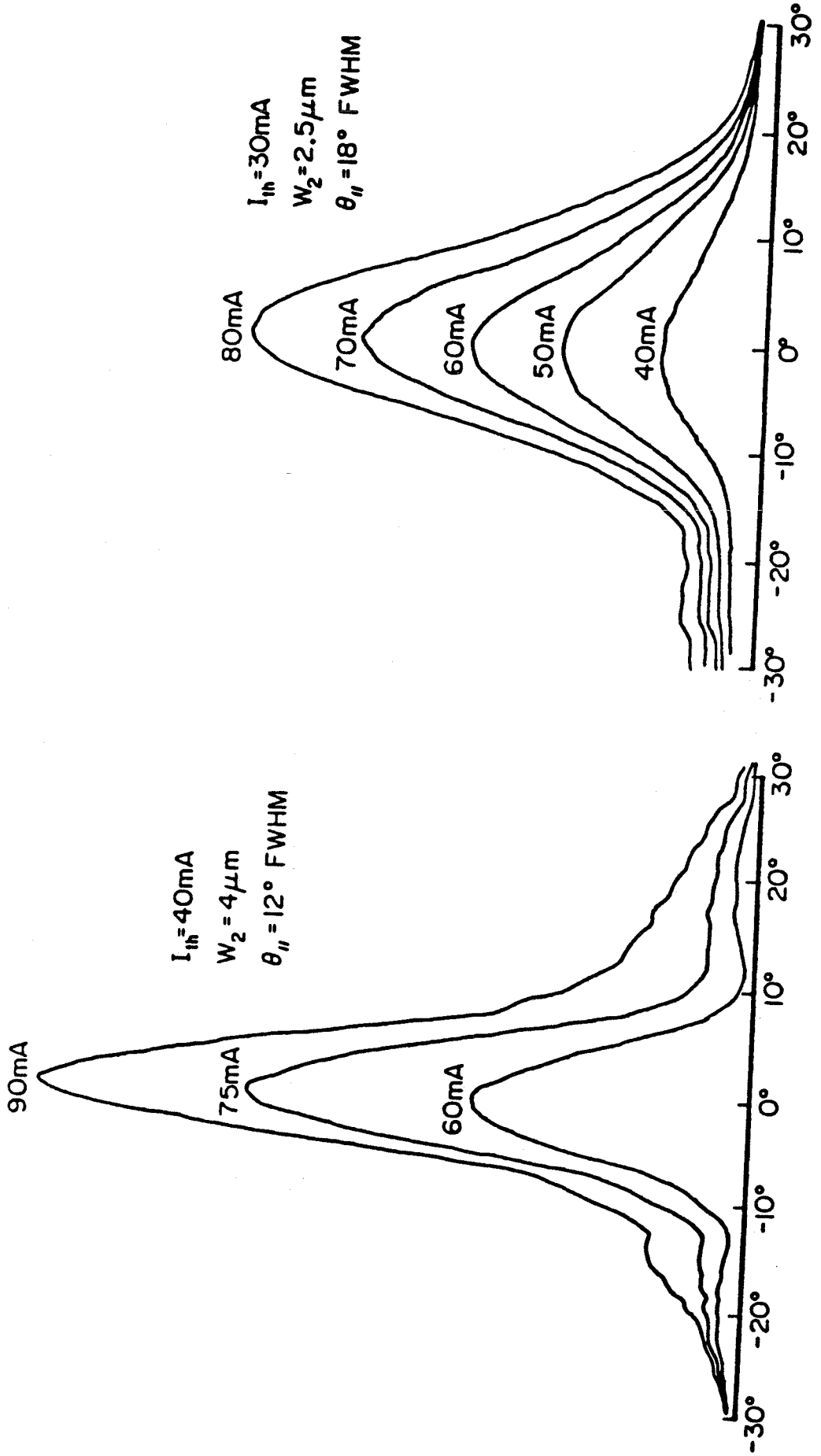

Fig. 7 Far field patterns of ISBH lasers

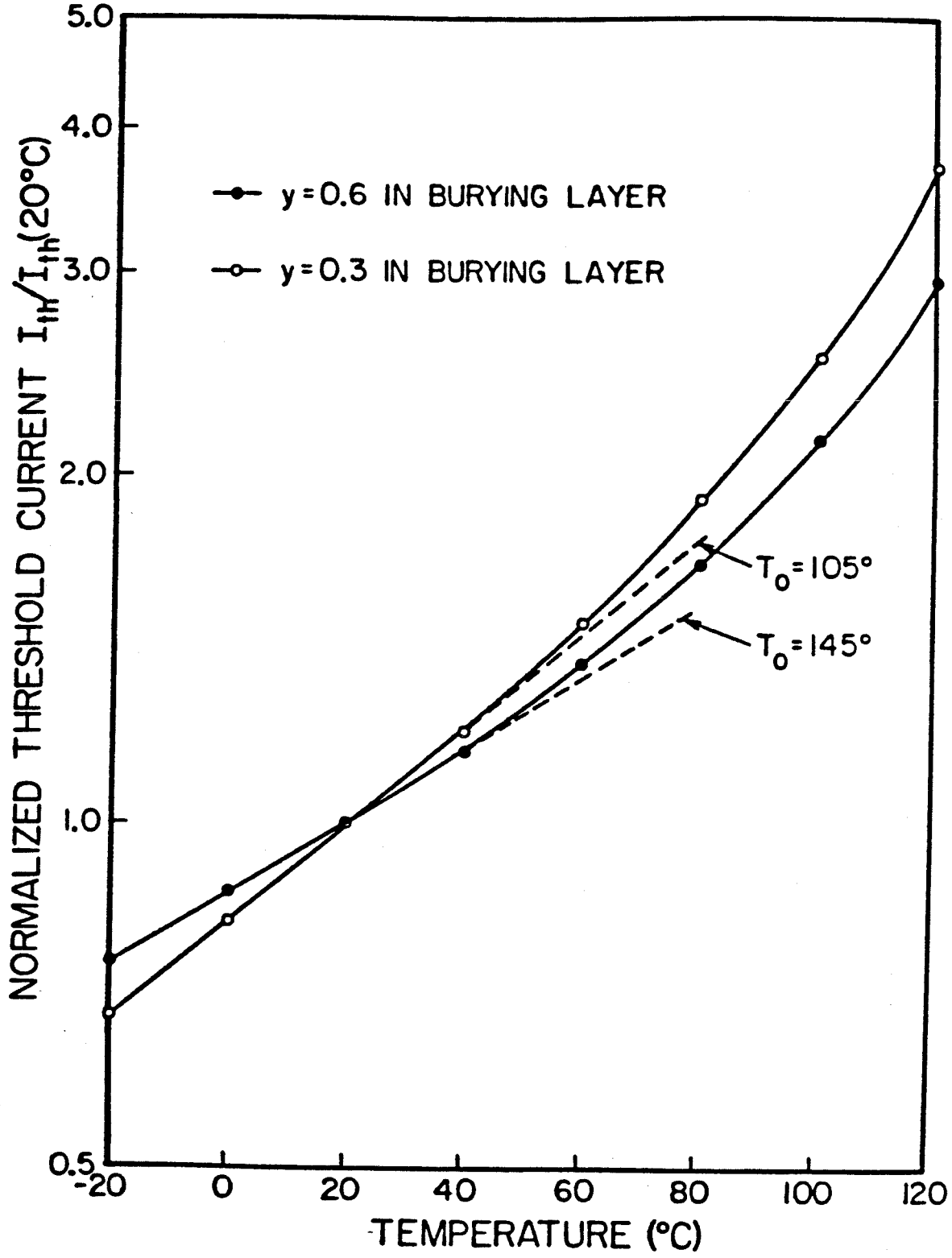

Fig. 8 Temperature dependence of the pulsed threshold current of ISBH lasers

lasers is shown in fig. 8. The improvement in the high temperature operating characteristics is believed to be due to the reduction in the shunt currents flowing on the sides of the mesa when high aluminum content burying layers are used. The shunt currents are expected to decrease due to both the higher bandgap of the burying layer and the larger resistivity that is typically obtained for layers with high aluminum contents.

In chapter 4, the fabrication of large optical cavity buried heterostructure window lasers in which the active layers did not extend to the mirrors[6] was described. These lasers were operated at powers up to 130 mW/μm stripe width per facet. This was three times the power density at which otherwise identical lasers in which the active layer extended to the mirrors failed by catastrophic mirror damage. Since the output power was limited by heating, even larger power densities should be possible from this structure by improving the thermal characteristics of these lasers. In the LOC BH window lasers, fundamental mode operation was achieved only for stripe widths up to 2 μm and the far fields were frequently highly irregular due to scattered light. However, the window laser technology is completely compatible with the ISBH laser structure and it is believed that the application of the window technology to the ISBH structure will result in significant improvements in output power and beam quality as compared to the LOC BH window lasers.

In conclusion, inverted strip buried heterostructure lasers have been fabricated which have threshold currents and quantum efficiencies that are comparable to those of conventional LOC BH lasers. However, predominantly fundamental transverse mode operation of ISBH lasers was obtained for stripe widths up to 4 μm which was twice as wide as fundamental mode operation was obtained in LOC BH lasers. The beam quality of ISBH lasers was found to be significantly improved as compared to LOC BH lasers which have been fabricated

in our lab. Finally, the ISBH laser structure is compatible with a recently developed window laser technology. Fabrication of ISBH window lasers may result in significant improvements in the output power and beam quality over that obtained with LOC BH window lasers.

References

1. N. Chinone, K. Saito, R. Ito, K. Aiki, N. Shige, 'Highly Efficient (GaAl)As Buried Heterostructure Lasers with Buried Optical Guide", Appl. Phys. Lett. **35** , pp 513-516 (1979).

2. H. Nakashima and K. Aiki, 'Transverse Mode Control and Reduction of Threshold Current in (GaAl)As Buried Heterostructure Lasers with a Buried Optical Guide Japan J. Appl. Phys. **19** , pp L591-L594 (1980).

3. W.T. Tsang and R. Logan, "GaAs-$Al_xGa_{1-x}As$ Strip Buried Heterostructure Lasers", IEEE J. Quantum Electron. **QE-15** ,pp 451-469, (1979).

4. H.C. Casey 'Room Temperature Threshold Current Dependence of GaAs $Al_xGa_{1-x}As$ Double Heterostructure Laser on X and Active Layer Thickness", J. Appl. Phys, **49** , pp 3684-3692 (1978).

5. C. Henry, R. Logan, and F. Merritt, 'Single Mode Operation of Buried Heterostructure Lasers by Loss Stabilization", IEEE J. Quantum Electron. **QE-17** , pp 2196-2204 (1981).

6. H. Blauvelt, S. Margalit, and A. Yariv, 'Large Optical Cavity Buried Heterostructure Window Lasers" Appl. Phys. Lett. **40** , pp 1029-1031 (1982).

Chapter VI

AlGaAs Buried Heterostructure Lasers with Narrow Carrier Injection

6.1 Introduction

Unlike most laser structures, which only require a single liquid phase epitaxial (LPE) growth, buried heterostructure (BH) lasers require two LPE growths. This is generally considered to be an undesirable feature of the BH lasers because it makes the task of achieving a high device yield substantially more difficult. However, the use of two LPE growths affords a large degree of flexibility, which makes possible the fabrication of many structures that are impossible with just a single LPE growth. The window BH and the inverted strip BH lasers described in chapter 3 and 4 are examples of the types of the devices that can be fabricated by exploiting the flexibility inherent in two LPE growth devices. In this chapter, another example of this flexibility will be described. In this case wide stripe (8 μm) BH lasers have been fabricated with the gain region confined to a narrow region in the center of the stripe. As was mentioned in chapter 3, this provides a strong mode selecting mechanism, which makes possible fundamental mode operation for much wider stripe widths than in a conventional BH laser.

This laser structure, which will be referred to as a narrow injection buried heterostructure (NIBH) laser is shown in fig 1. The most significant feature of this laser structure is that the current is forced to flow through a narrow injecting stripe (N GaAs) beneath the bottom cladding layer. This narrow injection is achieved by the incorporation of a reversed biased PN junction. In this structure, the active layer width and the width of the gain region are independent of one another. If the active layer width is chosen to be much larger than the gain width then NIBH lasers would be expected to behave like gain guided stripe lasers. If the active layer width is chosen to be the same width as the gain region, then NIBH lasers would be expected

Narrow Injection Buried Heterostructure Laser

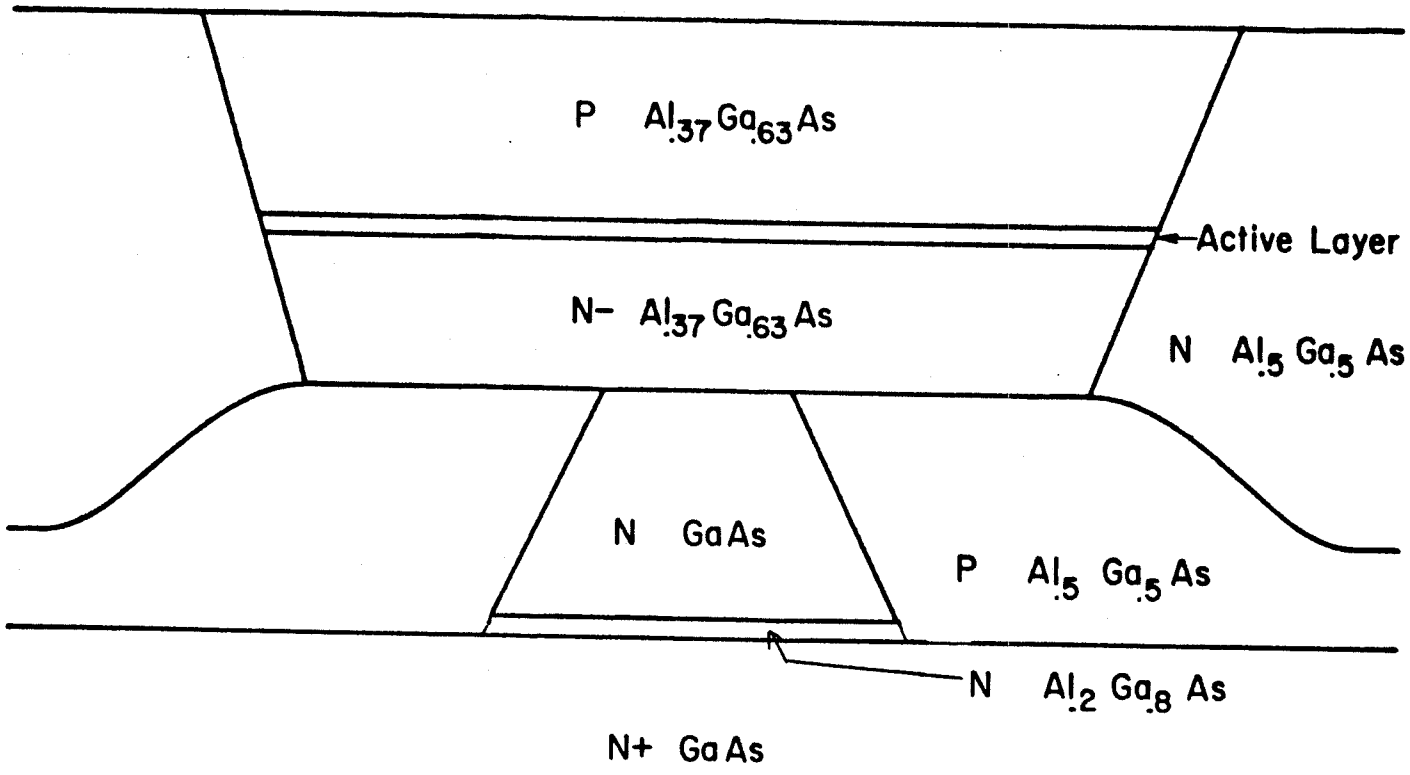

Fig. 1 Cross section of an NIBH laser

to behave like conventional BH lasers. The most interesting case, however, is the intermediate situation where the NIBH laser is behaving like a hybrid of the gain guided and BH lasers.

Before describing the properties of NIBH lasers, some of the more relevant properties of the gain guided lasers[1-4] and BH lasers[5-8] will be first reviewed. These properties are listed below:

BH Lasers

1. Very low threshold currents (8 mA/μm stripe width) and high differential quantum efficiency (typically 40-60%)
2. Single longitudinal mode
3. For narrow stripe widths(less than 2 μm), single and fundamental spatial mode
4. For wider stripe widths, higher order and multi-spatial mode operation occurs, spatial hole burning results in changes in the beam pattern as the power is increased.

Narrow Stripe Gain Guided Lasers

1. Relatively high threshold currents and lower quantum efficiency (30-40%). This is due to poor optical confinement in the lateral direction.
2. Many longitudinal modes.
3. For stripe widths less than about 5 μm the beam pattern is stable as the power is increased. However, the far field pattern is characterized by two peaks rather than a fundamental gaussian-like beam profile. For wider stripe widths the far field pattern is similar to a fundamental gaussian beam pattern at low power levels. At higher output power levels the beam pattern is distorted due to spatial hole burning.

For some applications of semiconductor lasers it would be desirable to combine some of the properties of these two types of lasers. For instance, for multimode fiber-optic communications it is desirable to have a laser that operates stably in the fundamental transverse spatial mode (properties of BH lasers), but oscillates simultaneously in many longitudinal modes (a property of gain guided lasers). The reason that many longitudinal modes are desirable is the attendant reduction of modal noise[10,11]. Another example of a potential advantage of the NIBH laser structure is for a high power single mode laser structure. As was explained in chapter 2, for high power operation it is desirable to increase the size of the emitting area as much as possible while still maintaining fundamental mode operation. The confinement of the gain to the center of the waveguide provides a very strong mode selecting mechanism because the fundamental mode is best confined to the center of the waveguide, thus exercising the maximum gain.

6.2 Fabrication of Narrow Injection Buried Heterostructure Lasers

The fabrication of NIBH lasers is similar to that of conventional BH lasers, requiring two LPE growths. The fabrication steps are illustrated in fig. 2. In the first growth, the layers grown are an N $Al_{.2}Ga_{.8}As$ layer (0.3 μm thick, Sn doped), an N GaAs layer (2 μm thick, Sn doped), an N $Al_{.40}Ga_{.60}As$ bottom cladding layer (1 μm thick, Sn doped), an $Al_{.12}Ga_{.88}As$ active layer (0.3 μm thick, undoped), and a P $Al_{.40}Ga_{.60}As$ top cladding layer (1 μm thick, Ge doped). Next mesas are etched down to the N GaAs epitaxial layer. Typically, the mesa etched is 6-8 μm wide at the active layer. Next the GaAs layer is selectively etched in H_2O_2 (pH=7). This etching is stopped when the width of the GaAs is approximately 3 μm. The H_2O_2 etch will etch AlGaAs layers of aluminum content less than 0.1. We choose aluminum content of the active layer to be 0.12, which is higher than normal, to minimize the etching of the active layer during the GaAs selective etching. The purpose of the lower $Al_{.2}Ga_{.8}As$ layer is to limit the amount of downward etching that occurs during the GaAs

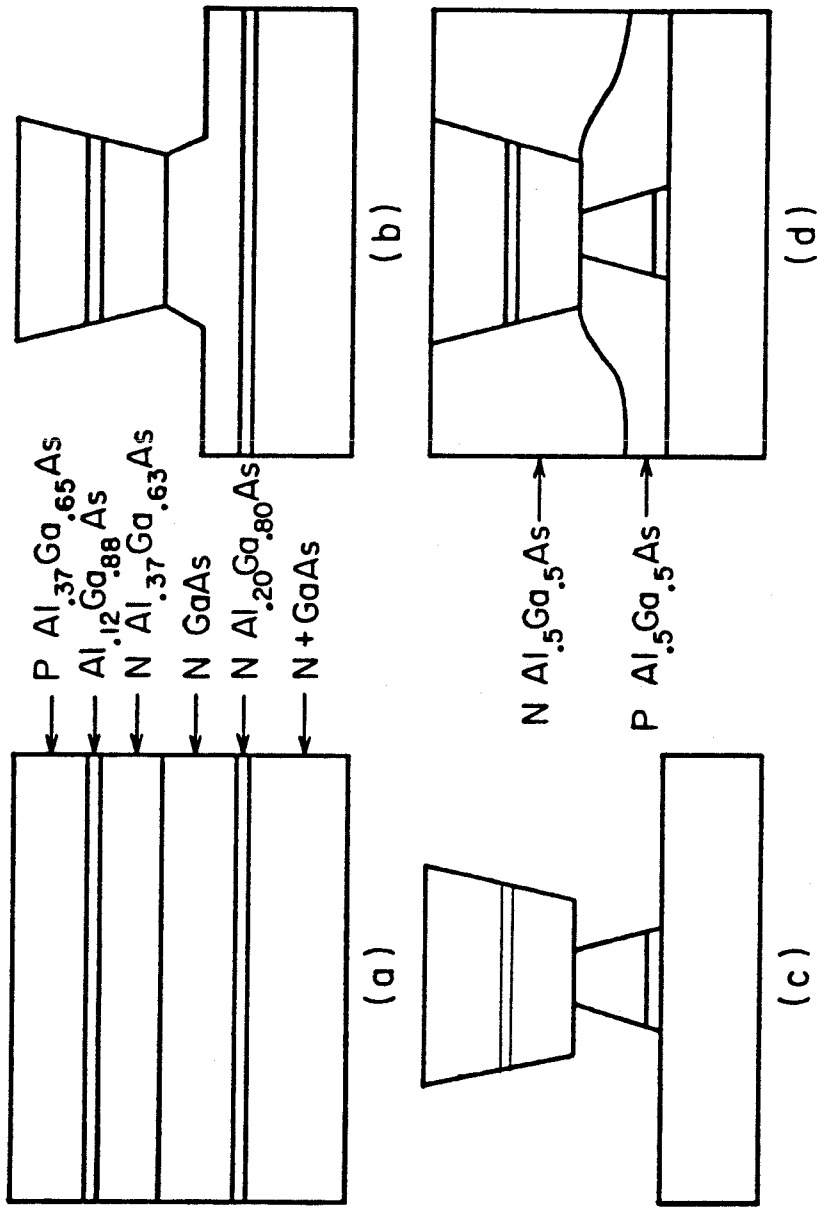

Fig. 2 Steps in the fabrication of NIBH lasers

selective etching. The selective H_2O_2 etch typically etches down twice as fast as it etches laterally. Next, two layers are grown in the second LPE growth. The first layer is a P $Al_{.5}Ga_{.5}As$. It is a property of LPE growth that the growth proceeds in such a manner as to flatten out any irregularities in the surface that were present prior to the growth. As a result, the P layer rapidly fills the undercut that resulted from the selective etching. This P layer provides a reversed biased PN junction, which restricts the current to flow through the narrow top of the N GaAs epitaxial layer. The second layer is N type $Al_{.5}Ga_{.5}As$ and this layer is grown until a flat top surface is obtained.

6.3 Characteristics of Narrow Injection Buried Heterostructure Lasers

The results to be presented for the narrow injection BH lasers were for devices with an active layer width of 6–8 μm and a lower injecting stripe width of 2-3 μm. A conventional BH laser with a stripe width this wide would operate in a high order spatial mode and, because of spatial hole burning, the mode profile would change as the power output is increased. The intention in the laser structure that was investigated was to obtain stable fundamental mode operation by having a narrow gain profile which is best matched to the fundamental spatial mode. Obtaining fundamental mode operation in wide stripe BH lasers would enable the fabrication of single mode lasers with significantly greater output powers. The far field pattern of one of these lasers is shown in fig. 3. As can be seen, for low output powers, the laser operates in the fundamental spatial mode. Fundamental spatial mode operation is never observed in BH lasers of 8 μm stripe width when the active layer is uniformly pumped. Achieving fundamental mode operation in wide stripe lasers is of great importance for high power laser operation since the maximum power available from a semiconductor laser is approximately proportional to the stripe width (see chapter 2). It can also be seen in fig. 3 that at higher output powers there is some distortion of the beam profile, which indicates the laser is operating in

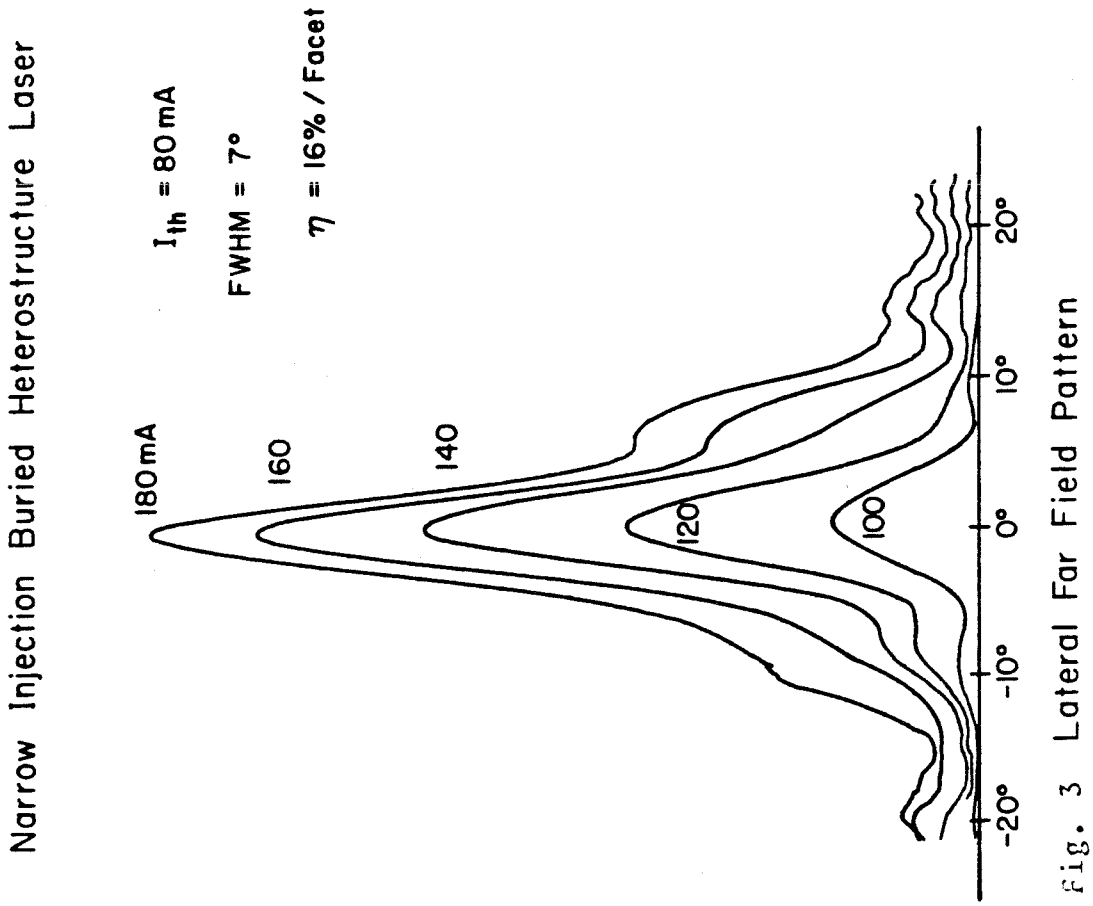

Fig. 3 Lateral Far Field Pattern

more than one spatial mode. For sufficiently narrow gain profiles, it would be expected that the laser would operate only in the fundamental mode at all power levels[11]. If the gain profile is sufficiently narrow, as compared to the optical mode that the optical intensity is nearly uniform over the gain region, then spatial hole burning is impossible. The reason for the failure of these lasers to do so is probably due to current spreading in the lower cladding layer. As a result of this current spreading the width of the gain profile is sufficiently large so that spatial hole burning effects become important. By increasing the sheet resistivity of this layer and narrowing the injecting stripe width, improved mode control shoud be possible in this structure.

As mentioned previously, NIBH lasers can be thought of as a hybrid between narrow stripe gain guided lasers and BH lasers. It is therefore of interest to see whether the characteristics of the laser described in the previous chapter correspond more to those of narrow stripe lasers or to those of BH lasers. Three important characteristics of a laser are the threshold currents, the differential quantum efficiency, and the spectrum. For the laser described above the threshold currents were typically 80-100 mA and the differential quantum efficiency was typically 15% per facet. In both cases, these figures are more characteristic of gain guided stripe lasers than BH lasers. A BH laser with an 8 μm wide active layer would be expected to have a threshold current of 50-60 mA and a quantum efficiency of 20-30% per facet. However, the spectrum of NIBH lasers is more characteristic of BH lasers, which typically operate in a single longitudinal mode. The spectrum of a NIBH laser is shown in fig. 4 . Although, the laser is not single longitudinal mode, there are many fewer modes than the typical 5-10 modes found in narrow stripe gain guided lasers (see chapter 7).

In conclusion, results for a buried heterostructure laser with narrow current injection have been presented in this chapter. These lasers are a hybrid of the

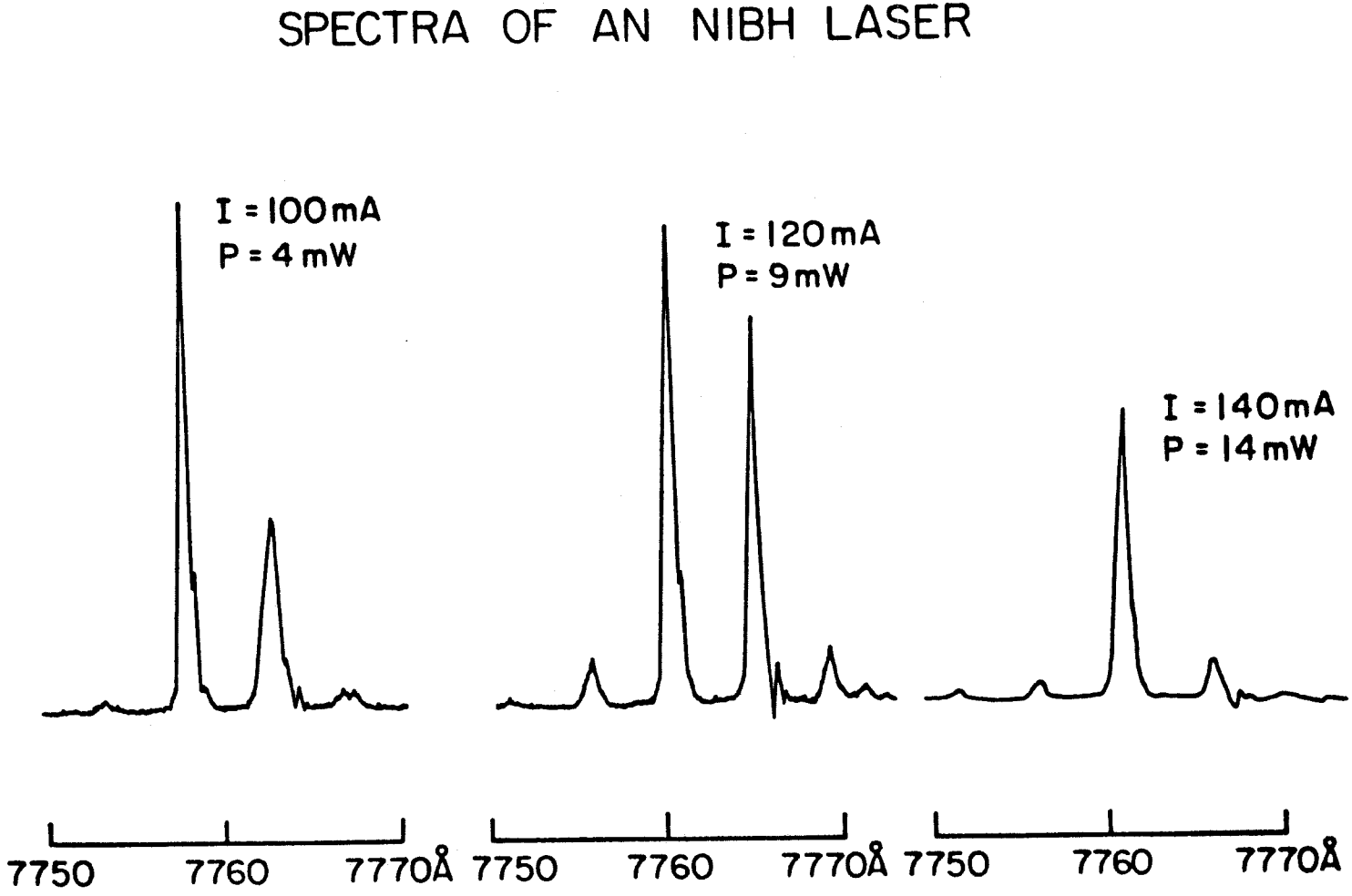

Fig. 4 Spectra of an NIBH laser

narrow stripe gain guided lasers and the buried heterostructure lasers and these lasers show some of the characteristics of each of these classes of lasers. The NIBH structure makes possible the fabrication of a continuum of laser structures in between the two extremes of gain guided lasers and BH lasers. By combining characteristics from the gain guided and BH lasers, it may be possible to fabricate lasers which are better suited to certain applications than are either of the extreme cases.

References for Chapter 6

1. F.R. Nash 'Mode Guidance Parallel to the Junction Plane of Double Heterostructure Lasers", J. Appl. Phys. **44** , pp4696-4707, (1973).

2. P.M. Asbeck, D. Cammack, J. Daniele, and V. Klebanoff. 'Lateral Mode Behavior in Narrow Stripe Lasers", IEEE J. Quant. Electron. **QE-15** ,pp 727-730, (1979).

3. R. Lang. 'Lateral Transverse Mode Instability and Its Stabilization in Stripe Geometry Injection Lasers", IEEE J. Quant. Electron. **QE-15** ,pp 718-726 (1979).

4. W. Streifer, R. Burnham, and D. Scifres. "An Analytic Study of (GaAl)/As Gain Guided Lasers at Threshold", IEEE J. Quant. Electron. **QE-18** ,pp 856-864 (1982).

5. T. Tsukada, "GaAs-$Ga_{1-x}Al_xAs$ Buried Heterostructure Injection Lasers", J. Appl. Phys. **45** ,pp 4899-4906 (1974).

6. K. Saito, R. Ito, 'Buried Heterostructure AlGaAs Lasers" IEEE J. Quantum Electron. **JQE-16** ,pp 205-215 (1980).

7. H. Nakashima and K. Aiki, "Transverse Mode Control and Reduction of Threshold Current in (GaAl)As Buried Heterostructure Lasers with a Buried Optical Guide" Japan. J. Appl. Phys. **19** ,pp L591-L594 (1980).

8. N. Chinone, K. Saito, R. Ito, K. Aiki, N. Shige, 'Highly Efficient (GaAl)As Buried Heterostructure Lasers with Buried Optical Guide", Appl. Phys. Lett. **35** , pp 513-516 (1979).

9. R. Epworth, 'The Phenomena of Modal Noise in Analog and Digital Optical Fiber Systems", Proc. 4th Eur. Conf. Optical Communications (Genoa Italy) , pp 492-501 (1978).

10. R. Epworth, 'The Phenomena of Modal Noise in Fiber Systems", Tech. Dig. Topical Meeting on Optical Fiber Communication (Washington DC) paper ThD1. 1979.

11. K.L. Yu, K.Y. Lau, U. Koren, T.R. Chen, and A. Yariv "Mode Stabilization Mechanism in Buried Waveguide Lasers with Lateral Diffused Junctions", submitted for publication.

Chapter VII

Narrow Stripe AlGaAs Lasers Using Double Current Confinement

7.1 Introduction

One of the most widely studied classes of injection lasers are the gain guided stripe geometry lasers. In these laser structures, there is no built in waveguide to confine the light in the lateral direction. The primary advantage of these laser structures is the simplicity of their fabrication. However, there are several disadvantages of gain guided stripe lasers, such as, higher threshold currents than the more complicated buried heterostructure and transverse junction stripe laser structures. Due to spatial hole burning, the transverse mode patterns of wide stripe, gain guided lasers do not remain stable if the current is increased much above threshold[1,2]. The output beams of gain guided lasers can also have a large amount of astigmatism. Recently, a great amount of work has been reported, both experimentally and theoretically[2,3,4] on the influence of the stripe width on the properties of gain guided lasers. The problem of spatial hole burning has been found to be greatly reduced in narrow stripe lasers, such as the V-groove laser[5]. Narrow stripe lasers having very large astigmatism factors have been reported[6]. These lasers oscillate simultaneously in many longitudinal modes which has been explained by the high spontaneous emission factors expected in lasers with large astigmatism[7,8]. In this chapter, gain guided lasers are described in which the current is confined to flow between two narrow stripes located above and below the active layer. A simple theoretical model of gain guided lasers is also presented which explains many of the characteristics mentioned above The laser structure described in this chapter is a modification of the double current confinement (DCC) configuration developed by Tsang and Logan[9] and is shown in fig. 1. In the original

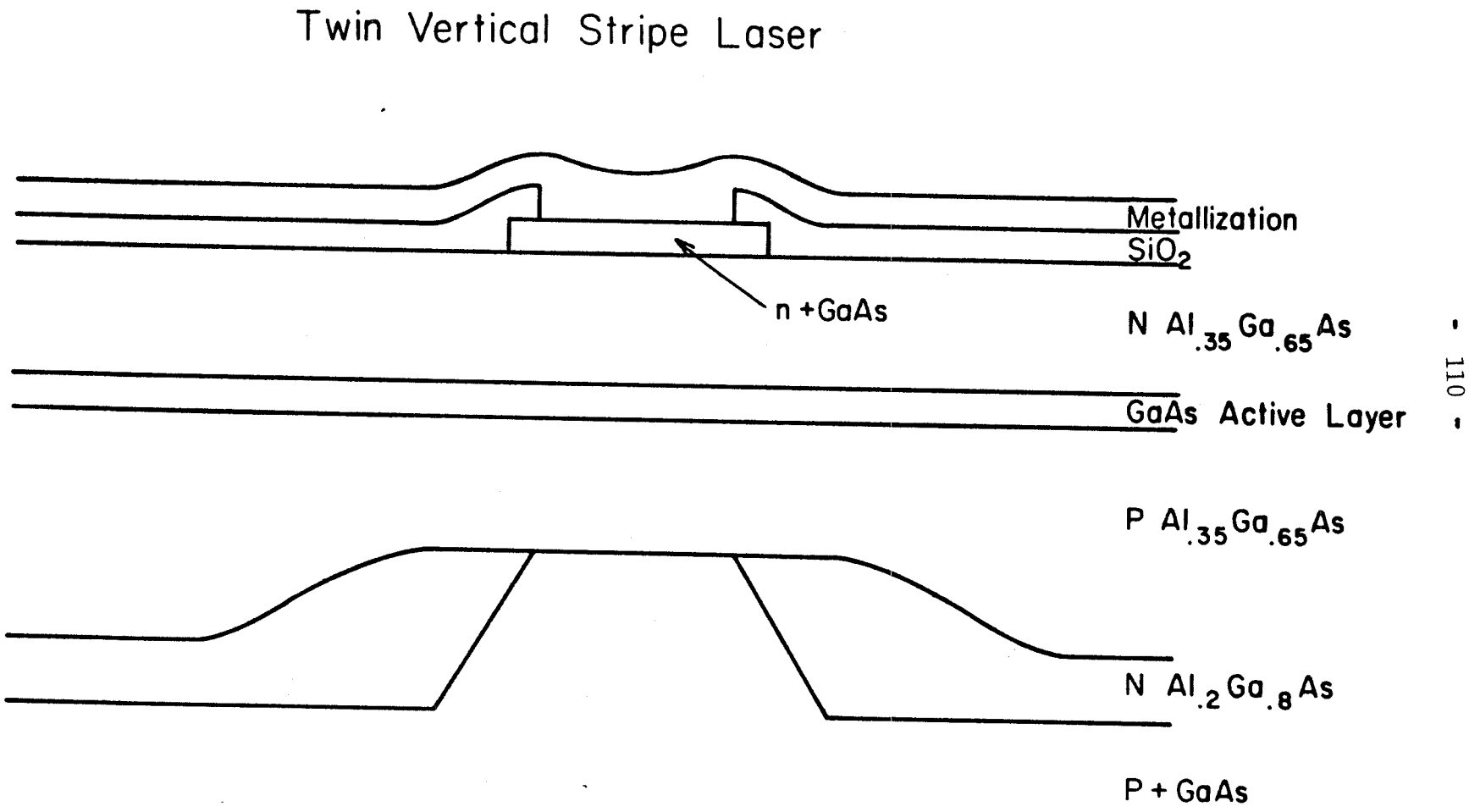

fig. 1 Schematic diagram of the narrow stripe DCC laser structure

DCC structure it was reported to be difficult to obtain injecting stripes with widths less than 10 microns. The structure which will be described is capable of restricting carrier injection to an extremely narrow width of the active layer. Injecting stripe widths of 2 microns were routinely obtained and injecting stripe widths as narrow as 0.5 microns have been obtained. The main emphasis in this chapter will be simply describing the structure and the properties of these lasers. However, it is believed that the narrow stripe DCC configuration has potential applications in the fabrication of low threshold lasers structures and arrays of optically coupled lasers.

7.2 Fabrication of Narrow Stripe Lasers with Double Current Confinement

Current confinement in the narrow stripe DCC lasers is provided by an oxide stripe above the active layer and by N-type blocking layers below the active layer. The fabrication of the narrow stripe DCC structure requires only one liquid phase epitaxial (LPE) growth and is based on the fact that LPE crystal growth proceeds in such a manner as to flatten out any features such as mesas or channels that are present in the substrate prior to the growth[10-12]. In the case of GaAs substrates with etched mesas, in the first stages of the LPE growth, the tops of the mesas can be being melted back at the same time that AlGaAs layers are being grown on the sides of the mesas. It has been shown from thermodynamic considerations[13] that for a given temperature, the surface curvature of a solid effects the chemical potential of the solid. If a liquid is in contact with a solid with a non-planar surface , to maintain equilibrium, variations in the chemical potential of a solid have to be matched by variations in the chemical potential of liquid. The chemical potential of the liquid is in turn directly related to the solute concentration. The deviation in the equilibrium solute concentration near a curved solid surface of radius R is given by the following relation[14]:

$$\frac{\Delta C}{C} = \frac{2\gamma V_m}{kTR} \tag{7.1}$$

where γ is the surface tension, V_m is the crystal molar volume, and R is taken to be positive for a convex solid surface. Thus curved solid surfaces will be in equilibrium at a temperature T_e with a solute concentration $C_e \pm \Delta C$, depending on whether the surface is convex or concave. A melt with a solute concentration of C_e at a temperature of T_e is therefore undersaturated if above a convex solid surface and supersaturated if above a concave solid surface. The undersaturated case results in a meltback of the solid surface and the supersaturated case results in rapid deposition on the solid surface.

Fig. 2a shows a scanning electron microscope (SEM) photograph of the mesas that were etched in the substrate before the growth. The surface of such a mesa is convex at the top and concave at the base. Thus the melt above the top surface is effectively undersaturated while the melt near the base is supersaturated. Fig. 2b shows the growth that results when the substrates were placed under a solution of gallium, saturated with GaAs, for 30 seconds. As can be seen, in this 30 seconds, the top of the mesa was melted back to approximately the position of the waist of the mesa, while at the same time layers were being grown on the sides of the mesa. In the narrow stripe DCC laser structure this effect is used to grow a blocking layer, which restricts the current to flow through a narrow mesa etched in the substrate prior to the growth. The layers grown for the narrow stripe DCC lasers are shown in fig 3. If the blocking layer is grown for a sufficiently short time it will not grow at all above the mesa. In practice, we found that when we used n type substrates that the I-V characteristics of the devices sometimes indicated the presence of a thin blocking layer above the mesa. However, if Zn doped substrates are used this problem is avoided due to the rapid diffusion of Zn through any thin blocking layers that may form above the mesas. LPE growth was carried out at an initial

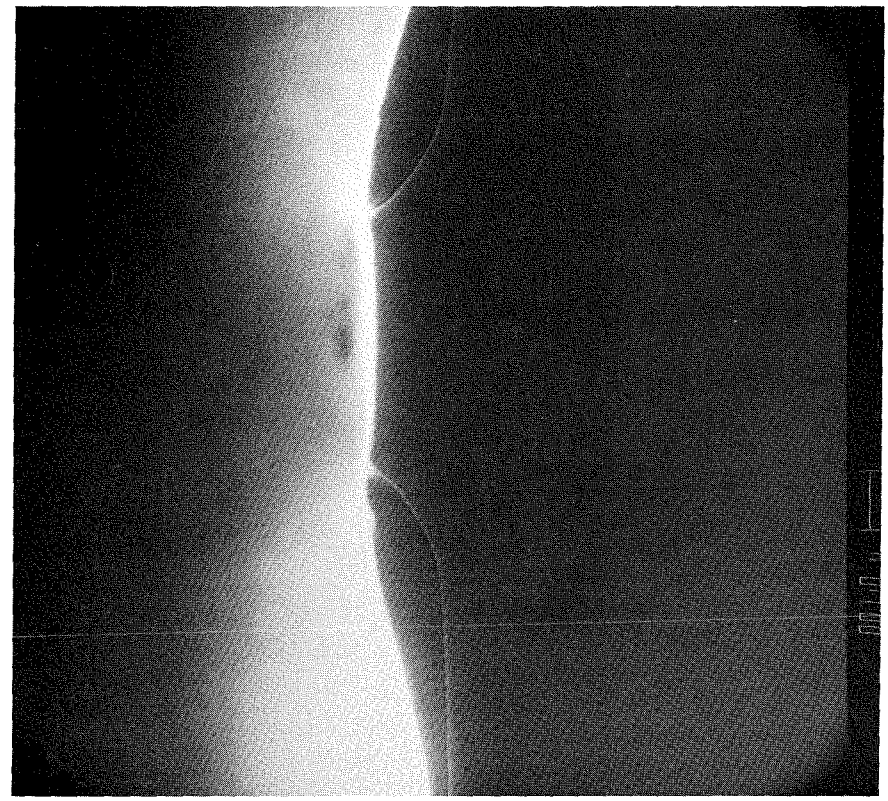

(b)

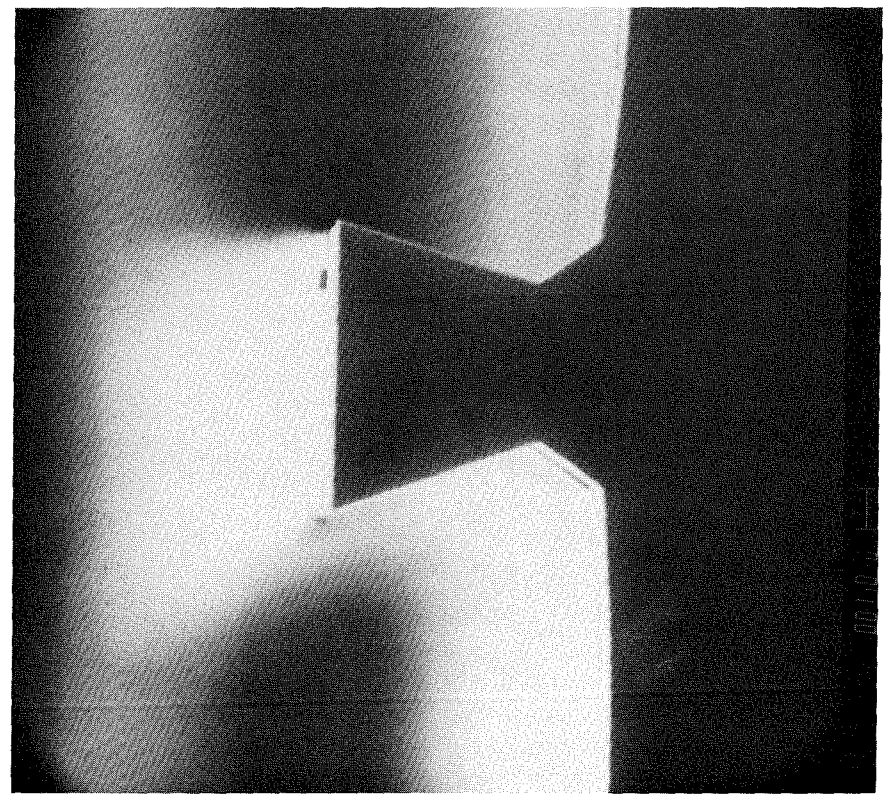

(a)

Fig. 2

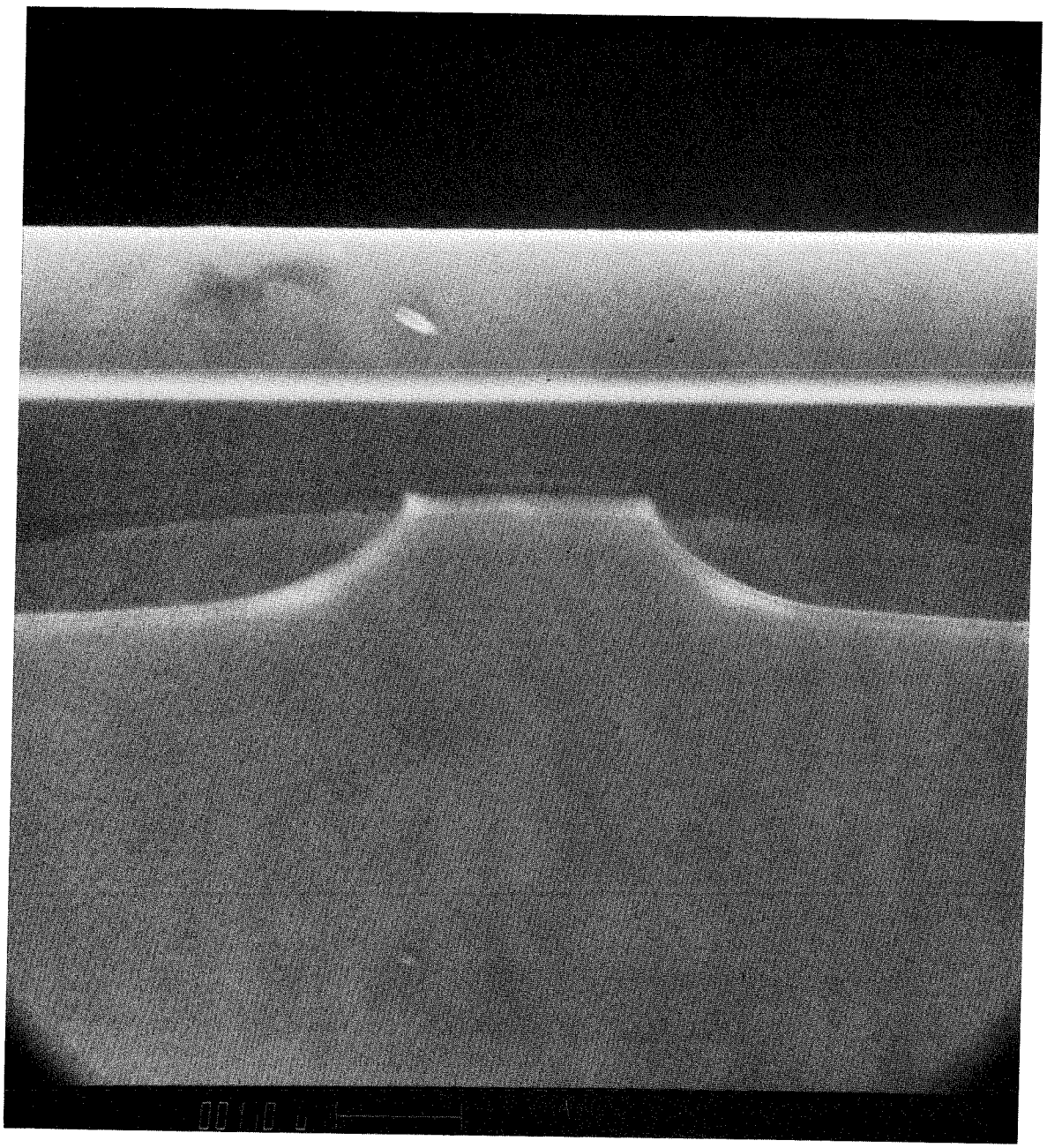

Fig. 3

temperature of 800°C and at a cooling rate of 0.4°C/min.. With these growth conditions the DCC configuration could be obtained for blocking layer growth times between 45 seconds and 3 minutes. For growth times less than 45 seconds the blocking layer is too thin or is discontinuous and for growth times greater than 3 minutes, growth on top of the mesas resulted. For growth times within this range the meltback and growth process was found to be very reproducible, provided the etching of the mesa in the substrate prior to the growth was done reproducibly. One significant feature of this structure is that the lower injecting stripe can be very narrow. Injecting stripes as narrow as 0.5 μm have been fabricated using this technique.

7.3 Properties of Narrow Stripe DCC Lasers

Narrow stripe DCC lasers were found to have several interesting properties. The results to be presented were obtained for a laser with the features listed below. The width of the top GaAs contact layer and the opening in the SiO_2 were 3 μm, the width of the lower injecting stripe was 2 μm, the lower and upper cladding layers were 1 μm thick and doped with Ge and Sn respectively to approximately $5x10^{16}cm^{-3}$. As is the case with other narrow stripe lasers the threshold currents of these lasers are relatively high. Threshold currents varied widely, ranging from 70-150 mA for 250 μm long devices. Differential quantum efficiencies were typically 15-20% per facet. For temperatures between 0°C and 70°C the threshold current was found to be given by the relation $I_{th}=I_{th}(0°C)\exp(T/T_o)$. The characteristic temperature, T_o, for these lasers was a relatively high 170°K.

One of the most interesting properties of these lasers are the far field patterns which are characteristic of a leaky guide. Fig. 4 shows the far field pattern of one of these lasers in the direction parallel to the junction. The lasers with threshold currents at the high end of the 70-150 mA range were found to have far field

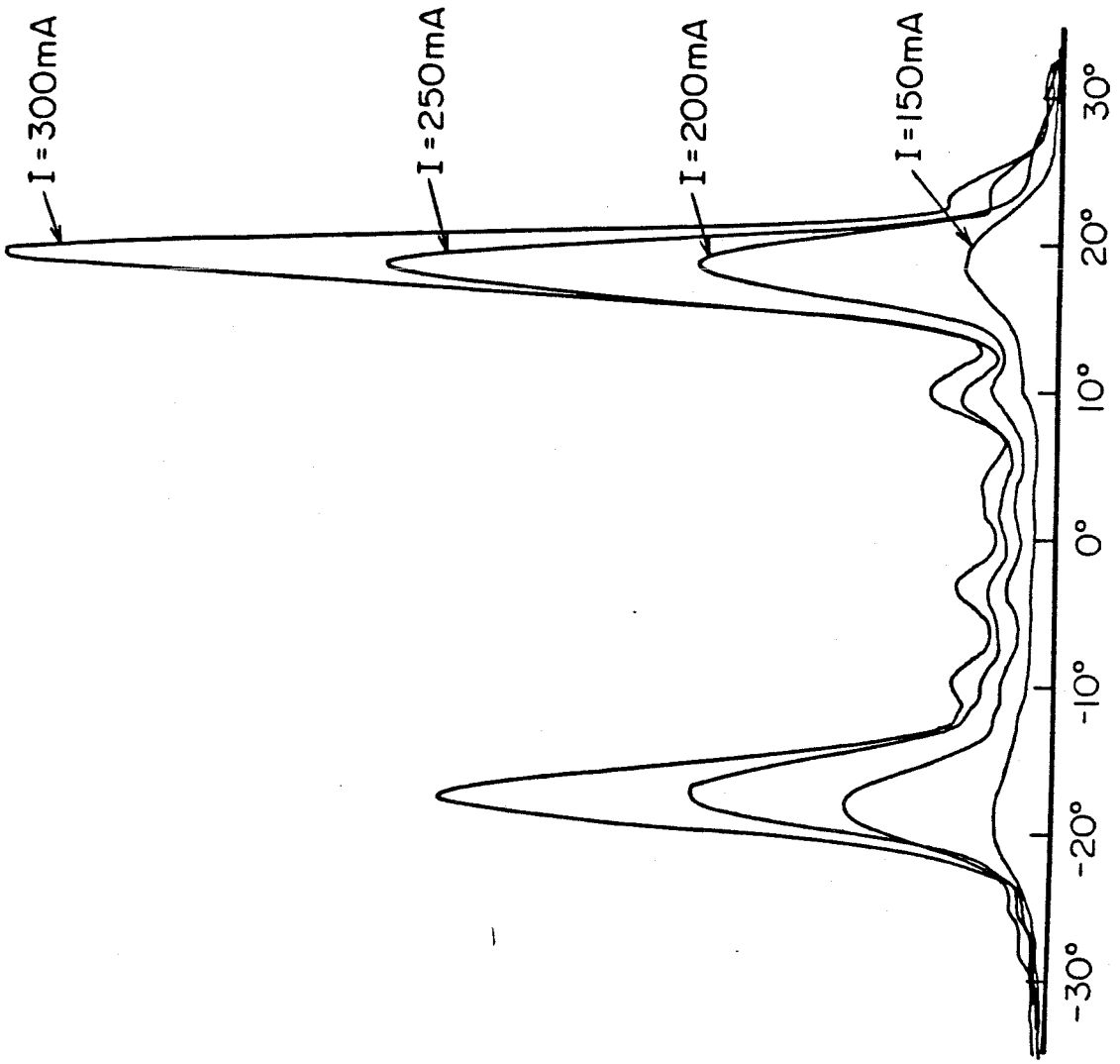

Fig. 4 Lateral far field pattern of a narrow stripe DCC laser

patterns with the most pronounced antiguiding characteristics. The variation in the threshold currents is believed to be due variations in the width of the injecting stripe with the high threshold lasers corresponding to the devices with the most narrow injection. Both the far field patterns and the relatively high threshold currents can be understood by the fact that the real index of refraction is suppressed in the gain region by the high carrier density present there. The resulting strong real index antiguiding causes both the leaky mode far field patterns and the high threshold currents. Far field patterns exhibiting leaky mode characteristics have been reported previously in narrow stripe lasers, however the effect was much more pronounced in these narrow stripe DCC lasers. This is an indication of the very narrow injection that can be achieved in these lasers.

The dependence of the far field pattern on the stripe width can be qualitatively understood by examining the following simple model. In this model the actual gain guided waveguide is represented by a dielectric slab waveguide which has gain in the center layer and loss on the sides. This waveguide is shown in fig. 5. The actual gain guided laser waveguide has continuously varying gain and real index of refraction and can only be solved properly by an elaborate calculation in which Poisson's equation and the wave equation are solved self consistently for the carrier distribution and the optical modes[4]. Nonetheless, most of the important features of the modes of a gain guided laser waveguide can be understood by considering the gain guided dielectric slab waveguide model, which can be solved exactly.

The modes of the gain guided dielectric slab waveguide are the solutions to the wave equation:

$$\nabla^2 E + (k^2 n^2 - \beta^2) E = 0 \qquad (7.2)$$

where n is the complex index of refraction and β is the complex propagation constant. Typically, the differences between the indices of refraction of the core

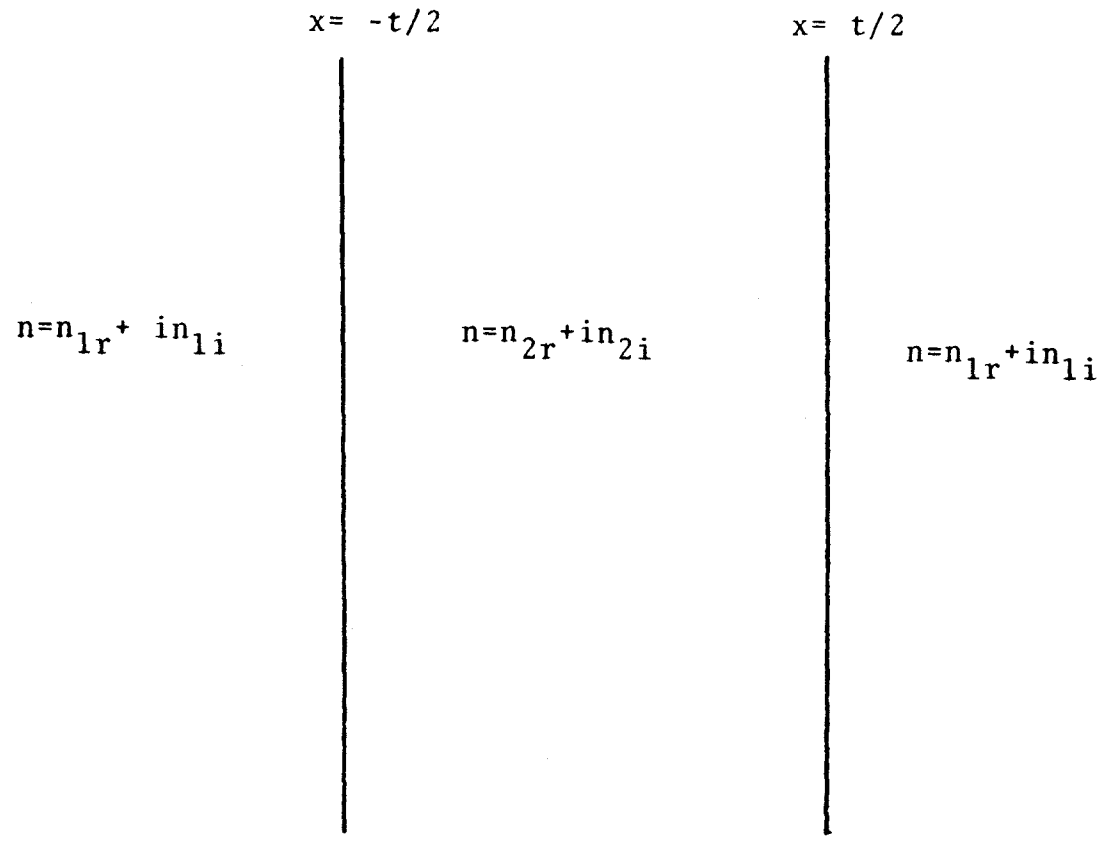

Fig. 5 Gain guided dielectric slab waveguide

layer and the cladding layers is very small and there is little difference between the TE and TM modes of this waveguide. The solutions of the wave equation are then given by:

$$E(x)=\cos(hx) \qquad x< t/2 \qquad (7.3)$$

$$E(x)=\cos(ht/2)\exp(-p|x|) \qquad |x| > t/2$$

for the even modes and

$$E(x)=\sin(hx) \qquad x< t/2$$

$$E(x)=\sin(ht/2)\exp(-px) \qquad x> t/2 \qquad (7.4)$$

$$E(x)=-\sin(ht/2)\exp(px) \qquad x< -t/2$$

for the odd modes.

where

$$h=(k^2n_2^2-\beta^2)^{1/2} \qquad (7.5)$$

and

$$p=(\beta^2-k^2n_1^2)^{1/2} \qquad (7.6)$$

β is determined by the requirement that $\frac{\partial E}{\partial x}$ be continuous. This is satisfied for

$$pt=(ht)\tan(ht/2) \qquad (7.7)$$

for the even modes and

$$pt=(ht)\cot(ht/2) \qquad (7.8)$$

for the odd modes. The lowest order mode of gain guided dielectric slab waveguides with stripe widths of 2,3,and 5 μm are shown in fig 6-9. In all cases the imaginary part of the index of refraction in the cladding layers was taken to be -0.0005, which corresponds to a loss of 38 cm^{-1}. The imaginary part of the index in the core layer

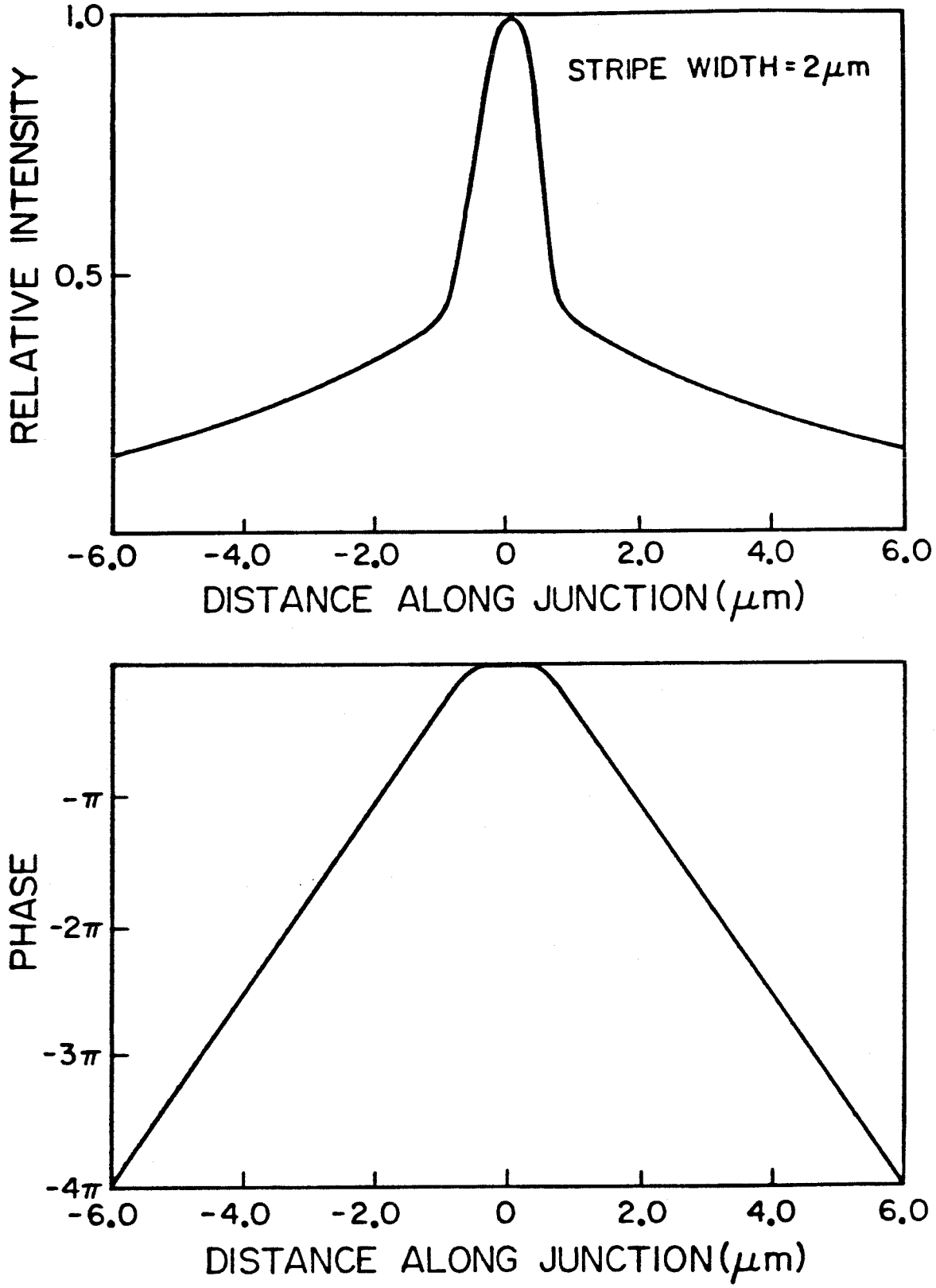

fig. 6 Near field intensity and phase for gain guided laser with 2 μm wide stripes

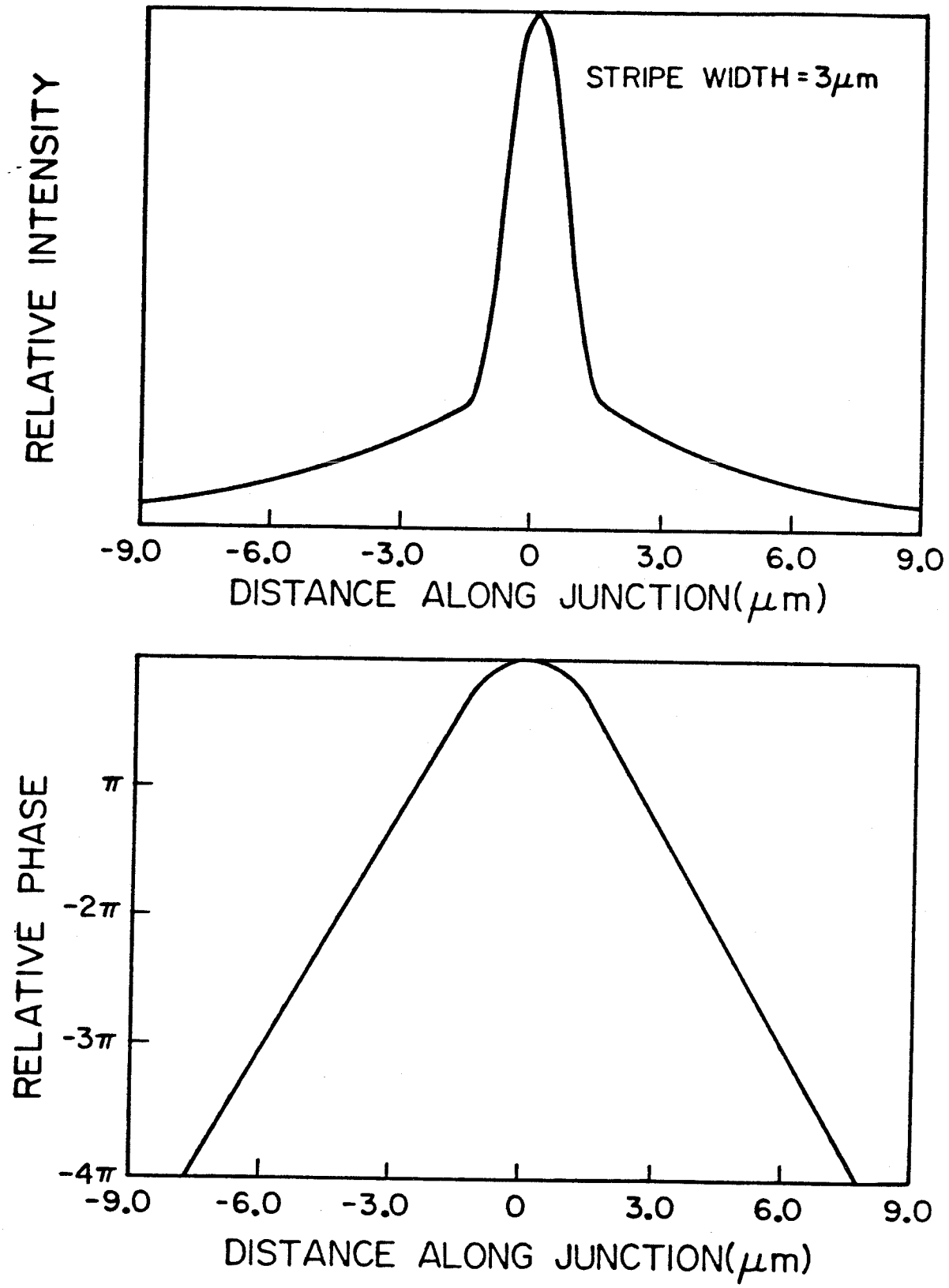

fig. 7 Near field intensity and phase for gain guided laser with 3 μm wide stripes

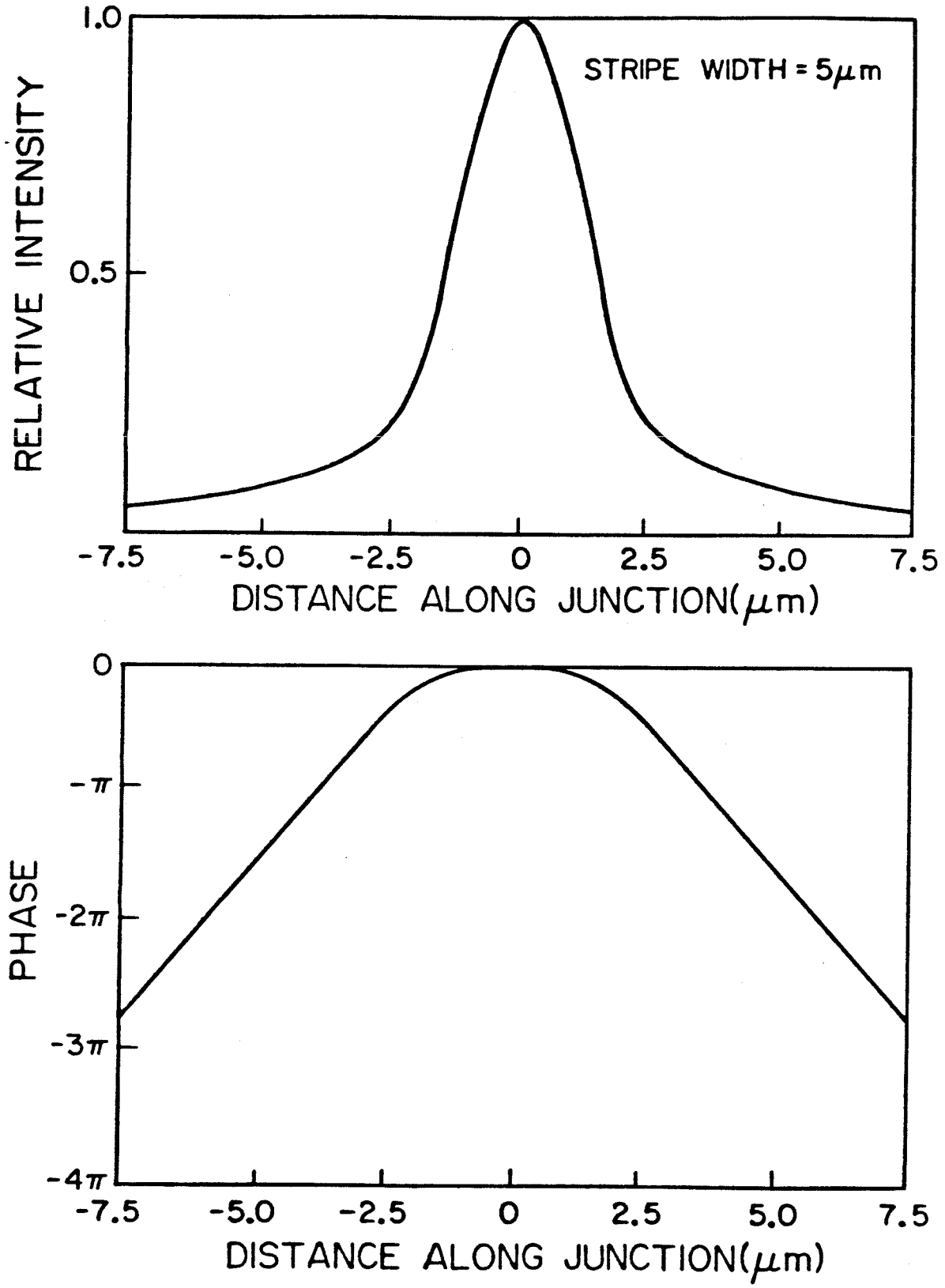

fig. 8 Near field intensity and phase for gain guided laser with 5 μm wide stripes

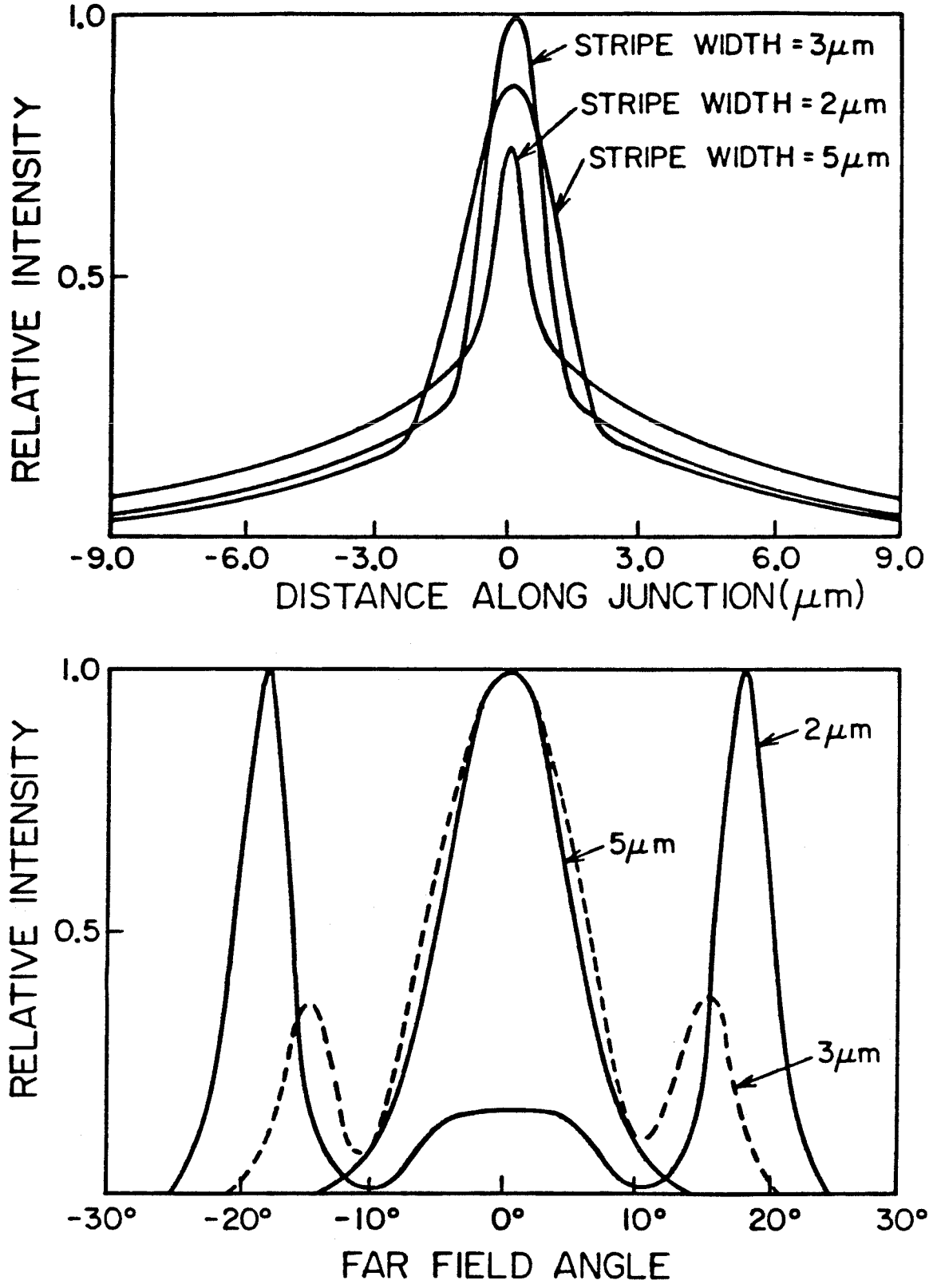

fig. 9 Near and far fields of modes of gain guided dielectric slab waveguides

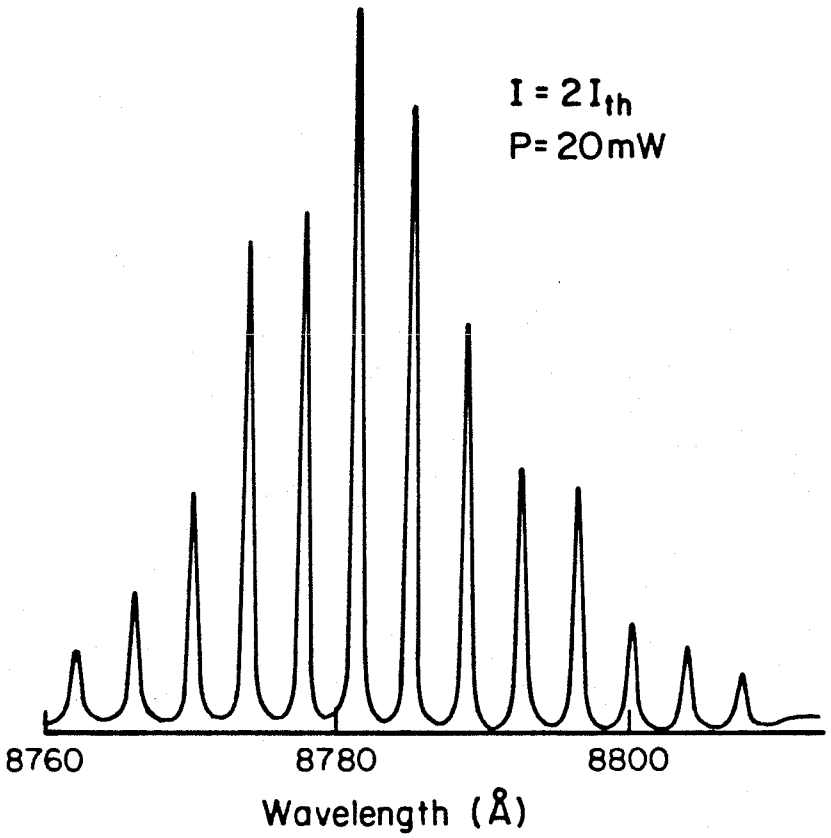

fig. 10 Spectrum of a narrow stripe DCC laser

was adjusted to give a mode gain of 40 cm^{-1}, which is approximately the mode gain at threshold for a typical laser. The real index suppression in the center layer was related to the gain by the expression

$$\Delta n_r = -3\Delta n_i \tag{7.9}$$

Because the indices of refraction of these waveguides are complex, p and h are also complex. The phase fronts of the modes are therefore not planar in gain guided lasers and the output beams are astigmatic. For instance the solutions in the lossy cladding layers of these waveguides are of the form

$$\exp(-p|x|)$$

where p is complex. The solutions are therefore plane waves, except that the amplitude decays exponentially away from the core.

The most striking feature of these gain guided modes is the appearance of pronounced side lobes in the far field patterns of the narrow stripe gain guided lasers. This can be understood by the fact that for narrow stripe widths, a large fraction of the power is propagating in the cladding layers. These decaying plane wave solutions in the cladding layers give rise to the side lobes in the far field, which are at an angle determined by the phase fronts of these decaying plane waves.

A second interesting property of narrow stripe DCC lasers was that they oscillate simultaneously in a large number of longitudinal modes. The spectrum of a narrow stripe DCC laser under pulsed operation is shown in fig. 10. This is consistent with previous findings that the number of longitudinal modes of narrow stripe lasers increases as the stripe width is decreased[6]. The reason narrow stripe lasers oscillate in many longitudinal modes is that as the stripe width is increased the astigmatism of the modes increases with the astigmatism factor being given by

$$K = \frac{\int |E|^2(y)dy}{\int E^2(y)dy} \tag{7.10}$$

The spontaneous emission into a mode with spontaneous emission factor K can be shown to be proportional to K^7. Thus as the stripe width decreases, the spontaneous emission into the modes increases. This in turn makes multilongitudinal mode operation more probable.

Although the primary purpose of this chapter is to report on the properties of DCC lasers with very narrow injection, it is believed that there are several advantages of the technique of injecting current though a narrow stripe in the substrate that may result in useful application for this technique. First, this technique allows the fabrication of narrow stripe lasers with broad area contacts, thus reducing contact resistance. In addition to lasers with a narrow top contact described above, lasers have been fabricated with top stripe widths of 15 μm. These lasers do not have as pronounced antiguiding characteristics as the narrow stripe DCC lasers. They also have lower threshold currents than the DCC lasers, with some devices having threshold currents as low as 50 mA. By incorporating some real index waveguiding mechanism, to provide good optical confinement, it may be possible to fabricate lasers with still lower thresholds using this technique of restricted injection through the substrate. In addition, we believe, that the leaky guide nature of the narrow stripe DCC structure combined with the simplicity of its fabrication makes the narrow stripe DCC structure an excellent choice for the fabrication of arrays of optically coupled lasers.

In conclusion, double current confinement lasers which feature very narrow carrier injection have been fabricated. These lasers exhibit strong antiguiding resulting in far fields characteristic of leaky waveguides. They have also been observed to operate in a large number of longitudinal modes. Finally, the technique

of current injection through a narrow stripe in the substrate appears to be well suited to several applications such as laser arrays, and also to low threshold laser structures if combined with a real index waveguiding mechanism.

References for Chapter 7

1. F.R. Nash 'Mode Guidance Parallel to the Junction Plane of Double Heterostructure Lasers", J. Appl. Phys. **44** , pp4696-4707, (1973).

2. P.M. Asbeck, D. Cammack, J. Daniele, and V. Klebanoff. 'Lateral Mode Behavior in Narrow Stripe Lasers", IEEE J. Quant. Electron. **QE-15** ,pp 727-730, (1979).

3. R. Lang. 'Lateral Transverse Mode Instability and Its Stabilization in Stripe Geometry Injection Lasers", IEEE J. Quant. Electron. **QE-15** ,pp 718-726 (1979).

4. W. Streifer, R. Burnham, and D. Scifres. "An Analytic Study of (GaAl)/As Gain Guided Lasers at Threshold", IEEE J. Quant. Electron. **QE-18** ,pp 856-864 (1982).

5. C. Wolk, H. Gottsmann, P. Marschall, K. Peterman, W. Pfister, and H. Vollmer "Criteria for Designing V-Groove Lasers", IEEE J. Quant. Electron. **QE-17** ,pp 756-759 (1981).

6. W. Streiffer, D. Scifres, and R. Burnham, "Spontaneous Emission Factor of Narrow Stripe Gain Guided Diode Lasers" Electronics Letters **17** ,pp 933-934 (1981).

7. K. Petermann. "Calculated Spontaneous Emission Factor for Double Heterostructure Injection Lasers with Gain Induced Guiding", IEEE J. Quant. Electron. **QE-15** ,pp 566-570 (1979).

8. W. Streiffer, D. Scifres, and R. Burnham. 'Longitudinal Mode Spectra of Diode Lasers", Appl. Phys. Lett. **40** ,pp 305-307 (1982).

9. W.T. Tsang and R Logan, 'Lateral Current Confinement in a GaAs Planar Stripe-Geometry and Channeled Substrate Buried DH Laser Using a Reversed-Biased P-N Junction", J. Appl. Phys. **49** ,pp 2629-2638 (1978).

10. D. Botez, W. Tsang, and S. Wang "Growth Characteristics of GaAs-$Ga_{1-x}Al_xAs$ Structures Fabricated by Liquid-Phase Epitaxy over Preferentially Etched

Channels", Appl.Phys. Lett. **28** ,pp 234-237 (1976).

11. P.A. Kirkby and G.H.B. Thompson "Channeled Substrate Buried Heterostructure GaAs-(GaAl)As Injection Lasers" J. Appl. Phys. **47** ,pp 4578-4589 (1976).

12. K. Funakoshi, A. Doi, K. Aiki, and R. Ito "Liquid Phase Epitaxial Growth of $Ga_{1-x}Al_xAs$ on Channeled Substrates" J. Cryst. Growth, **45** ,pp 252-257 (1978).

13. J.W. Cahn and D.W. Hoffman "A Vector Thermodynamics for Anisotropic Surfaces II. Curved and Faceted Surfaces" Acta Metallurgica, **22** ,pp 1205-1214 (1974).

14. D. Botez, "Constricted Double-Heterojunction AlGaAs Diode Lasers: Structures and Electrooptical Characteristics", IEEE J. Quantum Electron. **QE-17** ,pp 2290-2309 (1981).

Chapter VIII

Single Carrier Type Dominated Impact Ionization in Multilayer Structures

The noise generated by an avalanche photodiode (APD) is dependent on the statistics of the carrier multiplication process, since positive feedback effects, which exist when both electrons and holes produce secondary pairs, can greatly amplify any current fluctuations. Significantly more noise is generated if the electron and hole ionization rates (α,β) are equal than if only one carrier produces secondary pairs.[1] It is therefore highly desirable to have a detector in which the multiplication process is dominated by one carrier type. Unfortunately, most III-V materials have $\alpha \approx \beta$ .Recently, Chin etal.[2] proposed a multilayer GaAs-AlGaAs structure designed to enhance the ratio of the ionization rates α/β. This structure has been fabricated using molecular beam epitaxy (MBE) by Capasso et.al.[3]. The expected enhancement of α/β is due primarily to the fact that the discontinuity of the conduction band is larger than the discontinuity of the valence band. Thus, electrons enter the GaAs multiplication region with more kinetic energy than do holes and are therefore more likely to produce a secondary pair. This multilayer APD structure is shown in fig. 1. There is little impact ionization in the AlGaAs layers due to the higher ionization threshold of AlGaAs. In this chapter a proposed modification of this structure is described which is expected to significantly further increase α/β.

To illustrate the basic principles of this photodetector, first consider the hypothetical structure shown in fig. 2. A unit cell of this multilayer structure consists of five layers and two different materials. Material A has a low ionization threshold energy and is the material in which the multiplication occurs in this device. Material B has a much larger ionization threshold energy and negligible multiplication occurs in the layers of material B. The applied voltage is sufficiently

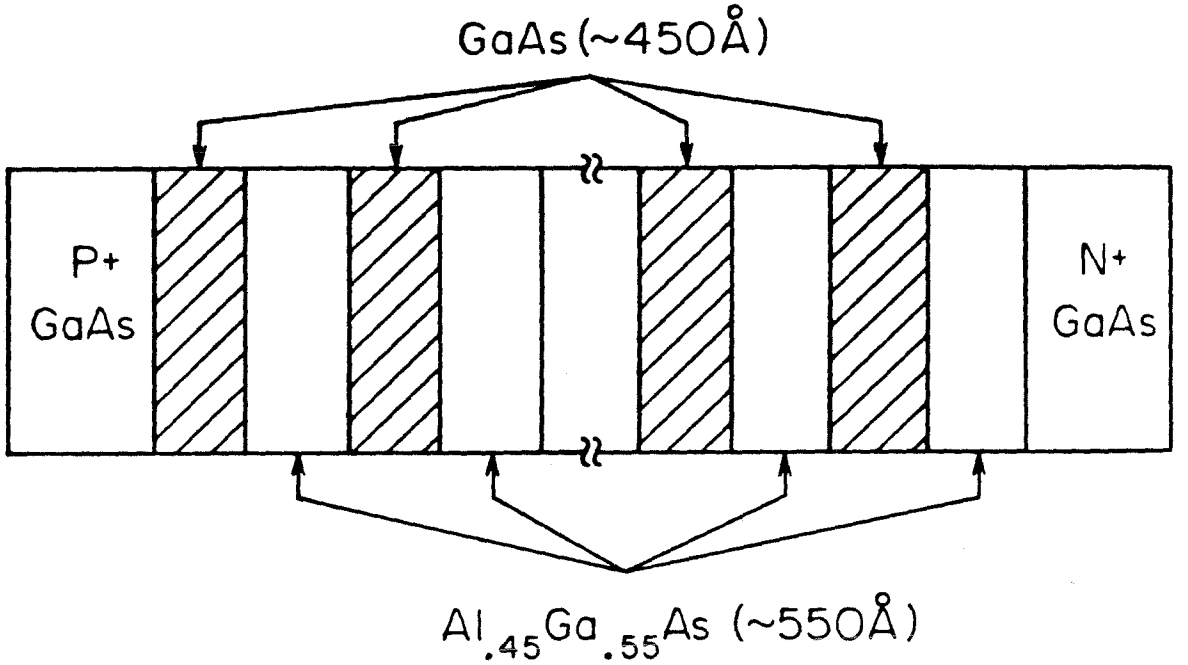

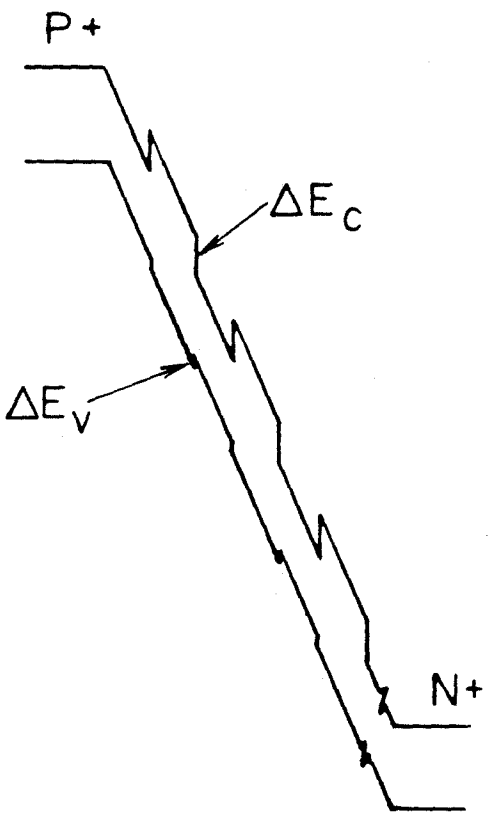

Fig. 1 a) Schematic diagram showing the layer structure of the superlattice APD grown by MBE[3].

b) Energy band diagram of the superlattice APD. The band edge discontinuities are ΔE_c=0.48eV, ΔE_v=0.08eV.

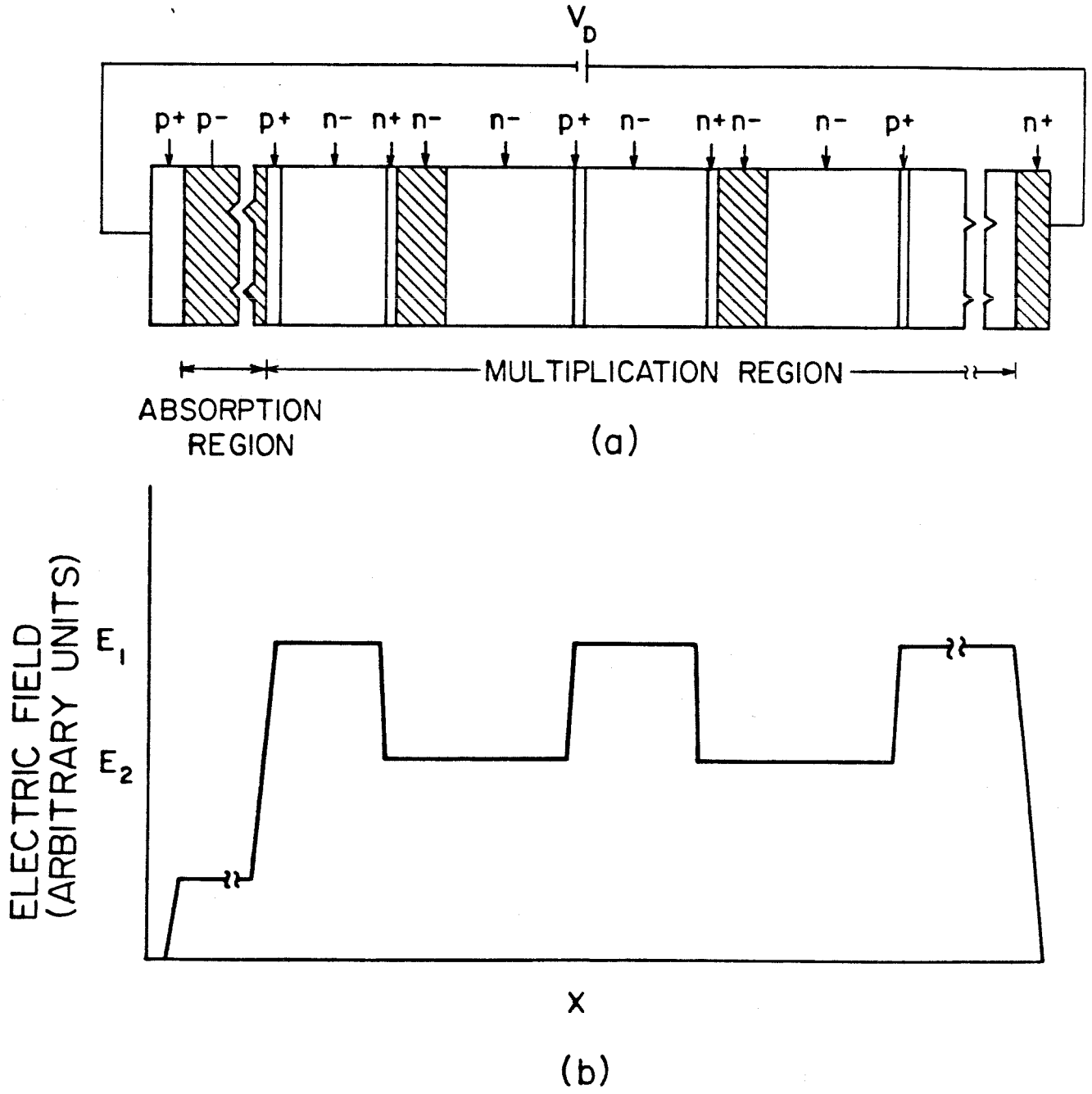

Fig. 2a) Schematic diagram of the multilayer APD structure showing the doping of each layer. Shaded regions are material A; white regions are material B.

b) Electric field in each layer of the multilayer structure.

large to fully deplete the absorption and multiplication regions. Typically, the layers of the multiplication region are fully depleted even at zero applied voltage. Since the gradient of the electric field in a depleted layer is proportional to the doping, the electric field changes abruptly in the thin, heavily doped layers. In the lightly doped layers, the field is nearly constant. By doping the layers as shown in fig. 2 the electric field on one side of material A (left side in fig. 1) can be made to be larger than the electric field on the other side of A. If the electrons are injected into A from the high field side and the holes are injected into A from the low field side, then the fraction of the electrons that are injected with energies above the ionization threshold can be significantly larger than the fraction of holes that are injected with energies above the ionization threshold.

To obtain the hypothetical avalanche photodetector just described all that is needed are two materials with sufficiently different ionization thresholds. Since the ionization thresholds of semiconductors are generally proportional to the bandgap, any two semiconductors with sufficiently different bandgaps could be used for the materials A and B. For the specific case of the ternary materials $Al_xGa_{1-x}As$, the bandgap increases as x increases. Since GaAs-AlGaAs superlattices can be fabricated using MBE, we expect GaAs (E_g=1.43eV) and $Al_{.45}Ga_{.55}As$ (E_g=2.0eV) to be suitable choices for materials A and B respectively.

Since the electric fields vary significantly over very short distances, the commonly used Baraff theory[4] cannot be readily applied to calculate the ionization rates of this device. However, to estimate the enhancement of α/β we have applied a simple model of impact ionization due to Shockley[5]. In this model impact ionizations occur only for the case of a carrier starting from zero energy and accelerating, without suffering any collisions, to an energy above the ionization threshold. In the Shockley model, the electron and hole ionization rates are proportional to $\exp(-D_n(E_{in})/L_n)$ and $\exp(-D_p(E_{ip})/L_p)$, where L_n and L_p are the optical phonon mean free

paths for electrons and holes respectively, $E_{in,p}$ are the electron and hole ionization threshold energies, and $D_{n,p}(E_i)$ are the distances the electrons and holes must travel without undergoing a collision to accelerate to the threshold energy for ionization. For this calculation the thicknesses of the GaAs, high field AlGaAs, and the low field AlGaAs layers were chosen to be 400 Å, 700 Å, and 900 Å respectively. For the ionization thresholds and optical phonon mean free paths we used the values given in Chin et al. These are ionization thresholds of 2.0 eV for electrons and 1.5 eV for holes and optical phonon mean free paths of 50 Å for electrons and 40 Å for holes. Fig. 3 shows a single unit cell of the structure for which the ionization ratio α/β was calculated. For the calculation the simplifying assumption was made that the electric field changes abruptly. This is equivalent to replacing the heavily doped layers of finite thickness by a sheet of charge of infinitesimal thickness.

In fig. 3 the position $x=-L_1$ satisfies:

$$\varphi(0)-\varphi(-L_1)=E_{in}-\delta E_c \tag{8.1}$$

the position $x=-L_2$ satisfies:

$$\varphi(D)-\varphi(-L_2)=E_{in}-\delta E_c \tag{8.2}$$

similarly

$$\varphi(L_3)-\varphi(-0)=E_{ip}-\delta E_v \tag{8.3}$$

$$\varphi(L_4)-\varphi(D)=E_{ip}-\delta E_v \tag{8.4}$$

for devices consisting of layers of GaAs and $Al_{.45}Ga_{.55}As$ $\delta E_c \approx 0.5$ eV and $\delta E_v \approx 0.1$ eV. The positions $x=-L_1,-L_2$ are therefore the starting points for electrons, which result in impact ionizations at x=0,D in the Shockley model x= 0,D respectively, assuming they suffer no collisions. Similarly the positions $x=L_3,L_4$ are the starting positions of holes that result in impact ionizations at x=0,D in the Shockley model.

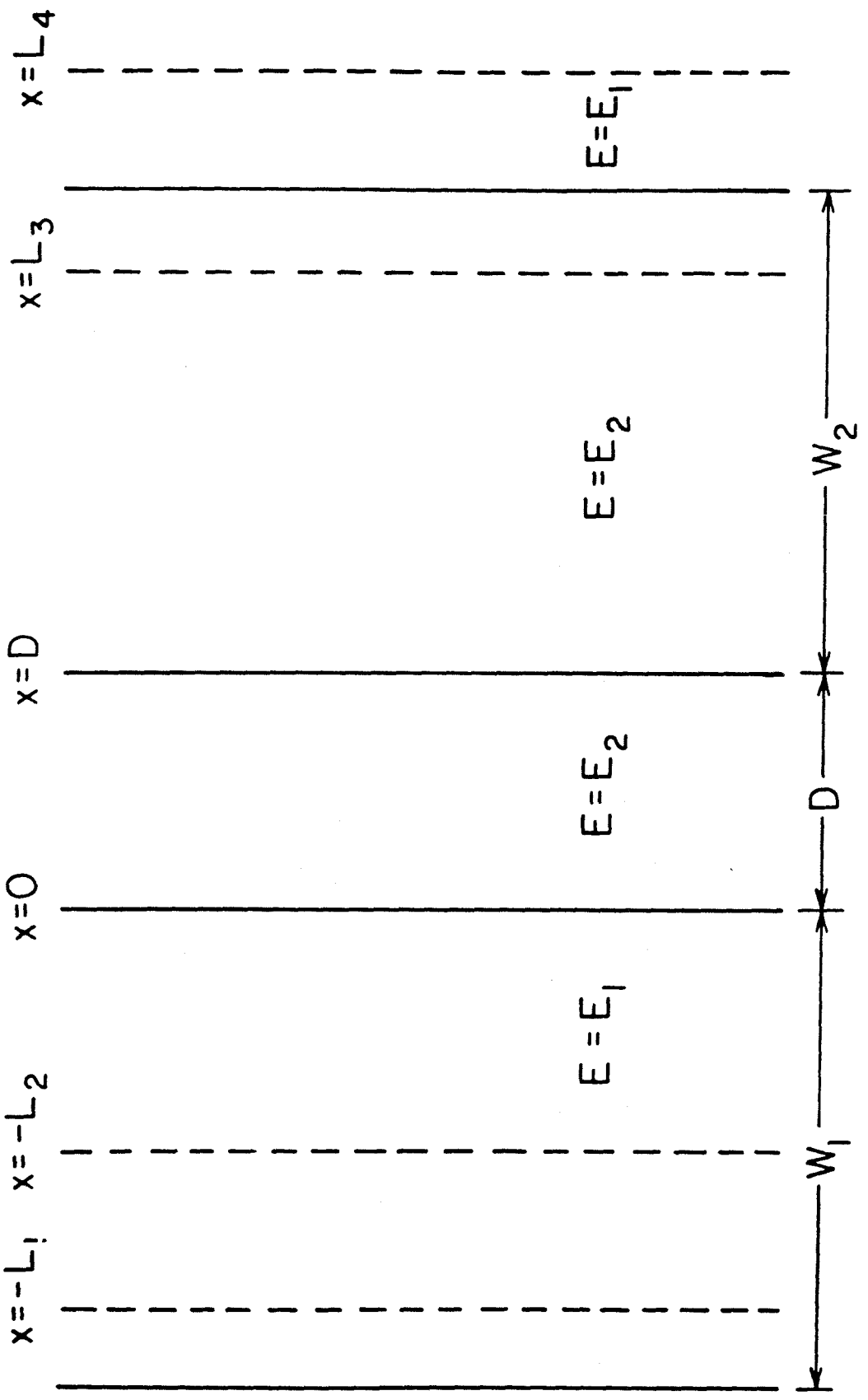

Fig. 3 A unit cell of the multilayer APD structure used in the Shockley model ionization rate calculation.

In this calculation, all of the relevant material parameters, except for the ionization threshold energy, are assumed to be the same in $Al_{.45}Ga_{.55}As$ as in GaAs. Although is certainly not the case, the enhancement of α/β in this structure as compared to that fabricated by Capasso et al. is significant for any reasonable set of assumptions about the material parameters.

To calculate the ionization ratio α/β, the probability for a carrier being accelerated so that it results in an impact ionization is first determined as a function of the starting position. Integrating over all starting positions then gives the total ionization rates. For electrons

$$P(x)= 0 \qquad x> -L_2$$

$$P(x) \sim \exp\left(\frac{-L_1+(x-L_1)\left(1-\frac{E_2}{E_1}\right)}{L_n}\right) \qquad -L_1< x< -L_2 \tag{8.5}$$

$$P(x) \sim \exp\left(\frac{-x}{L_n}\right) \qquad x< -L1$$

It is assumed that the high field region is sufficiently wide so that the fraction of the electrons contributing to the secondary multiplication that start outside of the high field region is negligible. A similar assumption for the holes is not always reasonable since the voltage drop across the low field region may be less than the ionization energy for some operating conditions of interest (this is actually the most desirable situation). The ionization probabilitics must therefore be separated into three cases depending on whether the positions $x=L_3,L_4$ are in the low or high field regions.

case 1: $L_4 < W_2+D$

$$P(x)=0 \qquad x< L_3 \tag{8.6}$$

$$P(x) \sim \exp\left(\frac{-L_3}{L_p}\right) \qquad L_3< x< L_4$$

$$P(x) \sim \exp\left(\frac{-(x-D)}{L_p}\right) \qquad x> L_4$$

case 2: $L_3 < (W_2+D) < L_4$

$$P(x)=0 \qquad x< L_3 \tag{8.7}$$

$$P(x) \sim \exp\left(\frac{-L_3}{L_p}\right) \qquad L_3< x< W_2+D$$

$$P(x) \sim \exp\left(\frac{-L_3+(x-(W_2+D))(1-\frac{E_2}{E_1})}{L_p}\right) \qquad W_2+D< x< L_4$$

$$P(x) \sim \exp\left(\frac{-(x-D)}{L_p}\right) \qquad x> L_4$$

case 3: $L_3 > W_2+D$

$$P(x)=0 \qquad x< L_3 \tag{8.8}$$

$$P(x) \sim \exp\left(\frac{-L_3+(x-L_3)(1-\frac{E_2}{E_1})}{L_p}\right) \qquad L_3< x< L_4$$

$$P(x) \sim \exp\left(\frac{-(x-D)}{L_p}\right) \qquad x> L_4$$

Integrating over all starting positions the electron and hole ionization rates are obtained.

$$\alpha \sim \left[L_n+L_{no}\left(1-\exp\left(\frac{-T}{L_{no}}\right)\right)\right]\exp\left(\frac{-L_2}{L_n}\right) \tag{8.9}$$

and

$$\beta \sim (D+L_p)\exp\left(\frac{-L_3}{L_p}\right) \qquad \text{case1} \tag{8.10}$$

$$\beta \sim \left[L_{po}\left(\exp\left(\frac{(L_4-D-W_2)}{L_{po}}\right)-1\right)+L_p\exp\left(\frac{(L_4-D-W_2)}{L_{po}}\right)+D+W_2-L_3\right]\exp\left(\frac{-L_3}{L_p}\right) \qquad \text{case2}$$

$$\beta \sim \left[L_{po}\left(\exp\left(\frac{D(2-\frac{E_2}{E_1})}{L_{po}}\right)-1\right)+L_p\exp\left(\frac{D(2-\frac{E_2}{E_1})}{L_{po}}\right)\right]\exp\left(\frac{-L_4}{L_p}\right) \qquad \text{case3}$$

where

$$L_{no} = \frac{L_n E_2}{E_1 - E_2} \tag{8.11}$$

$$L_{po} = \frac{L_p E_2}{E_1 - E_2} \tag{8.12}$$

and

$$T = D\frac{E_2}{E_1} \tag{8.13}$$

The values of α/β calculated from the Shockley model are shown in fig. 4. The curve for $\Delta E=0$, corresponds to a detector similar to that reported by Capasso etal.[3]. The main purpose of this calculation is to show that significant enhancement of α/β is expected for $\Delta E \neq 0$. The enhancement of α/β is most likely somewhat exagerated for the upper left hand part of fig. 4 due to shortcomings of the Shockley model. This calculation has been repeated for other commonly quoted values for the ionization thresholds and optical phonon mean free paths, which are consistent with experimentally measured ionization rates of GaAs The predicted enhancement of α/β was found to be relatively insensitive to which set of parameters we chose. The enhancement of α/β for $\Delta E \neq 0$ is most pronounced for lower electric field strengths. However, even with higher fields, which means greater multiplication per unit cell, the enhancement of α/β is significant. To reduce the complexity of fabricating such a detector it is desirable to have no more than 10-15 unit cells (with an external

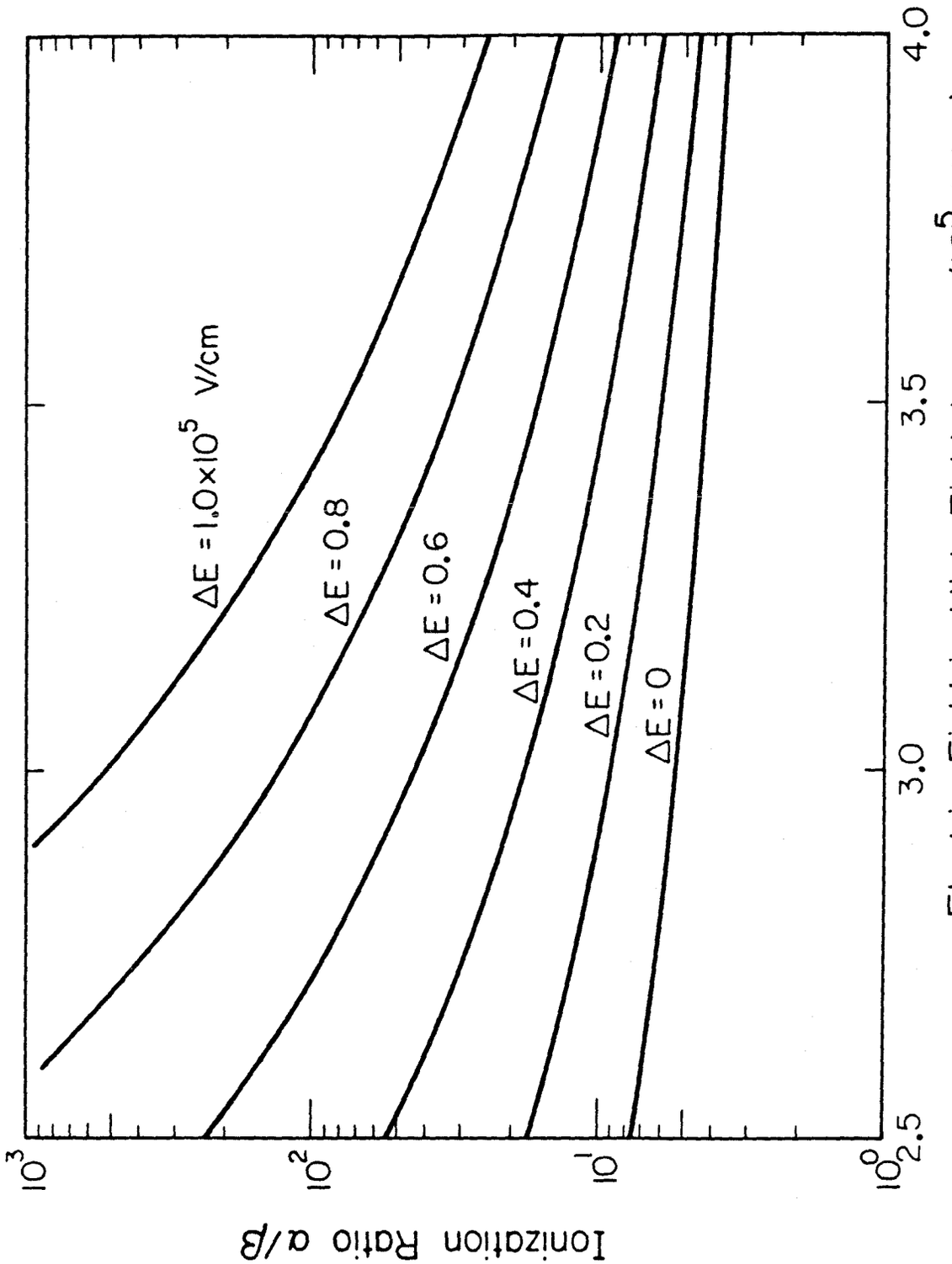

Fig. 4 Ionization ratio for various values of the electric fields in the high and low field layers.

bias of 6-10 volts per cell). A practical detector would therefore probably have electric field strengths corresponding to the right hand side of fig. 4 since higher electric fields would mean that fewer unit cells would be required.

To optimize the design of the proposed detector, it would be necessary to calculate the electron and hole energy distribution functions $f_e(\varepsilon)$,$f_h(\varepsilon)$ at each position as the carriers move through the layers of the detector. Such a calculation can be done using a Monte Carlo simulation[6], however this has not been attempted for this structure. Although the Shockley model is useful for estimating α/β, it can not be used to accurately calculate $f_e(\varepsilon)$ and $f_h(\varepsilon)$. However, several qualitative features of the detector design can be stated without precisely knowing the energy distribution functions. First, the n+ AlGaAs layers should be as thin as possible, so that the hot electrons do not lose much energy in these layers. The high field AlGaAs layers should have thicknesses and electric fields such that a significant fraction of the electrons are injected into the GaAs layers with enough energy to produce secondary pairs. However, it is undesirable for the fields to be so high that multiplication in the AlGaAs layers becomes significant. To minimize secondary ionization by holes the low field layers have to be sufficiently thick that holes can lose (by phonon collision) the kinetic energy gained in the preceding high field layer. In addition, the difference between the electric fields in the high and low field regions should be as large as is practical. A 50 Å thick n+ layer with a doping of $2x10^{18}$ cm^{-3} will result in a change, ΔE, in the electric field of approximately $1.6x10^5$ V/cm. It is also desirable to have the total number of donors in a unit cell nearly equal to the total number of acceptors, so that the electric field pattern repeats itself in each unit cell. One final consideration is that electrons that flow across an abrupt interface from GaAs to $Al_{.45}Ga_{.55}As$ have to overcome an energy barrier of nearly 0.5 eV. For this reason, it may be desirable to grade the interfaces between the GaAs and the n- $Al_{.45}Ga_{.55}As$ layers.

In conclusion a new III-V avalanche photodetector in which the multiplication process is dominated by a single carrier type has been proposed. For a GaAs-$Al_{.45}Ga_{.55}As$ detector of this type α/β has been estimated based on a simple model. The results of this calculation suggest that detectors with greatly enhanced ratios of α/β should be practical.

References

1. R.J. McIntyre 'Multiplication Noise in Uniform Avalanche Diodes". *IEEE Trans.* **ED-13** , 1966, pp164-167

2. R. Chin, N. Holonyak, G.E. Stillman, J.Y. Tang, and K. Hess, 'Impact Ionisation in Multilayered Heterojunction Structures", *Electron. Lett.*, **16** , 1980, pp 467-469

3. F. Capasso, W.T. Tsang, A.L. Hutchinson, and G.F. Williams, *Appl. Phys. Lett.* **40** , Jan. 1 1982, pp 38-40

4. G.Baraff, *Phys. Rev.* **128** , 1962 pp 2507-

5. W. Shockley 'Problems Related to P-N Junctions in Silicon" *Solid State Electron.*, **2** , 1961 pp 35-67

6. P. Price, Monte Carlo Calculation of Electron Transport in Solids", in Semiconductors and Semimetals vol. 14 ch. 4. R.K. Willardson and A. Beer eds. Academic Press, New York, 1979.